Prediction of Ice Accretion on a Swept NACA 0012 Airfoil and Comparisons to Flight Test Results

Andrew L. Reehorst
Lewis Research Center
Cleveland, Ohio

NASA

PREDICTION OF ICE ACCRETION ON A SWEPT NACA 0012 AIRFOIL AND COMPARISONS TO FLIGHT TEST RESULTS

Andrew L. Reehorst
National Aeronautics and Space Administration
Lewis Research Center
Cleveland, Ohio 44135

E-6746

Abstract

In the winter of 1989-90, an icing research flight project was conducted to obtain swept wing ice accretion data. Utilizing the NASA Lewis Research Center's DHC-6 DeHavilland Twin Otter aircraft, research flights were made into known icing conditions in Northeastern Ohio. The icing cloud environment and aircraft flight data were measured and recorded by an onboard data acquisition system. Upon entry into the icing environment, a 24-in. span, 15-in. chord NACA 0012 airfoil was extended from the aircraft and set to the desired sweep angle. After the growth of a well defined ice shape, the airfoil was retracted into the aircraft cabin for ice shape documentation. The ice accretions were recorded by ice tracings and photographs. Ice accretions were mostly of the glaze type and exhibited scalloping. The ice was accreted at sweep angles of 0°, 30°, and 45°. A three-dimensional ice accretion prediction code was used to predict ice profiles for five selected flight test runs, which include sweep angles of 0°, 30°, and 45°. The code's roughness input parameter was adjusted for best agreement. A simple procedure was added to the code to account for three-dimensional ice scalloping effects. The predicted ice profiles are compared to their respective flight test counterparts. This is the first attempt to predict ice profiles on swept wings with significant scalloped ice formations.

Nomenclature

AIRFAC	a density correction to correct for ice scallops
Alpha	angle of attack, deg
Alt	altitude, m and ft
k_{s2D}	equivalent sand grain roughness calculated for two-dimensional LEWICE, m
k_{s3D}	equivalent sand grain roughness calculated for LEWICE3D, m
LWC	liquid water content, g/m^3
JW LWC	liquid water content measured by the Johnson-Williams liquid water content sensor
Laser LWC	liquid water content measure by the particle measuring systems laser droplet sizing instruments
MVD	droplet mean volume diameter, μm
SAT	static air temperature, °C
Sweep	sweep angle, deg
TAS	aircraft true airspeed, km/hr and kn
Time	exposure time, min

Introduction

This report has two purposes: the first is to present the results from a swept airfoil icing flight test, and the second is to present the results of a comparison between these measured swept wing ice accretions and ice profiles predicted by a three-dimensional ice accretion code. Eleven sets of flight data and discussion are presented in the experimental section. The data consists of time plots of icing environment data, statistical information from these plots, tracings of the resultant ice shapes, and photographs of the ice shapes.

Five sets of comparisons between the predicted ice profiles from a three-dimensional ice accretion prediction code and flight ice accretion tracings are presented in the analysis section. Only the predicted and flight ice accretions are compared. No comparisons were attempted for resultant lift or drag. A description of the quality of agreement is included along with a discussion of the steps required to achieve this agreement.

The NASA Lewis Research Center has been actively involved in icing flight testing since 1982. Flight research has been utilized to validate wind tunnel and computational fluid dynamics analysis results. In recent years a great deal of effort has been expended towards three-dimensional computer icing analysis. A two-dimensional ice accretion code, LEWICE, was developed by the University of Dayton Research Institute (Ref. 1) and later modified by Ruff (Ref. 2). Potapczuk and Bidwell extended this technology to three-dimensional with the development of the LEWICE3D ice accretion code (Ref. 3). LEWICE3D had shown good agreement to the existing three-dimensional ice accretion database, however, this database was small and contained no natural icing data.

A test was designed utilizing a NACA0012 airfoil to begin building an inflight icing database for three-dimensional bodies. Eleven sets of ice tracings and environmental data for sweep angles between 0° and 45° are the results of this test and are presented here. Most of the ice accreted in flight was of the glaze type and exhibited significant scalloping.

The calculation of ice profiles with LEWICE3D to compare to this flight test data represents the first attempts at dealing with the presence of ice scallops with a three-dimensional ice accretion code. Detailed discussions are included on the adjustments of surface roughness factor and ice density that were made in an attempt to achieve agreement with flight measured ice accretions with scalloping.

Test Facility

The test aircraft is a DeHavilland DHC-6 Twin Otter (Fig. 1), a twin turboprop STOL commuter aircraft. It has been extensively modified to permit the acquisition of aircraft icing data. The wings, wing and gear struts, and all tail surfaces are protected by pneumatic de-icer boots. Small experiments may be introduced to the icing environment via the experiment elevator which extends out the overhead access hatch.

Instrumentation

In addition to the standard flight instruments, this aircraft is equipped with a great deal of research instrumentation (Ref. 4). Airspeed, altitude, angle of attack, and angle of sideslip are measured with Rosemount pressure transducers connected to a Rosemount model 858 five-hole pneumatic sensor located at the end of the research instrumentation nose boom. On the nose of the aircraft are located a General Eastern dew point sensor, two Rosemount temperature sensors, a Rosemount ice detector, and a Johnson/Williams liquid water content sensor. Two Particle Measuring Systems laser droplet sizing instruments (Optical Array Probe and Forward Scattering Spectrometer Probe) are located beneath the left wing. These laser probes provide droplet size and liquid water content measurements. All data is processed by an onboard Particle Measuring Systems data acquisition system and stored in binary format on nine-track magnetic tape.

Swept Wing Hardware

The test body used for this test was a wooden NACA0012 airfoil, with a 0.609 m (24-in.) span and a 0.381 m (15-in.) chord (Fig. 2). The airfoil can be pivoted to a desired angle of sweep between 0° and 45°. The pivot point of the airfoil is 7.62 cm (3 in.) from the lower edge and is even with the aircraft skin when the airfoil is fully extended. The boundary layer thickness above the hatch

2

has been measured to be approximately 15 cm (6 in.). This places the center of the airfoil above the boundary layer at all times. When extended, the airfoil chord is aligned with the longitudinal axis of the aircraft. Angle-of-attack of the airfoil is equal to and controlled by sideslip angle of the aircraft.

Test Procedure

Several steps were involved in the test of the swept airfoil in natural icing conditions. After icing conditions were identified from FAA PIREPS (pilot reports), the Twin Otter was launched and the pilots and FAA air traffic controllers coordinated a flight path to intersect the known icing region. When the icing conditions were encountered a holding pattern was coordinated. The aircraft was trimmed to hold the desired angle of sideslip, the NACA0012 airfoil was extended from the overhead hatch and swept to the desired angle, and the time was recorded. During the icing encounter the environmental data was constantly monitored by the test engineer and also recorded to tape by the data acquisition system. After a well defined ice shape had formed, the airfoil was unswept and retracted back into the aircraft cabin and the time was recorded. At this time ice shape photographs and ice tracings were taken. Tracings were made at center span and at one quarter or three quarter span locations. The tracings were made by first making a cut through the ice perpendicular to the leading edge with a heated aluminum template, and then manually tracing the ice shape to a cardboard template. The airfoil was then cleaned and the procedure was repeated.

Data Reduction

After each flight, data was reduced to engineering units and plotted using a desktop personal computer with a nine-track magnetic tape drive. The data is presented in tabular and graphical formats.

The tabular data includes important statistical data for each flight. Time averages and standard deviation for the following data is presented in Table 1: airfoil sweep angle (degrees); airfoil angle of attack (degrees); aircraft true airspeed (km/hr); liquid water content as measured by the Johnson/Williams probe (kg/m^3); droplet size (MVD) as measured by the laser probes (μm); time of airfoil exposure (min); static air temperature (°C); liquid water content as measured by the laser probes (kg/m^3); and altitude (m). For most of the cases presented the time averages and standard deviations were calculated for the entire airfoil exposure times. Exceptions to this are discussed below.

The graphical data includes plots showing the following parameters as a function of airfoil exposure time: aircraft true airspeed (kn); liquid water content as measured by the Johnson/Williams probe (kg/m^3); liquid water content as measured by the laser probes (kg/m^3); droplet size (MVD) as measured by the laser probes (μm); static air temperature (°C); and altitude (ft).

The reader should note that the true airspeed presented here is the aircraft's airspeed. From previous flight tests it is known that the airspeed for the area where the swept airfoil was tested is uniformly about 10 percent higher than the aircraft airspeed (Fig. 3).

Data for Each Flight

The icing environment and ice accretion documentation for each flight can be found in Figs. 4 to 14. For each airfoil exposure, environment data versus time plots are presented followed by airfoil ice tracings and then iced airfoil photographs.

Flight 90-4 Data. Figures 4 (Run 1) and 5 (Run 2): Ice was accreted at 45° sweep for this flight. The resultant ice was a mixed ice shape (rime and glaze mixture), an opaque, white ice with a shape between that of a pure rime or glaze with no significant scalloping. During the reduction of the environment data some MVD data was removed during very low LWC periods, this is done

3

because the MVD data is inaccurate at low LWC's. The data system was not recording altitude for this flight; the reported altitude for this flight was hand recorded during airfoil exposures.

Flight 90-5 Data. Figures 6 (Run 1) and 7 (Run 2): Ice was accreted at 45° sweep for this flight. The resultant ice was a glaze ice shape, a translucent ice with well defined scalloping (moderately sized in Run 1 and large in Run 2). During the reduction of the environment data, in addition to removing MVD data at short low LWC periods, the first 2 min of laser probe data (laser LWC and MVD) from the second run were removed because of very low LWC. The data system was not recording altitude for this flight; the reported altitude for this flight was hand recorded during airfoil exposures.

Flight 90-7 Data. Figures 8 (Run 1), 9 (Run 2), and 10 (Run 3): Ice was accreted at 30° sweep for this flight. The resultant ice was a glaze ice shape, a clear ice with well defined, large scalloping. During the reduction of the environment data several minutes of the laser probe data was removed for the third run because the laser instruments had briefly frozen over. The data system was not recording altitude for this flight; the reported altitude for this flight was hand recorded during airfoil exposures.

Flight 90-8 Data. Figures 11 (Run 1) and 12 (Run 2): Ice was accreted at 30° sweep for this flight. The resultant ice was a glaze ice shape, a clear ice with very rough, irregular, large scalloping.

Flight 90-11 Data. Figures 13 (Run 1) and 14 (Run 2): Ice was accreted at 0° sweep for this flight. The resultant ice was a mixed ice shape, clear near stagnation region turning white near impingement limits with the ice shape generally uniform in spanwise direction (no scalloping).

Analysis for Selected Cases

Comparison cases were run with the NASA LEWICE3D code (Ref. 3). LEWICE3D is a three-dimensional ice accretion code made up of a three-dimensional Hess-Smith panel code, a three-dimensional particle trajectory code, and the two-dimensional LEWICE code. LEWICE (the two-dimensional code) is applied along surface streamlines calculated by the three-dimensional panel code.

Five cases were selected for analysis to study the effect of sweep angle, two cases for 30° of sweep angle, two cases for 45°, and one case for 0°. Since LEWICE has had documented difficulty with glaze shapes with horns very large relative to the rest of the ice shape (Ref. 2), flight cases demonstrating this profile were avoided. All ice accretion predictions were performed using a single time step. The 10 percent aircraft airspeed correction discussed above was included for these calculations to account for the higher velocities above the overhead hatch. Time averaged temperature, LWC, and MVD values from Table 1 were used for the calculations. Eighty-seven chordwise panel elements were used to represent the airfoil profile and between 8 and 14 spanwise panel elements were used to represent the finite wing (number of spanwise stations dependent on sweep angle) (Fig. 15). Droplet trajectories were calculated at three spanwise stations to determine profile uniformity. Profiles were found to be reasonably uniform over the length of the airfoil, so for this report only the center span data is presented. CPU time for calculating one ice profile was about 1200 sec on the NASA Lewis Research Center Cray X-MP computer system.

The calculated ice profiles were compared to the tracings of the flight ice accretions. The tracings represent the outermost envelope of the ice shape in the region of the cut

(including scallops). Since LEWICE3D has no mechanism for modeling scallops, the resultant predicted ice profile can be expected to be smaller than the ice tracings. This difference between the tracings and predicted ice profiles shall be further explained in the next section.

Accounting for Three-Dimensional Scalloping Effects

When the first attempts were made to calculate ice accretions to compare to the swept wing flight cases, the calculated ice profiles were consistently too small. Initially it was thought that the time dependent nature of the liquid water content from the flight data was the reason for the discrepancy between the amount of ice predicted and the ice measured from flight, but very extreme adjustments in liquid water content were required to produce agreement. These adjustments were on the order of three times the values measured in flight. No justification could be seen for this severe adjustment of the flight measured variables. It is also interesting to note that these differences appear to be peculiar to flight data comparisons. Computer predictions (unpublished at this time) for NASA Icing Research Tunnel (IRT) generated ice profiles for this swept NACA0012 airfoil appear to predict the correct amount of ice. Upon inspection, the flight data had much more severe scalloping than the IRT data. It is not clear if the greater scalloping is due to the low liquid water content levels seen in these flight cases or the low flight turbulence levels. In either case, LEWICE3D has no mechanism for modeling scalloping. A simple adjustment of the ice density calculated by LEWICE3D was adopted as a first order approximation of the effects of the ice scalloping. While by no means does this adjustment model the physics involved in the microscopic icing process, it can satisfy the conservation of mass over the final macroscopic ice shape. This adjustment was made with a multiplicative factor, AIRFAC, which is defined as the ratio of the total flight ice volume divided by the total enclosed ice shape volume as

obtained by the tracing method. This is illustrated in Fig. 16, where assuming a constant ice profile,

$$\text{AIRFAC} = L_{ice}/(L_{ice}+L_{air}).$$

When this factor is applied to the LEWICE calculated ice density, the resulting predicted ice profile should have the correct size and profile, but without the air gaps caused by the scalloping. For this effort AIRFAC was estimated by reviewing the photographs of the ice shapes and then further refined by trial-and-error. The final values of AIRFAC used for each case is included in the discussion of the cases below.

Adjustment of Roughness Parameter

A significant parameter that controls where the calculated ice freezes (in single time step cases) is the equivalent sand grain roughness. This term controls the local heat transfer coefficient which in turn can influence the shape of ice predicted. Ruff and Berkowitz (Ref. 2) describe the calculation of the two-dimensional LEWICE equivalent sand grain roughness, k_{s2D}, using an empirical correlation. This calculation is based upon a baseline value of $k_{s2D}/c)_{base}$ equal to 0.00117 for ice accreted in the IRT at specific icing conditions. Since this baseline value is facility specific, it can not be expected to be appropriate for all sites. For comparisons to ice accreted in facilities other than the IRT, the roughness is generally determined by trial and error. Berkowitz and Riley (Ref. 5) showed that a new value of 25 percent of the IRT baseline value gave marked improvement in comparisons to ice accreted in flight on the Twin Otter wing. This modification to the baseline value was assumed to come from the lower free-stream turbulence in flight compared to that in the IRT.

Adjustment of the roughness parameter has been investigated by Potapczuk and Bidwell for use in LEWICE3D (Ref. 3). They found that an order of magnitude increase of k_{s2D} was necessary to produced a value for

use with LEWICE3D, k_{s3D}, which achieved good agreement with ice shapes accreted at 30° of sweep in the IRT. The use of this factor is assumed to arise from the addition and influence of spanwise flow. The spanwise flow can be reasoned to raise the heat transfer over that of a pure two-dimensional flow for which the Ruff/Berkowitz correlation was derived.

A linear combination of the Berkowitz-Riley adjustment and the Potapczuk-Bidwell adjustment was used as a starting point for a trial-and-error search for the value of k_{s3D} which yielded the best agreement to flight data:

$$k_{s3D)initial} = 0.25^*10^*(k_{s2D}) = 2.5(k_{s2D})$$

The individual surface roughness values used for these cases are presented later in the discussion of flight/analytical data agreement.

Calculation Procedure

The procedure for the trial and error search for the best ice accretion agreement began with the calculation of $k_{s3D)initial}$ as discussed above. This value along with the flight test values for airspeed, liquid water content, droplet size, altitude, and exposure time, along with the initial value of 1.0 for AIRFAC made up the input data set for LEWICE3D. For a single time step calculation, the roughness and density effects were investigated separately. Roughness was adjusted first to get the best agreement in profile geometry. Once the best possible ice profile agreement was produced, then the ice density was adjusted with AIRFAC to produce the best agreement in size. By adjusting the ice density, the profiles remain geometrically similar, but scale up in cross-sectional area as density is reduced. Since the droplet trajectory calculations are the time consuming portion of the ice profile prediction calculation and are independent of k_{s3D} and AIRFAC, the trajectory results can be stored. This allows the trial and error process of determin-

ing the optimal values to proceed without expending a great deal of CPU time.

Comparison Between Flight Results and Computer Predictions

The discussion of agreement for each pair of flight and analytical profiles in this section is based upon (1) impingement limits, (2) cross-sectional area (volume of ice), and (3) shape. This section also contains discussion of efforts to improve agreement. The key parameters input to LEWICE3D for these cases are listed in Table 2.

Flight 4, Run 1. For this 45° of sweep case, the general agreement was good (Fig. 17). The calculated limits of impingement were smaller than those seen in the flight data. The impingement agreement is rated fair. The volume of ice predicted agrees very well with the flight data and the ice shape agreement is seen to be good. For this case AIRFAC = 0.6 was used. A roughness value of $k_{s3D} = 0.0009$ m produced the best agreement with flight data. To achieve this value, the calculated two-dimensional roughness level of $k_{s2D} = 0.00036$ m was multiplied by 2.5.

Flight 5, Run 1. Agreement for this 45° of sweep case is very similar to the previous case (Fig. 18). Overall agreement is good, based upon fair ice impingement limit agreement, very good ice volume agreement, and good shape agreement. In this case the required value for AIRFAC was 0.4. A roughness value of $k_{s3D} = 0.0024$ m produced the best agreement here. This requires the two-dimensional roughness level of $k_{s2D} = 0.00041$ m be multiplied by 5.8.

Flight 7, Run 2. Sweep angle was 30°. Agreement for this case is very good (Fig. 19). Generally poor agreement was achieved when an Angle-of-Attack of 3° was utilized for this calculation, so 0° was used and resulted in the demonstrated agreement. It is theorized that the true flow angle may be significantly

6

less than the aircraft angle of sideslip. This case demonstrates the need to determine the true flow angle above the Icing Research Aircraft's overhead hatch. The calculated limits of impingement were somewhat greater than the flight data. Both ice volume and shape were made to agree very well. The value of AIRFAC used was 0.4. The roughness value $k_{s3D} = 0.0010$ m was used to achieve the best agreement. The calculated two-dimensional roughness value of $k_{s2D} = 0.00038$ m must be multiplied by 2.6.

Flight 7, Run 3. Agreement for this 30° of sweep case is good (Fig. 20). The calculated agreement with flight data is very good for both the limits of impingement and the volume of ice. The shape agreement is only fair. Similar to the previous case, the calculation for this case was carried out at 0° angle of attack. The value of AIRFAC used here was 0.3. A roughness value $k_{s3D} = 0.0015$ m was used to achieve the best agreement. The calculated two-dimensional roughness value of $k_{s2D} = 0.00036$ m must be multiplied by 4.2.

Flight 11, Run 1. Agreement for this 0° of sweep case is very good (Fig. 21). The calculated impingement limits, volume of ice, and general shape agree very well. It is very important to note that for this 0° of sweep case, AIRFAC was held at 1.0, representing no density adjustment. A roughness value $k_{s3D} = 0.0005$ m was used to achieve best agreement. The calculated two-dimensional roughness value of $k_{s2D} = 0.00027$ m must be multiplied by 1.9. It should be noted that this roughness correction does not conform with that from previous analysis of flight test cases (Ref. 5), by being almost 8 times larger. This discrepancy may be influenced by the chord lengths of the airfoils examined (NACA0012 examined here has a chord of 15 in. and the Twin Otter airfoil examined in Ref. 5 has a chord of 6.5 ft). However, no definitive explanation has been established.

Discussion of Comparisons

Three interesting trends become apparent when observing these above cases as a group. The trends are related to roughness, density and scalloping. For the following discussion of trends, it is helpful to refer to Table 2.

The first trend is that the density values used by the code (after AIRFAC adjustment) decrease as scalloping becomes more severe. The level of scalloping severity can be seen to start with no scalloping in the Flight 90-11, Run 1 data, moving to minimal scalloping in the Flight 90-4, Run 1 data, on to moderate scalloping in Flight 90-5, Run 1 and Flight 90-7, Run 2, and ending with severe scalloping in Flight 90-7, Run 3. This is also the order exhibited by the density correction, AIRFAC. This is the trend that is desired and seen to be appropriate to correctly model swept airfoil scalloping.

The second trend is that the greater the sweep angle and the greater the level of scalloping, the greater the level of required roughness correction. This can be seen by reviewing the values of k_{s3D}/k_{s2D} and sweep angle in Table 2 and the scalloping severity discussion above. This trend is most likely due to combination of the spanwise flow and the complex flow about the scallops. As Potapczuk and Bidwell theorized that three-dimensional spanwise flow increases the heat transfer from that of a pure two-dimensional case, it can also be theorized that this spanwise flow coupled with flow about the scallops will further elevate the local heat transfer coefficients. Since k_{s3D} controls heat transfer, it follows that this term should follow this trend.

The third trend is that the density correction is consistently greater than would be expected by looking at the photos of the flight ice shapes. Two factors that may be

contributing to this disparity are code over-estimation of ice density and single time step calculation.

The ice density is calculated using the LEWICE form of the Macklin ice density expression (Ref. 2) which can vary from 0.1 g/cm^3 for a feathery rime to 0.9 g/cm^3 for a clear ice. But for the cases examined here, the Macklin correlation gave values of ice density that corresponded to a pure glaze condition for all regions of all the examined cases. This disagrees with some of the photos taken in flight which show distinct regions of rime ice. Also, the Macklin correlation was derived from low speed, two-dimensional wind tunnel data (Ref. 6). Therefore, it is argued that the density values predicted by the Macklin expression may need to be reduced and varied along the chordwise surface distance for three-dimensional applications, especially in cases where scalloping is very pronounced. In addition, the use of a constant density adjustment, AIRFAC, for a given ice profile may not be the best approach. Clearly evident in the flight photos is a varying level of air space in the scallops. Near the stagnation point there is little to no space, where at the impingement limits there is a maximum spacing between ice scallops. The shape agreement should be improved if AIRFAC was allowed to vary along the chordwise surface distance.

As would be expected, the general tendency seen in previously reported efforts (Ref. 2) has been that multiple time steps give better agreement for glaze cases than single time step calculations. As an ice shape begins to form, the local collection efficiency distribution is altered thus altering the growth pattern of the ice shape. Single step calculations were performed to save computation time, however in the future, multiple step accretion calculations will need to be performed to quantify the level of error introduced by this factor.

Conclusions

Comparisons between measured and analytically predicted ice profiles were made for 5 of 11 flight test cases. It was found that density and roughness factor corrections were required to achieve reasonable agreement. To account for the ice scalloping observed in the flight data, the LEWICE3D density term was modified by a multiplicative factor AIRFAC. This term was determined by trial and error, but appears to be related to the level of ice scalloping. The surface roughness factor k_{s3D} was also determined by trial and error, and is significantly larger than the two-dimensional version, k_{s2D}. The correction ratio required to get from k_{s2D} to k_{s3D} tends to increase with sweep angle and the level of scalloping.

Based upon this study, further investigation is required to refine the extension of the two-dimensional LEWICE heat transfer and ice density correlations to three dimensions. Besides the measurement of environmental conditions and resulting ice shapes, future tests should include the measurement of overall and local ice densities and detailed studies of ice scalloping and roughness. This testing will allow the development of improved ice density correlations, improved modeling of the scalloping, and improved surface roughness correlations. Future tests on the NASA Lewis Research Center's Twin Otter should further investigate the airspeed and flow angularity in the overhead hatch area.

References

1. MacArthur, C.D., Keller, J.L., and Leurs, J.K., "Mathematical Modeling of Ice Accretion on Airfoils," AIAA Paper 82-0284, Jan. 1982.

2. Ruff, G.A. and Berkowitz, B.M., "Users Manual for the NASA Lewis Ice Accretion Prediction Code (LEWICE), " NASA CR-185129, 1990.

3. Potapczuk, M.G. and Bidwell, C.S., "Numerical Simulation of Ice Growth on a MS-317 Swept Wing Geometry," AIAA Paper 91-0263, Jan. 1991 (also, NASA TM-103705).

4. Ide, R.F. and Richter, G.P., "Comparison of Icing Cloud Instruments for 1982-1983 Icing Season Flight Program," AIAA Paper 84-0020, Jan. 1984 (also, NASA TM-83569).

5. Berkowitz, B.M. and Riley, J.T., "Analytical Ice Shape Predictions for Flight in Natural Icing Conditions," NASA CR-182234, DOT/FAA/CT-88/19, 1988.

6. Macklin, W.C., "The Density and Structure of Ice Formed by Accretion." Quarterly Journal of the Royal Meteorological Society, Vol. 88, Jan. 1962, pp. 30-50.

TABLE 1.—FLIGHT DATA SUMMARY[a]

Flight number	Run	Sweep	Alpha	TAS[c]	JW LWC	MVD	Time	SAT	Laser LWC	Alt
90-4	1	45	0	244.8/11.1	0.13/0.04	17.98/0.86	25.0	-9.53/0.23	0.24/0.07	[b]3657/---
90-4	2	45	3.5	245.9/7.0	0.07/0.07	18.4/2.6	29.3	-9.77/0.32	0.11/0.09	[c]3657/---
90-5	1	45	0	238.3/9.3	0.15/0.12	17.8/2.4	9.83	-5.77/0.34	0.22/0.12	[c]1585/---
90-5	2	45	4	228.7/6.5	0.19/0.13	25.1/3.8	12.0	-5.23/0.28	0.32/0.15	[c]1676/---
90-7	1	30	3	233.5/4.6	0.26/0.04	23.5/1.5	17.0	-3.65/0.47	0.37/0.10	[c]1006/---
90-7	2	30	3	236.5/3.5	0.22/0.06	13.74/1.26	20.8	-2.98/0.36	0.28/0.07	[c]1128/---
90-7	3	30	3	229.8/6.5	0.19/0.09	14.8/0.12	20.5	-4.72/0.49	0.28/0.12	[c]975/---
90-8	1	30	0	270.6/6.7	0.49/0.06	15.4/0.9	10.5	-3.77/0.27	0.41/0.06	[c]2255/53
90-8	2	30	3	237.5/5.0	0.38/0.05	15.4/1.1	11.0	-3.4/0.2	0.43/0.05	[c]2153/22
90-11	1	0	0	298.2/8.3	0.12/0.1	17.9/2.4	12.5	-8.7/0.26	0.12/0.08	[c]2505/34
90-11	2	0	4	294.5/10.6	0.14/0.11	16.6/4.1	19.5	-8.7/0.26	0.14/0.12	[c]2525/30

[a]Averages/standard deviations.

[b]No standard deviations are available for altitude for flights 90-4 to 90-7.

[c]Airspeed data is for the aircraft, airspeed for the swept airfoil is approximately 10 percent higher airspeed due to position effects.

TABLE 2.—LEWICE3D PARAMETERS

	90-4, Run 1	90-5, Run 1	90-7, Run 2	90-7, Run 3	90-11, Run 1
Sweep, deg	45.0	45.0	30.0	30.0	0.0
Velocity, m/s	74.9	72.9	72.4	70.3	91.1
LWC, g/m^3	0.13	0.15	0.22	0.19	0.12
MVD, μm	18.0	17.8	13.75	15.0	17.9
Temperature, K	263.6	267.4	270.2	268.4	264.4
Time, sec	1500	590	1248	1230	750
k_{s3D}	0.0009	0.0024	0.0010	0.0015	0.0005
AIRFAC	0.6	0.4	0.4	0.3	1.0
k_{s3D}/k_{s2D}	2.5	5.8	2.6	4.2	1.9
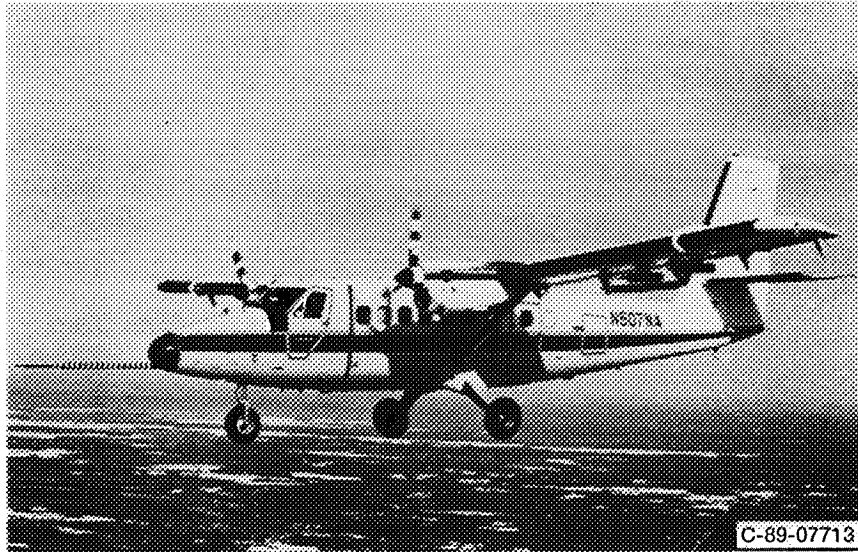
Figure 1.—NASA Lewis Research Center icing research aircraft (DHC-6 Twin Otter Aircraft).
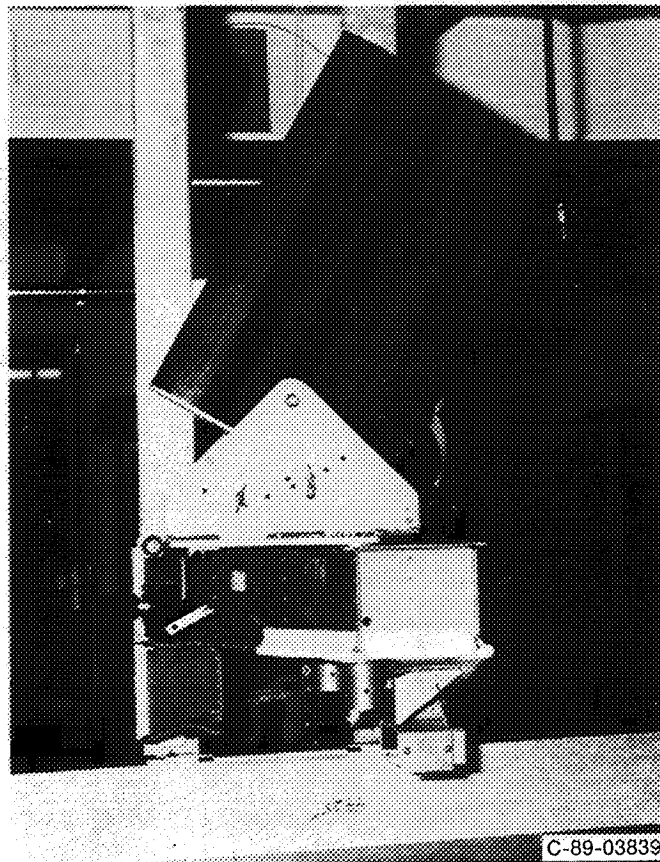
Figure 2.—Swept wing apparatus.
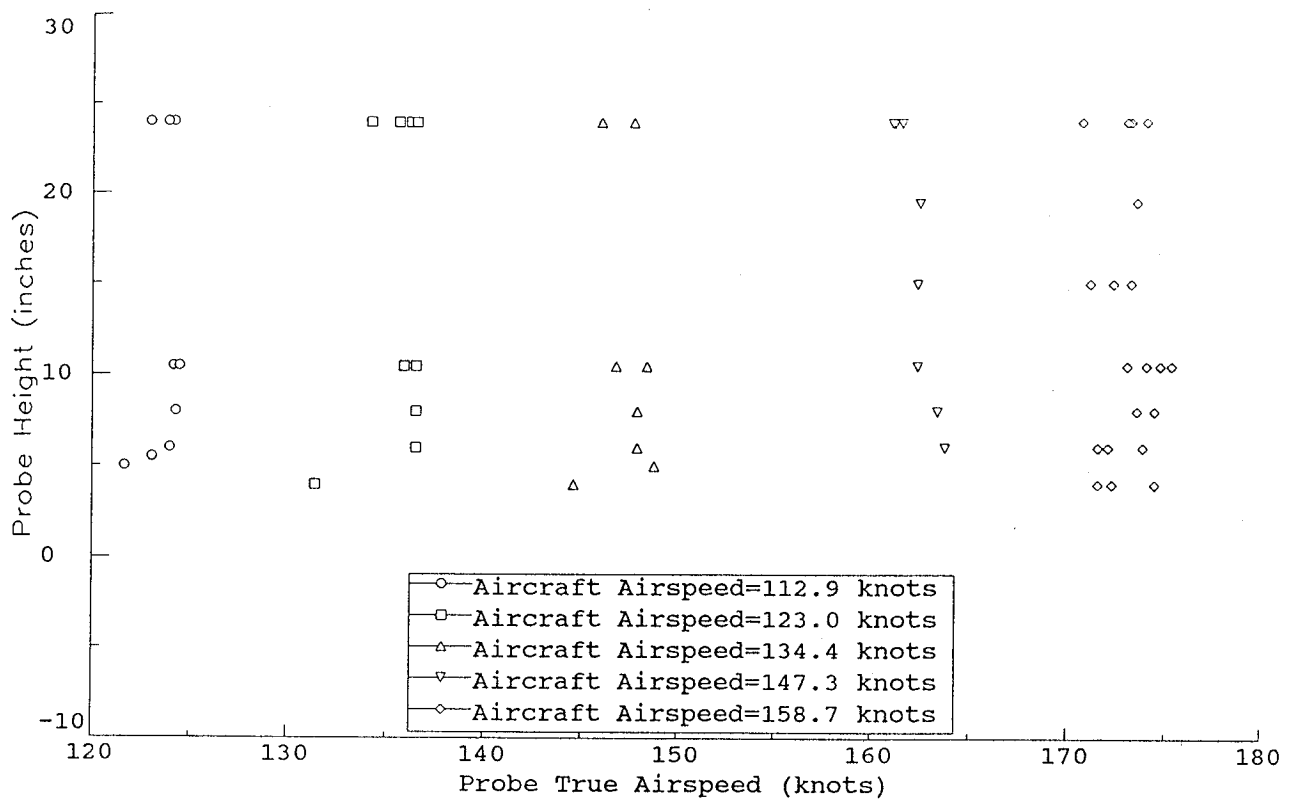
Figure 3.—Local velocity profiles above the hatch.
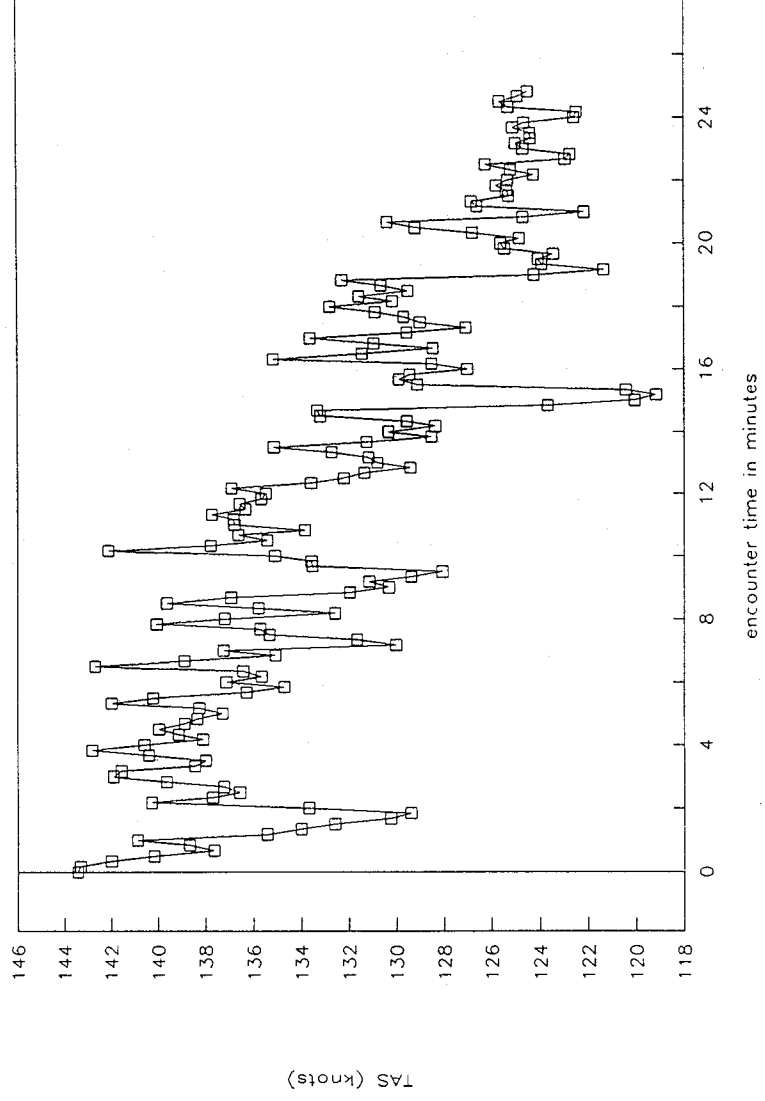
Figure 4a.—Aircraft true airspeed (in knots) for flight 90-4, run 1; average = 132.1, standard deviation = .6.
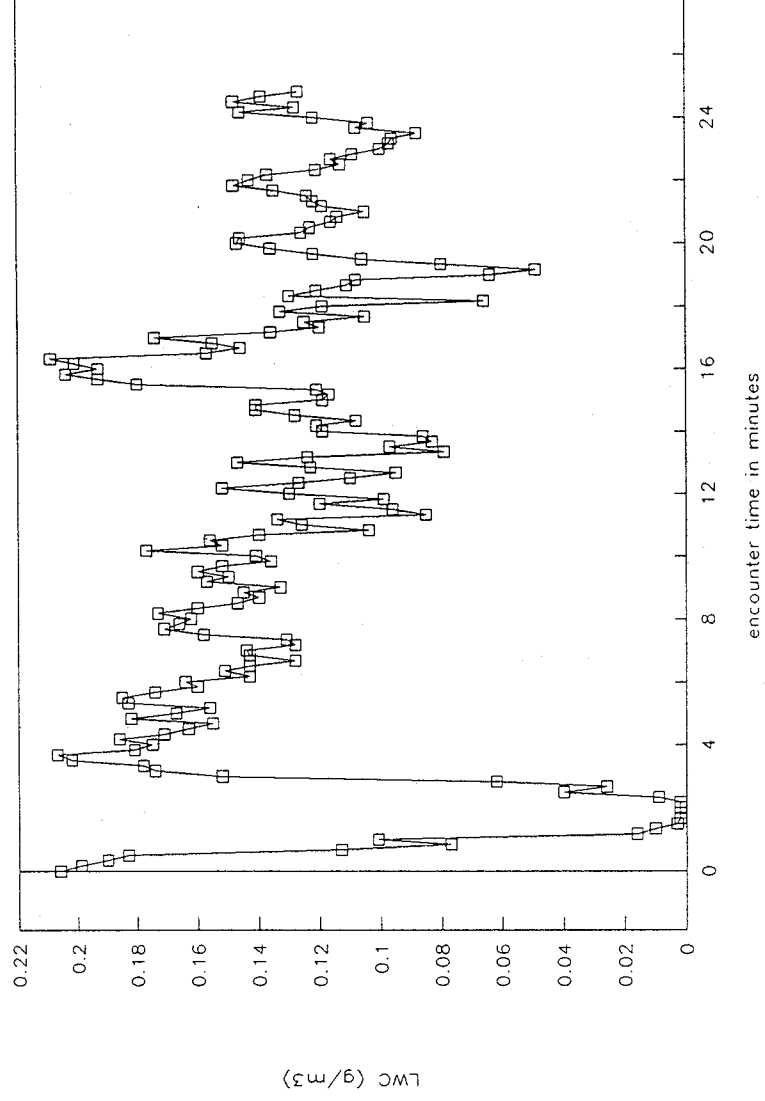
Figure 4b.—Johnson-Williams liquid water content for flight 90-4, run 1; average = .13, standard deviation = .04.
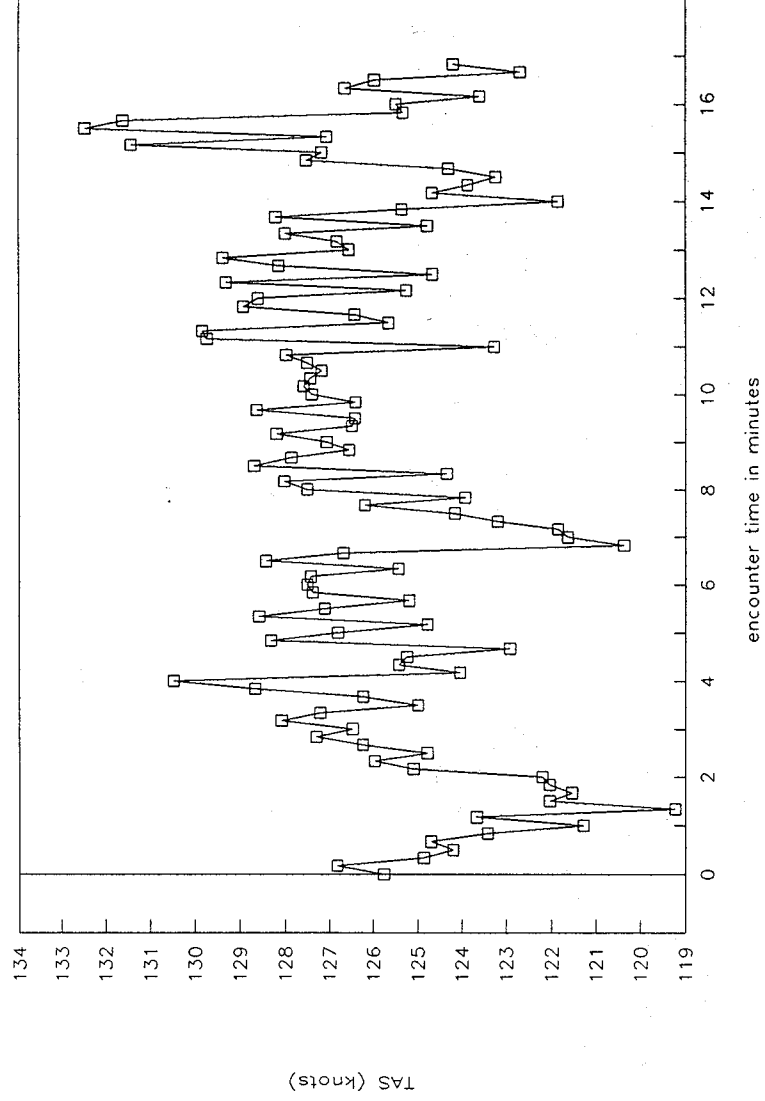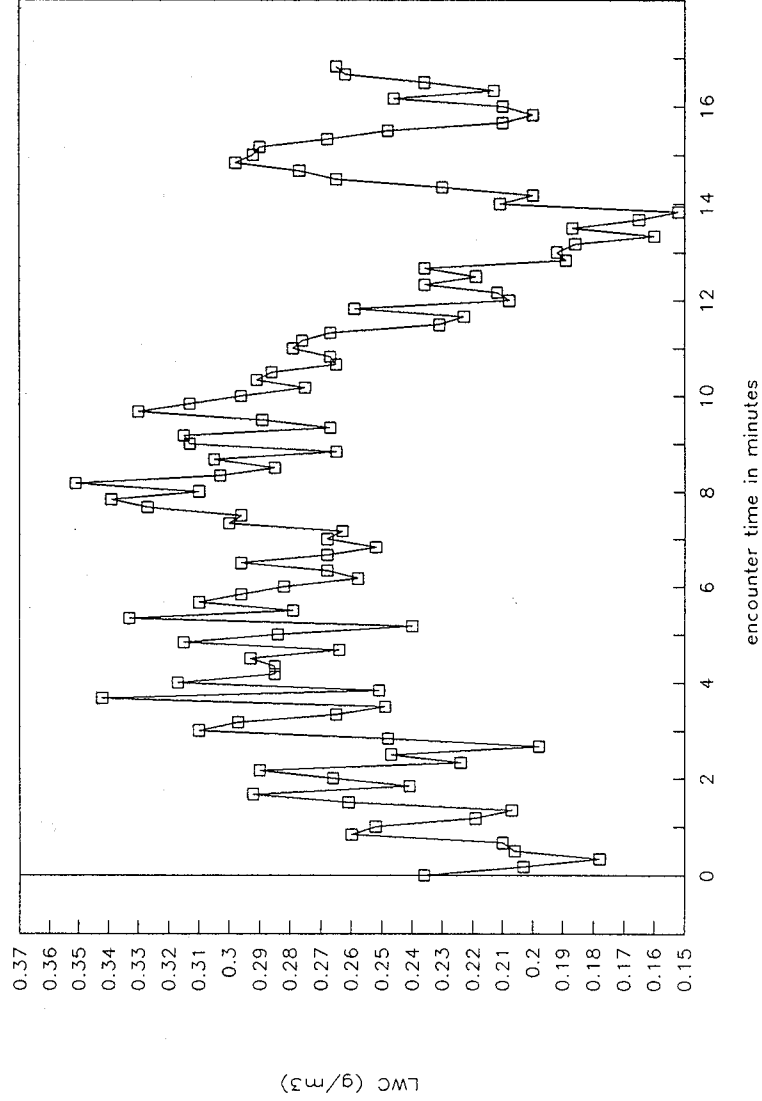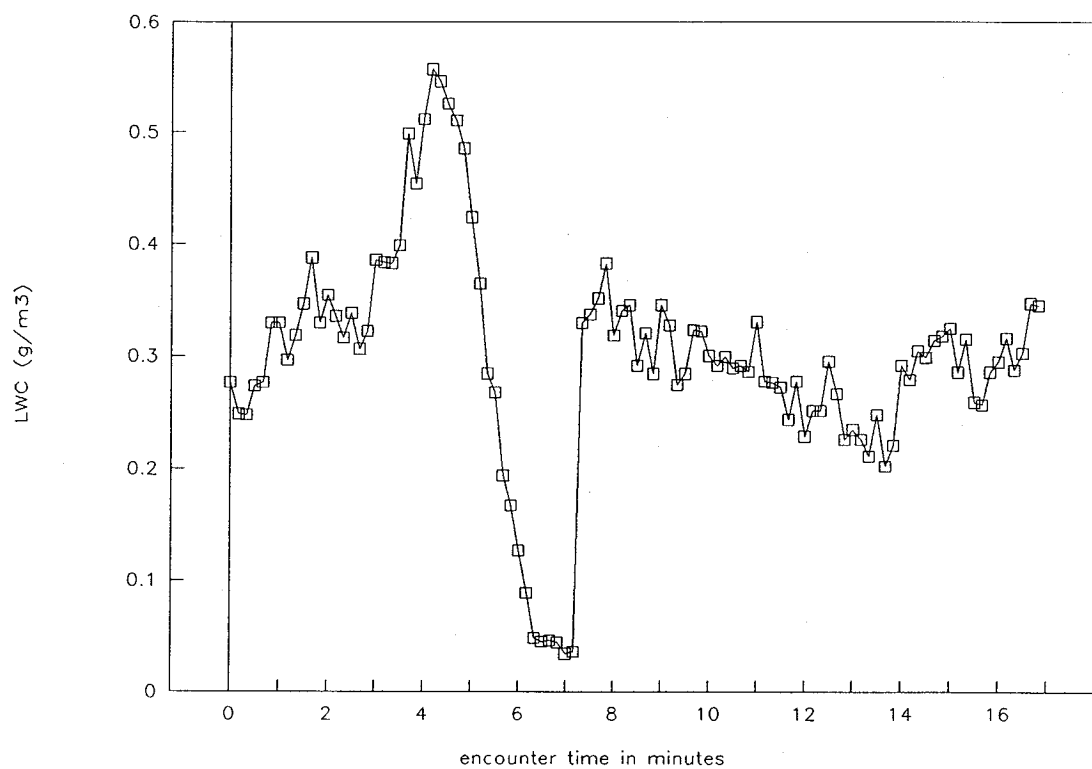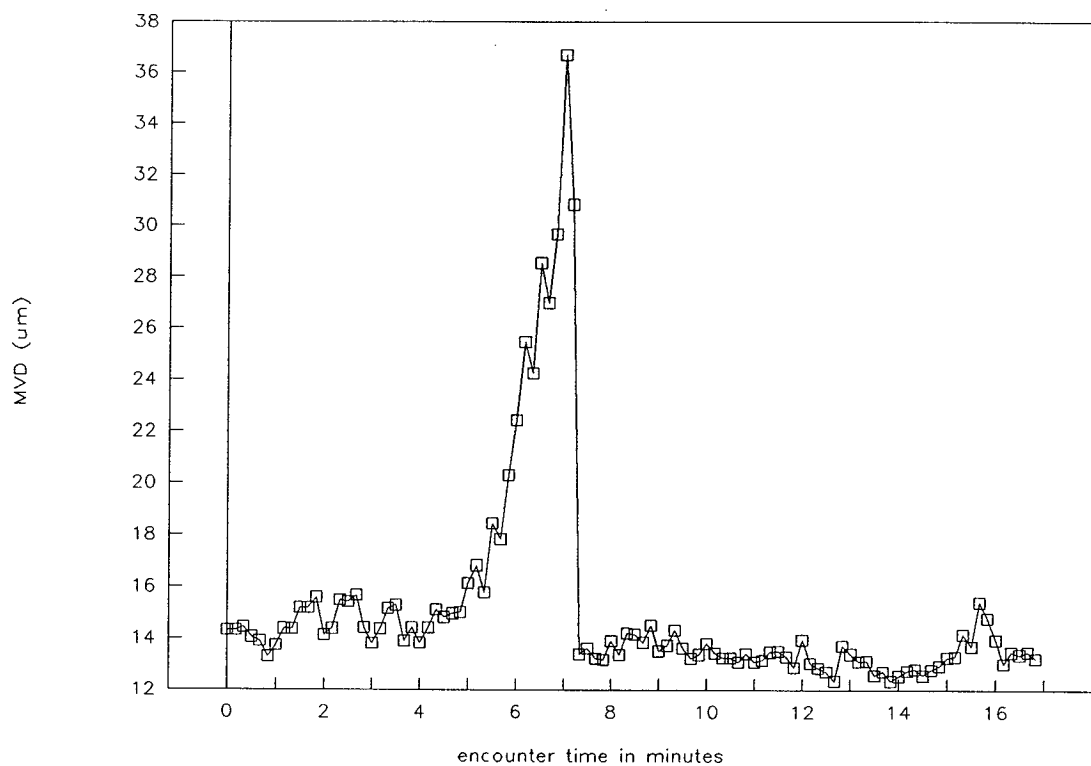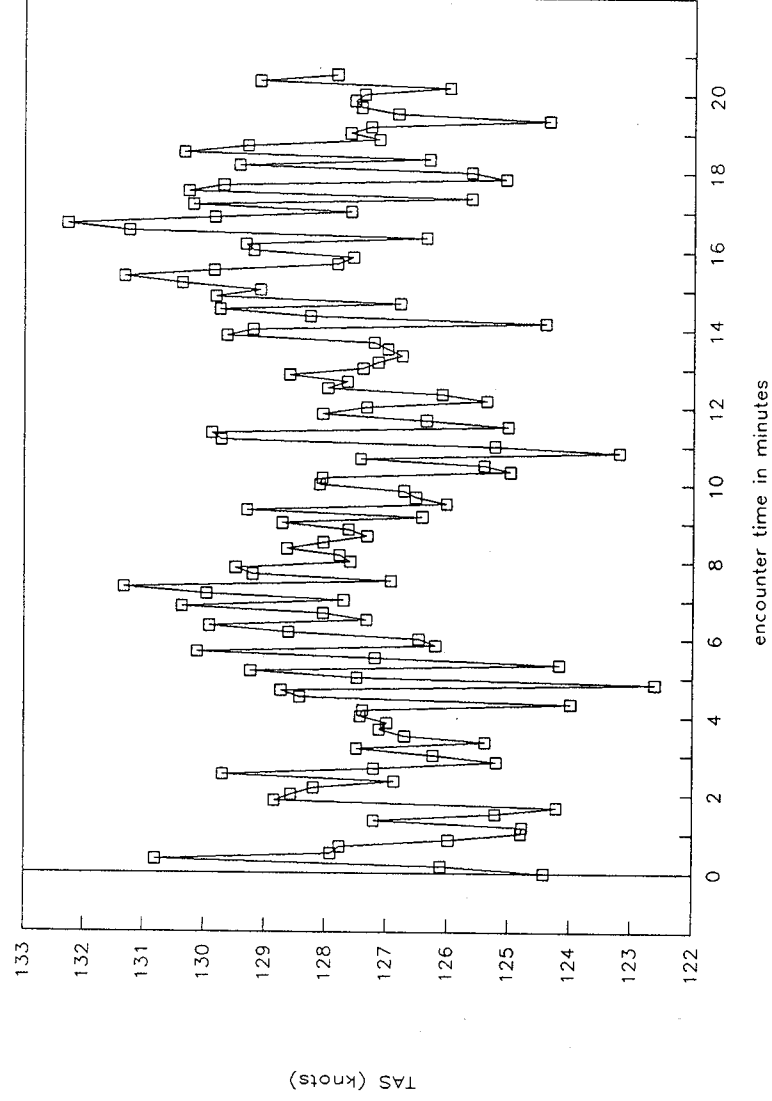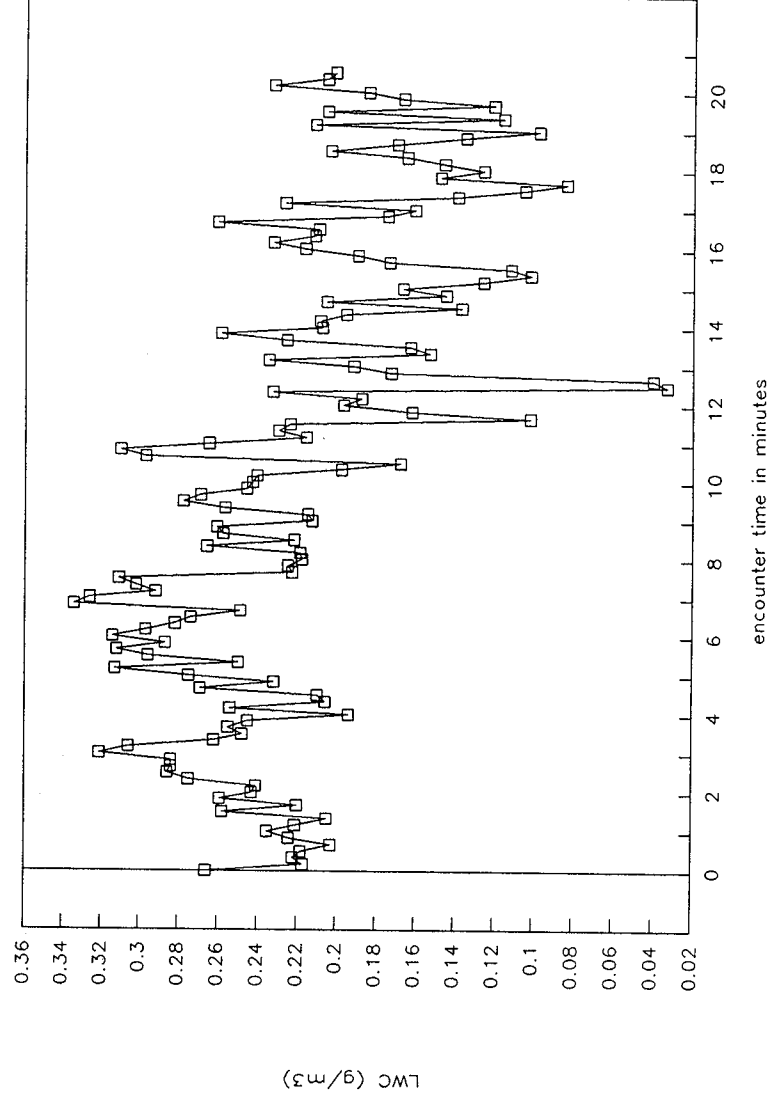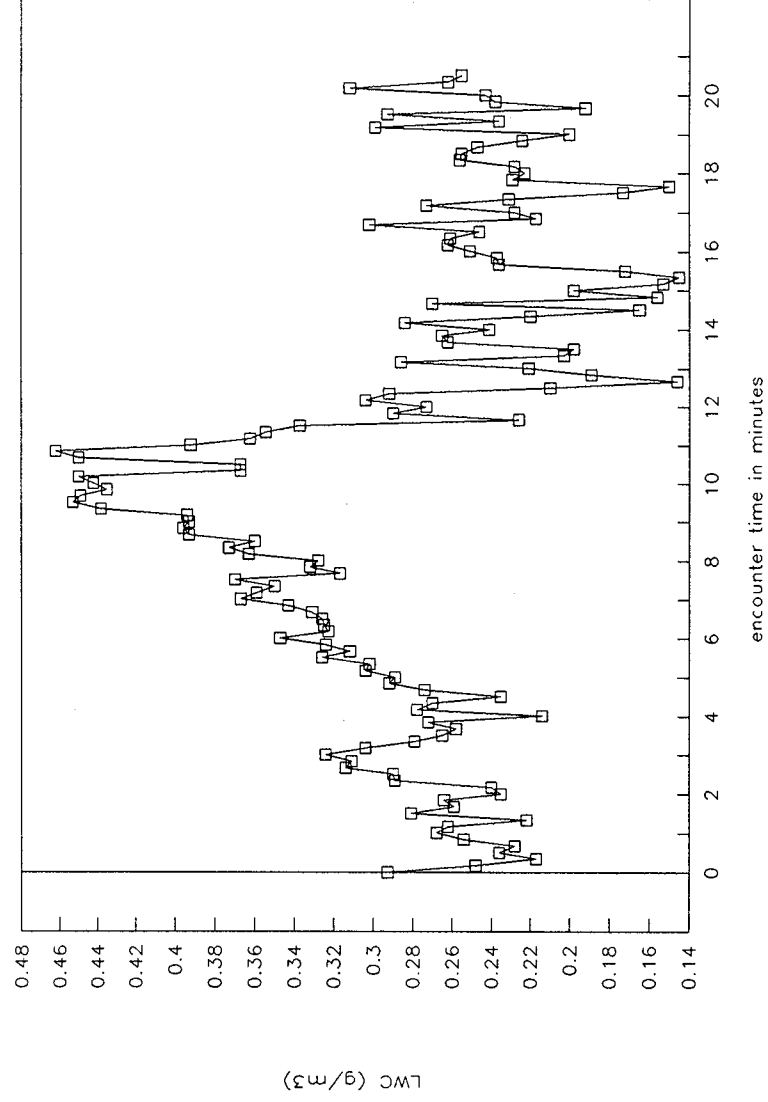
12
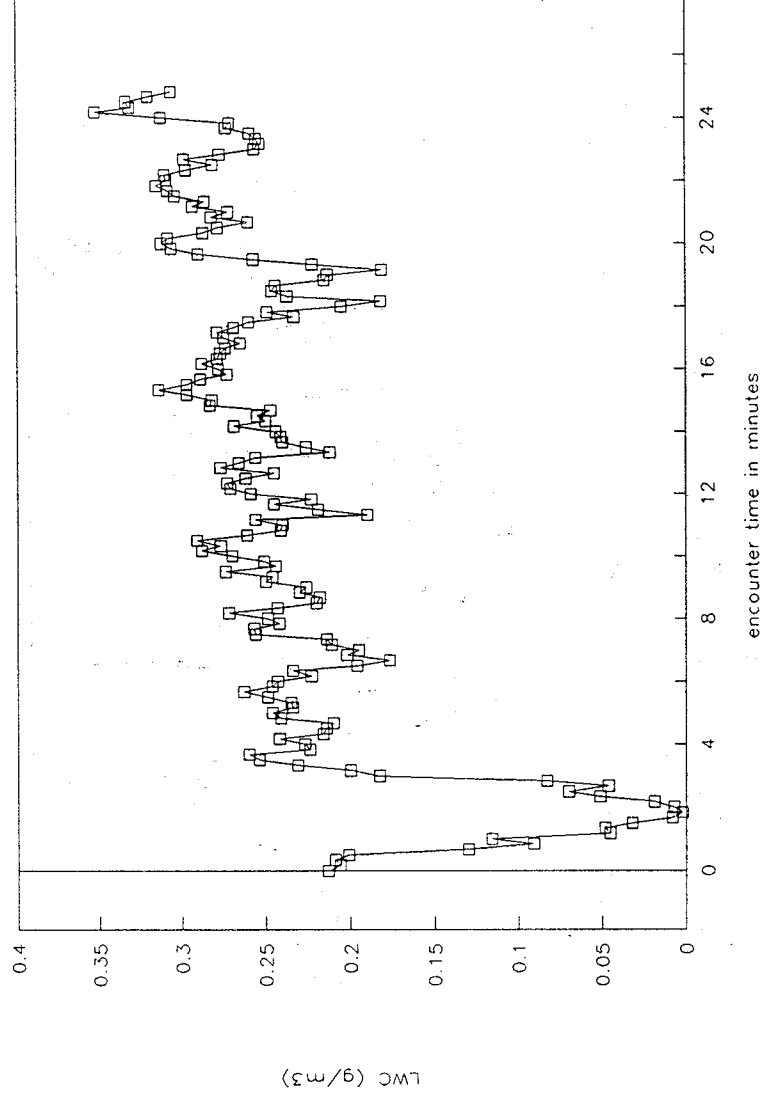
Figure 4c.—Laser probe liquid water content for flight 90-4, run 1; average = .24, standard deviation = .07.
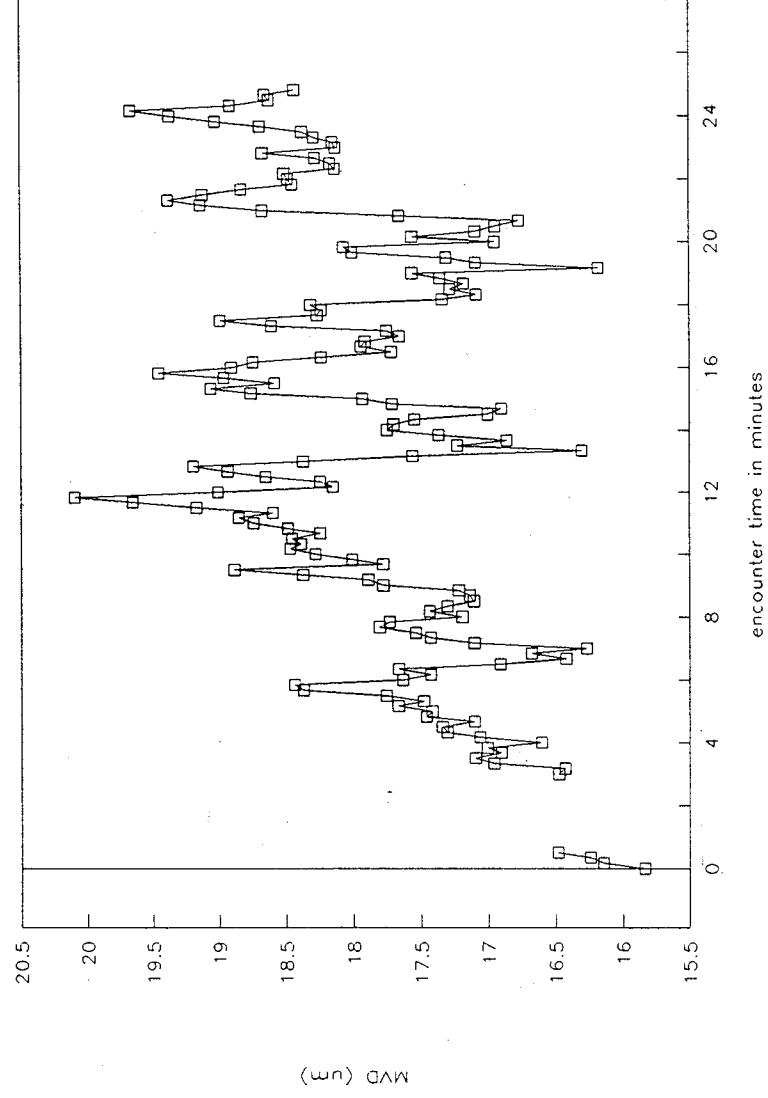
Figure 4d.—Droplet mean volume diameter for flight 90-4, run 1; average = 17.98, standard deviation = .86.

13
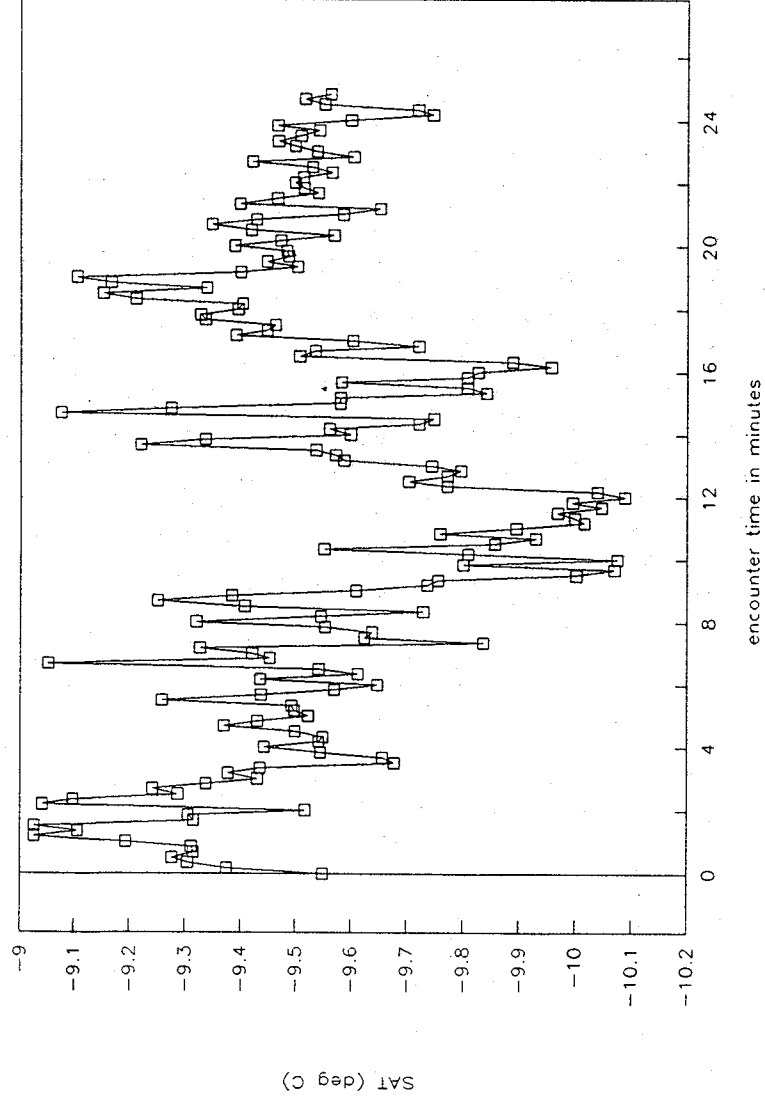
Figure 4e.—Static air temperature for flight 90-4, run 1; average = -9.53, standard deviation = .23.
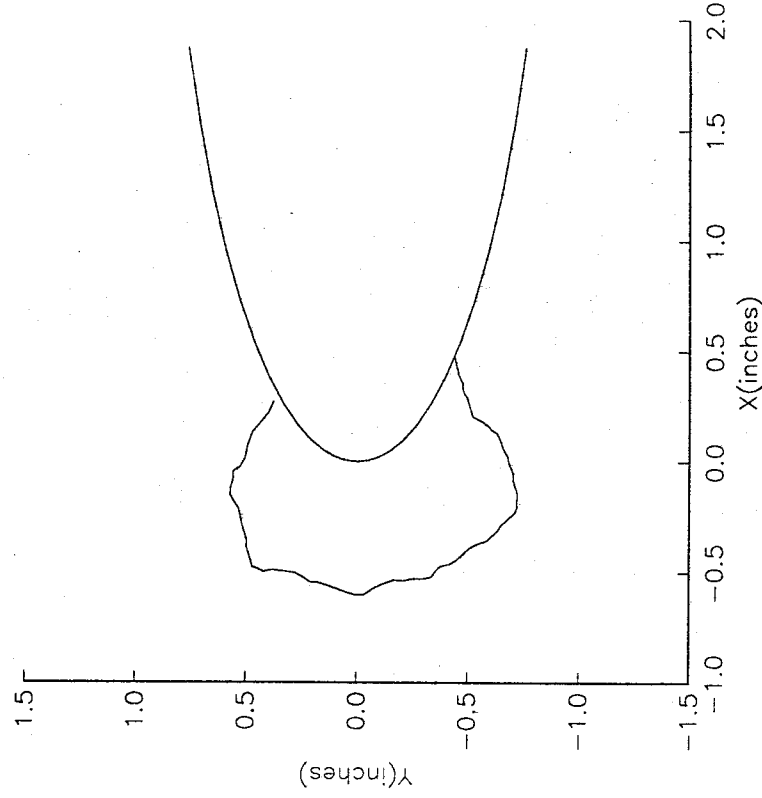
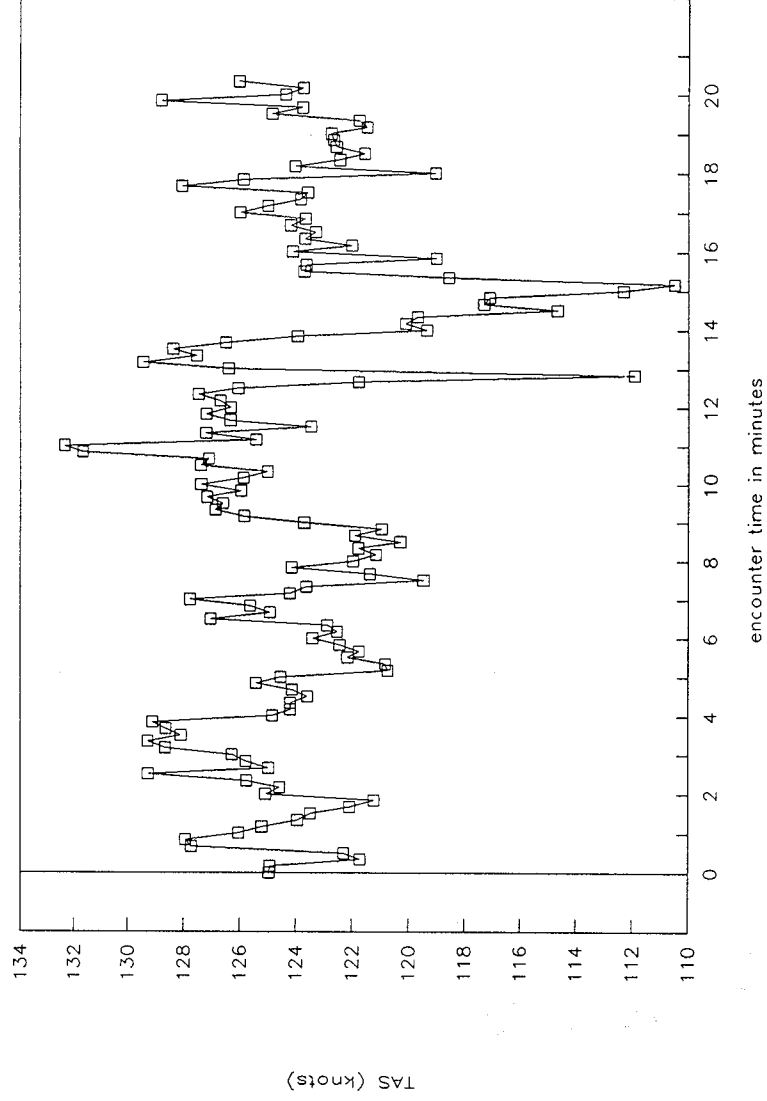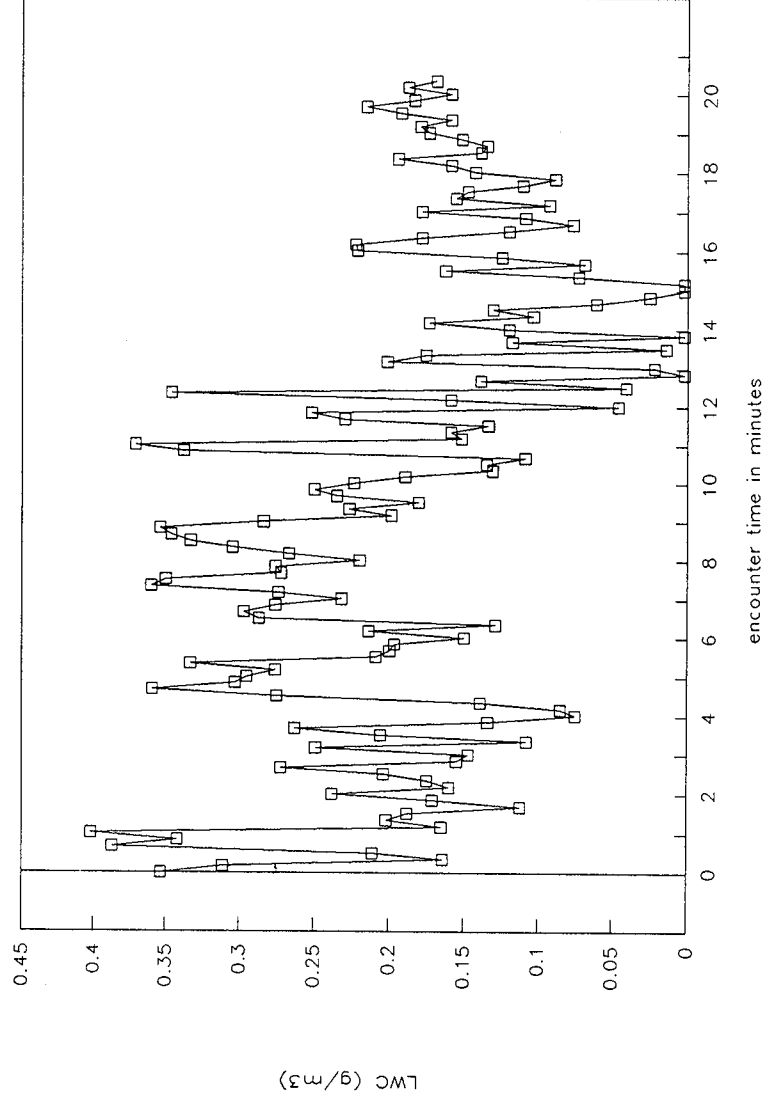Figure 4f.—Center span tracing of ice from flight 90-4, run 1.
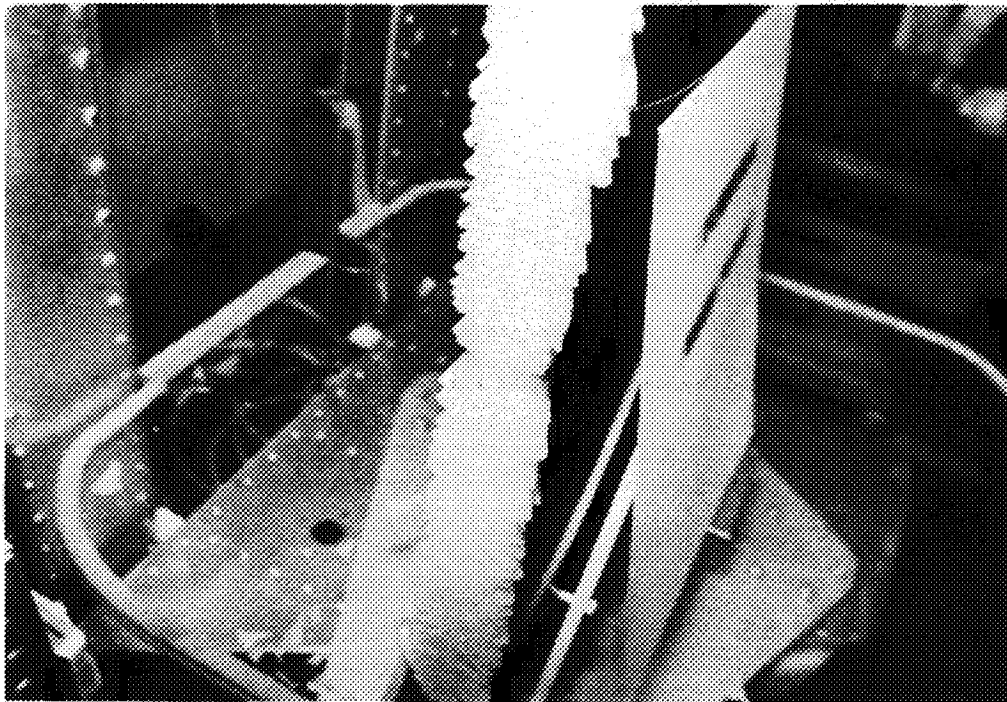
Figure 4g.—Photograph of ice from flight 90-4, run 1.
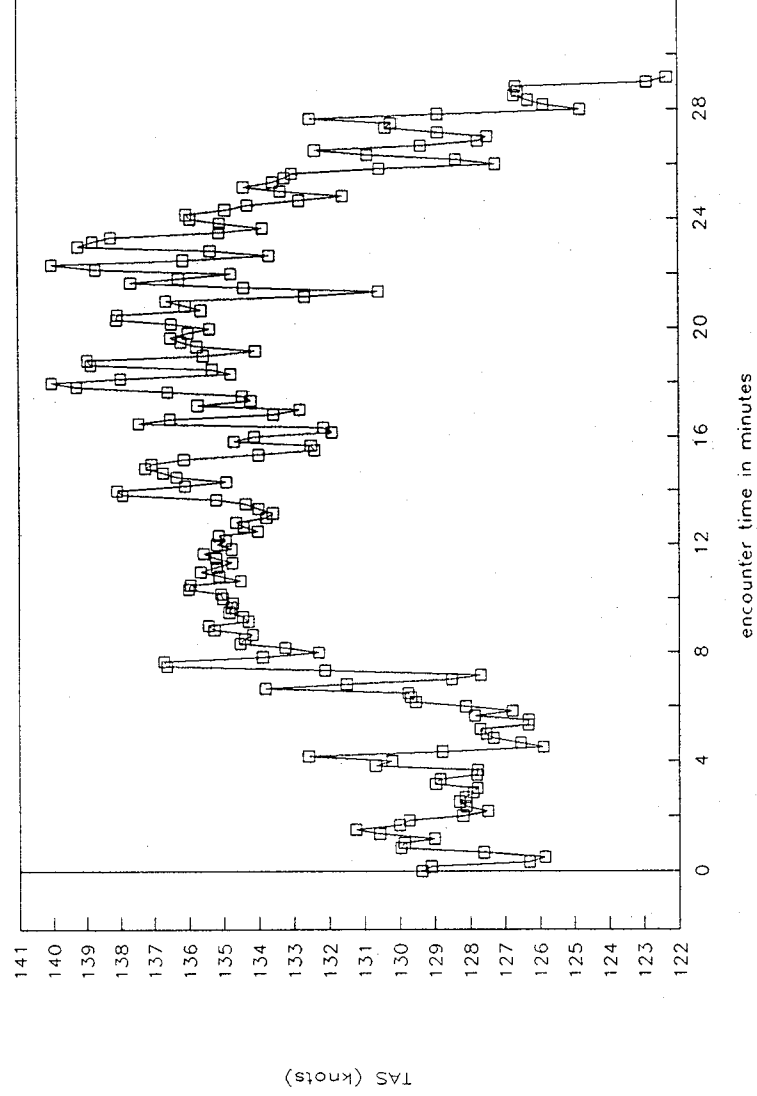
Figure 5a.—Aircraft true airspeed (in knots) for flight 90-4, run 2; average 132.7, standard deviation = 3.8.
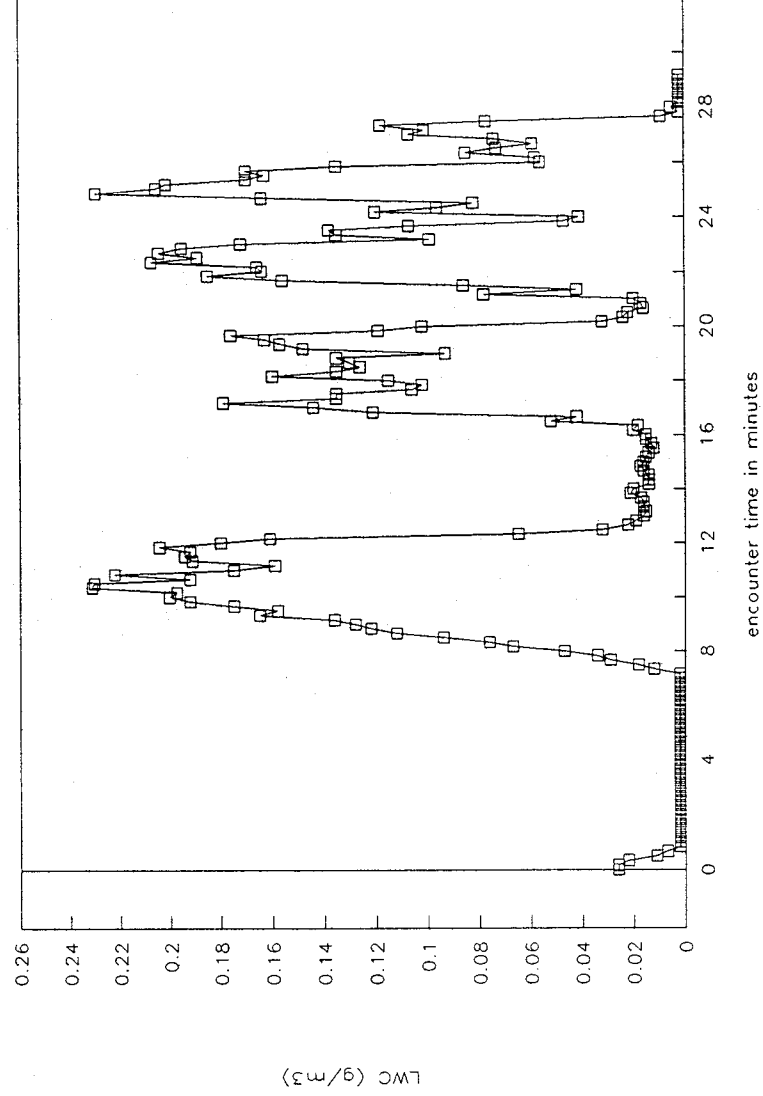
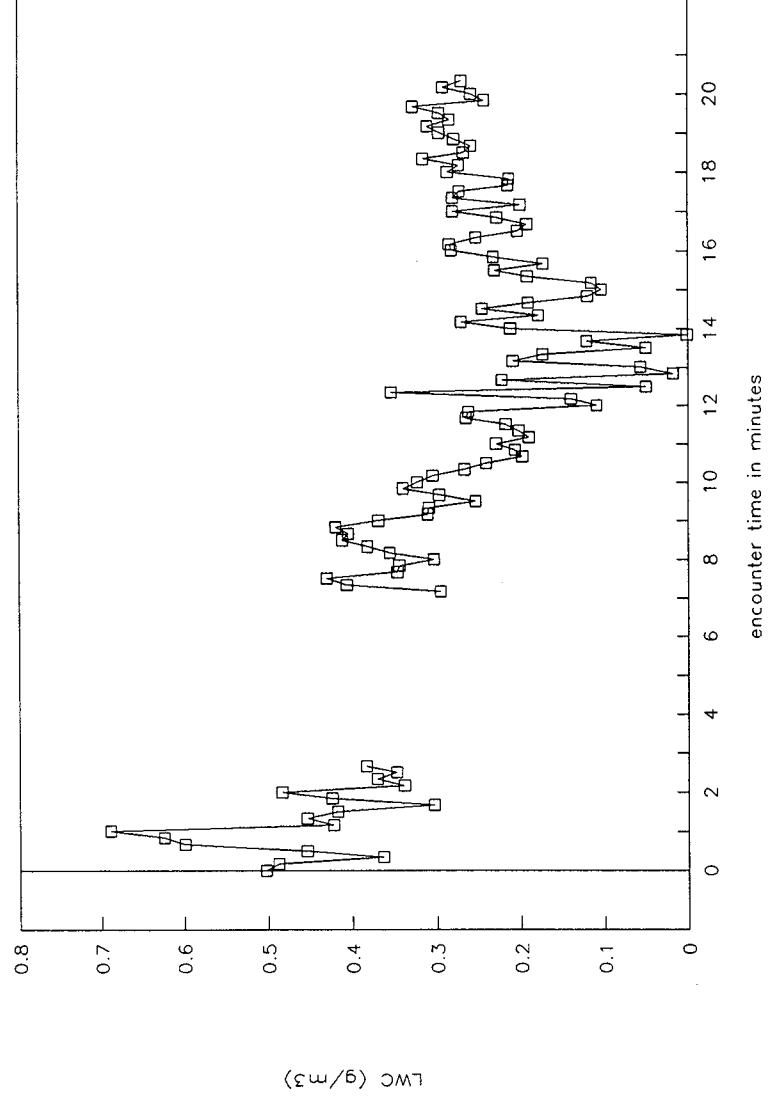Figure 5b.—Johnson-Williams liquid water content for flight 90-4, run 2; average = .07, standard deviation = .07.

16
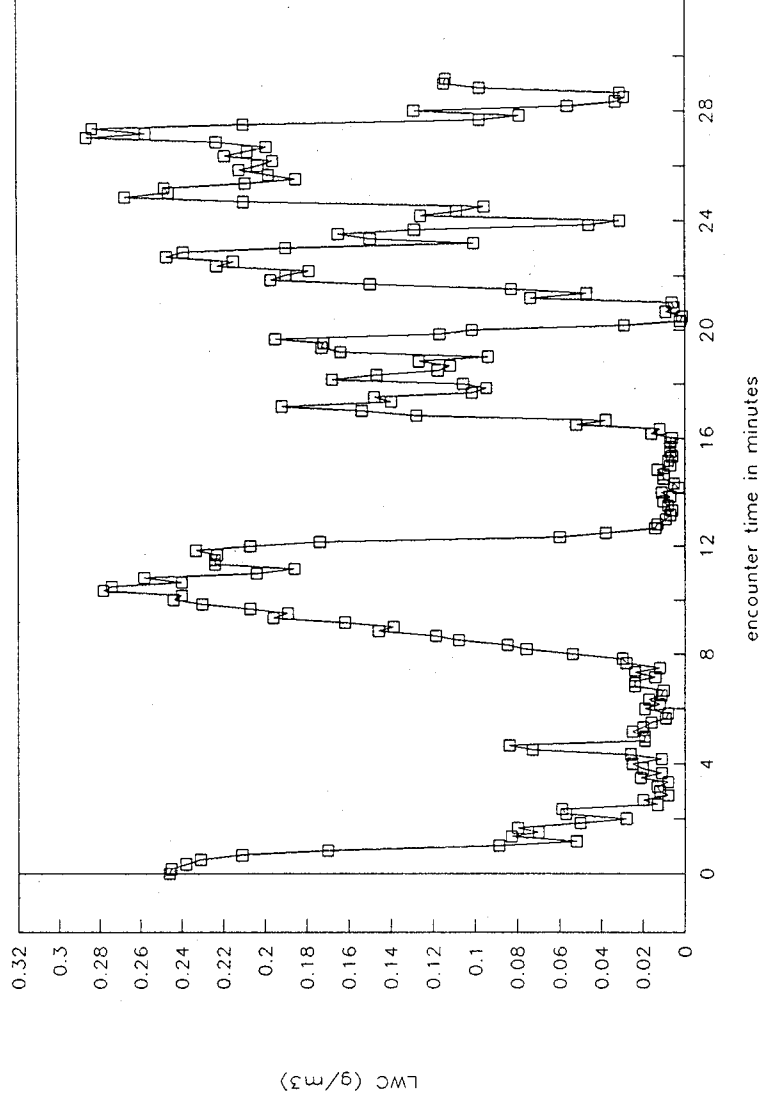
Figure 5c.—Laser probe liquid water content for flight 90-4, run 2; average = .11, standard deviation = .09.
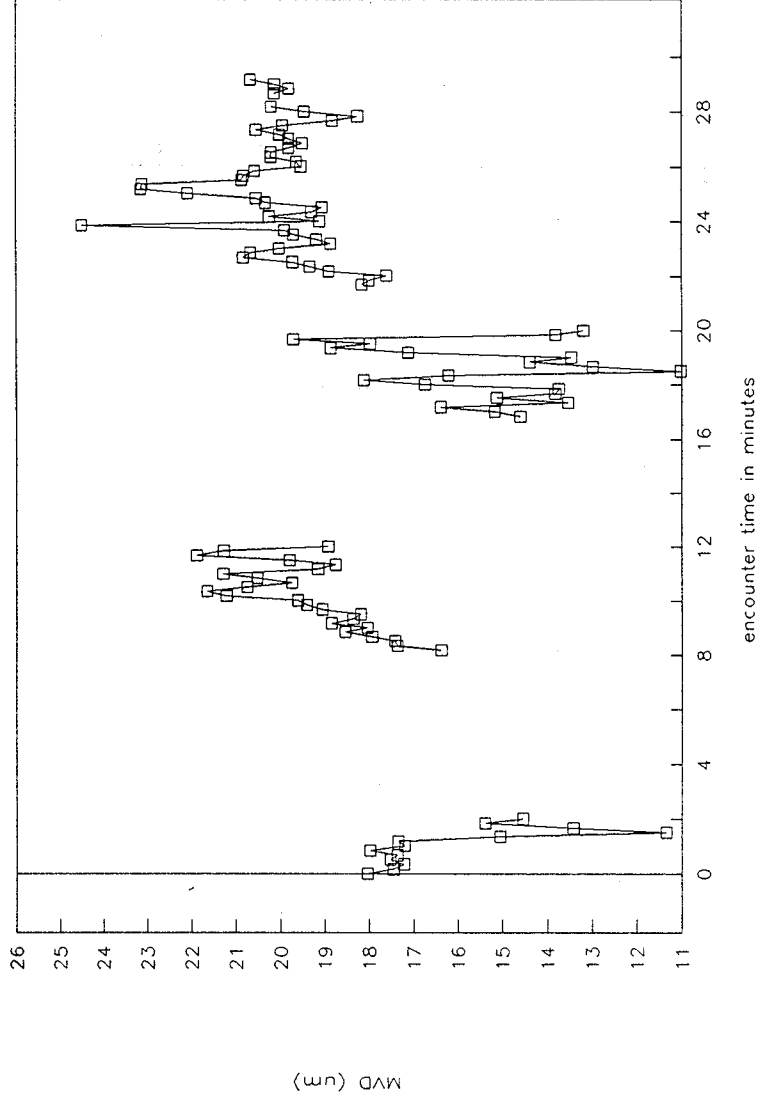
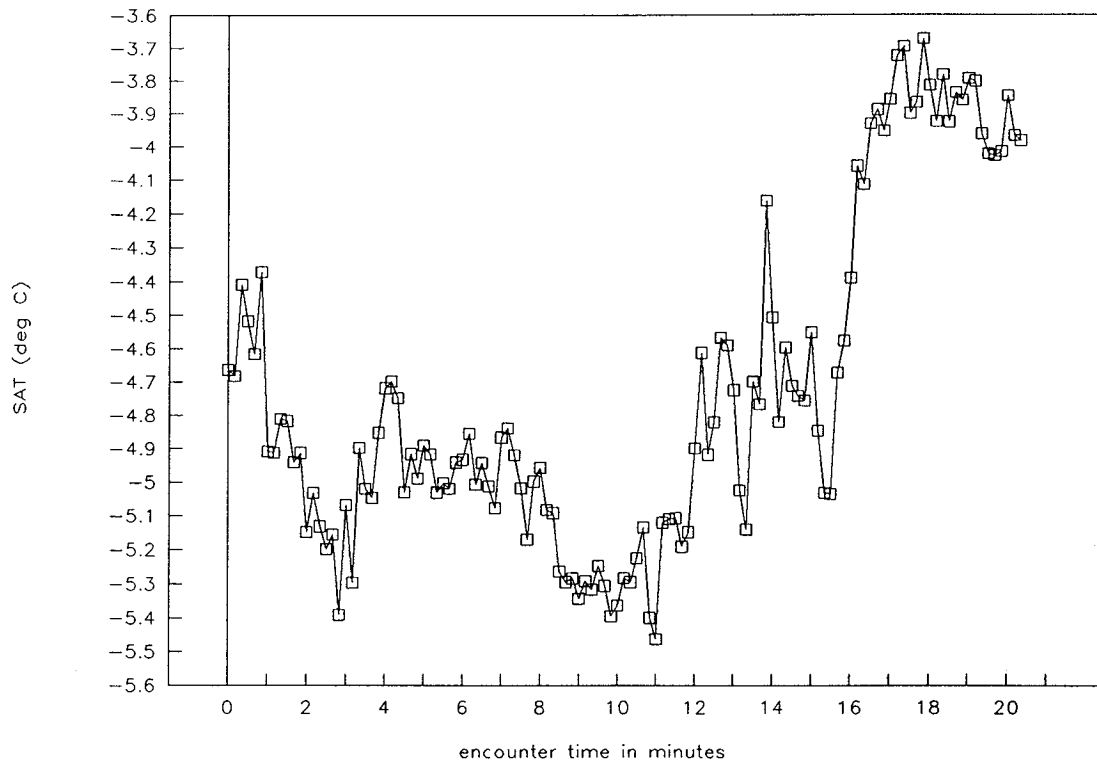Figure 5d.—Droplet mean volume diameter for flight 90-4, run 2; average = 18.4, standard deviation = 2.6.

17
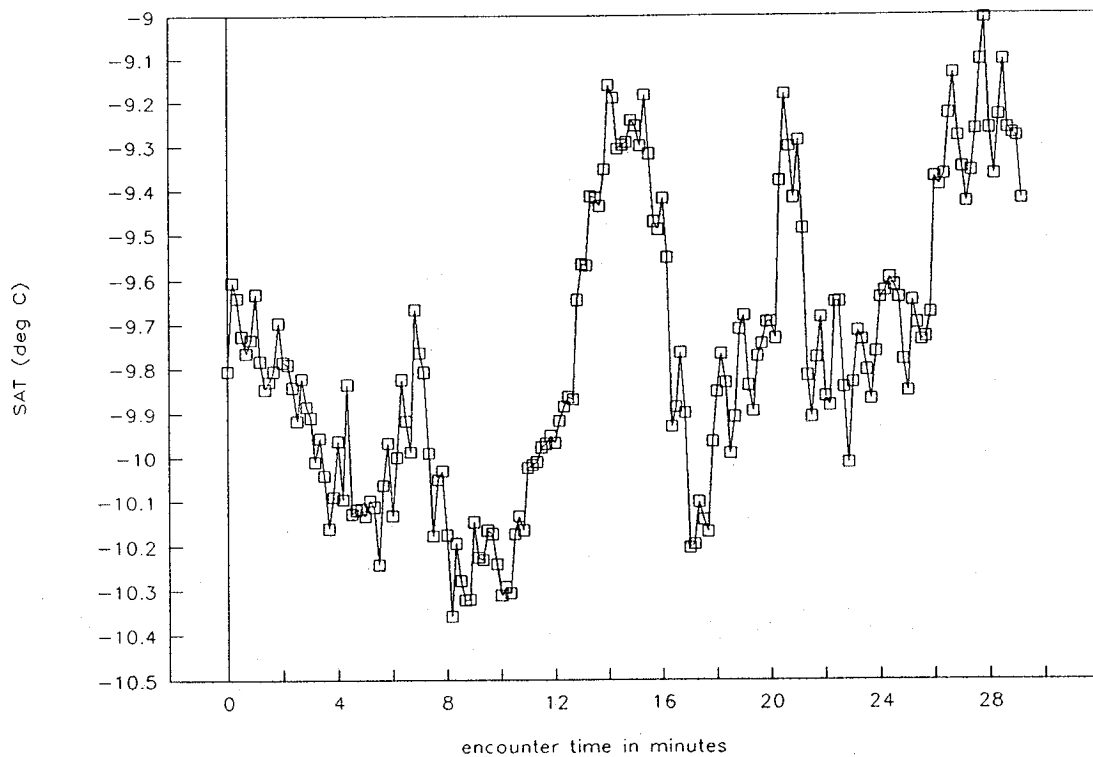
Figure 5e.—Static air temperature for flight 90-4, run 2; average = –9.77, standard deviation = .32.
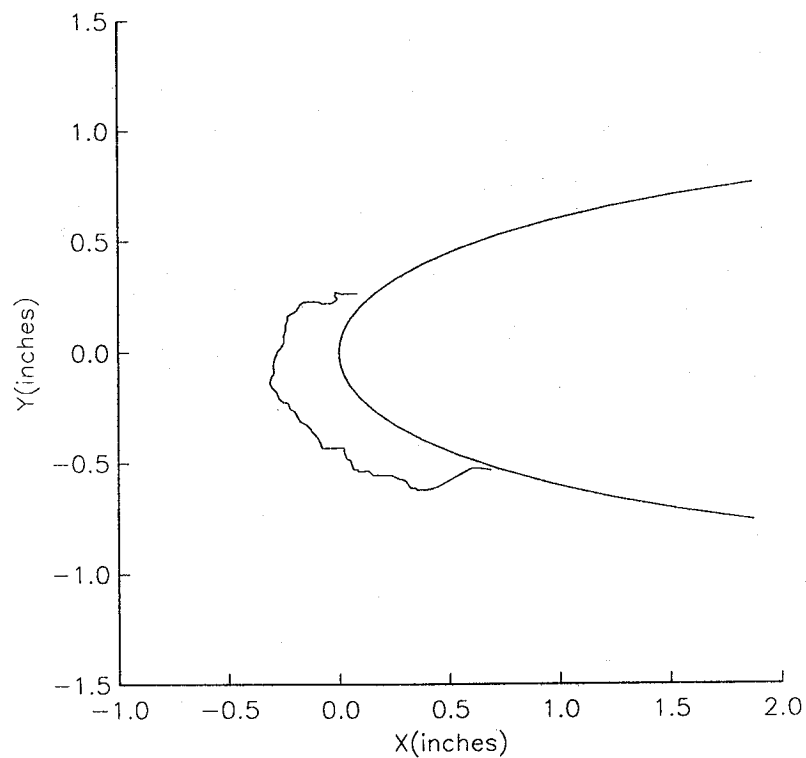
Figure 5f.—Center span tracing of ice from flight 90-4, run 2.

18
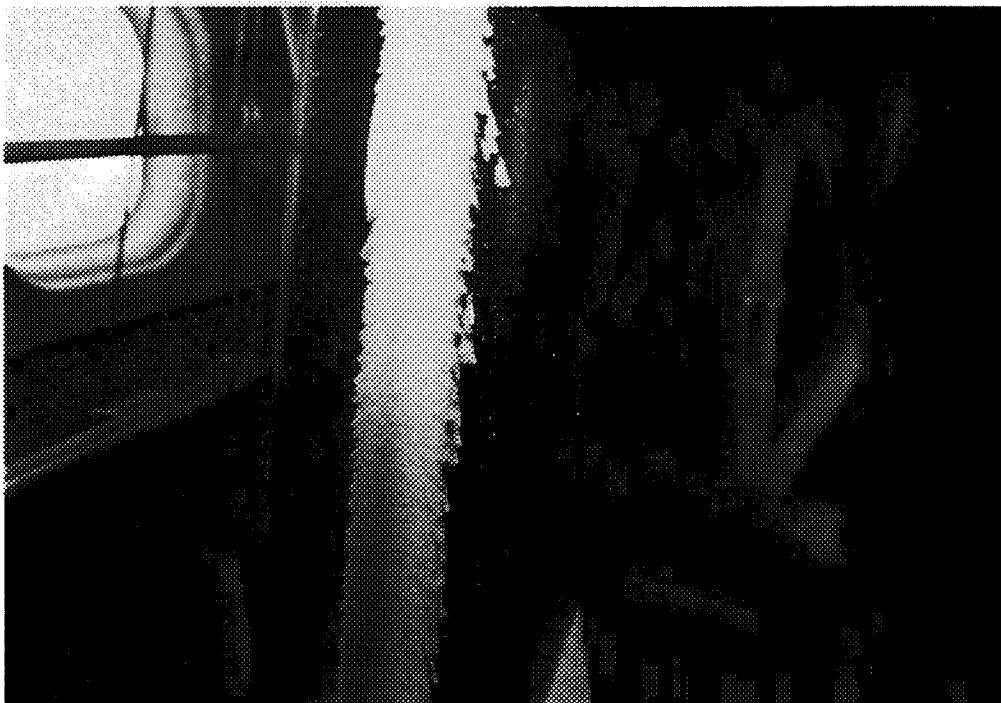
Figure 5g.—Photograph of ice from flight 90-4, run 2.
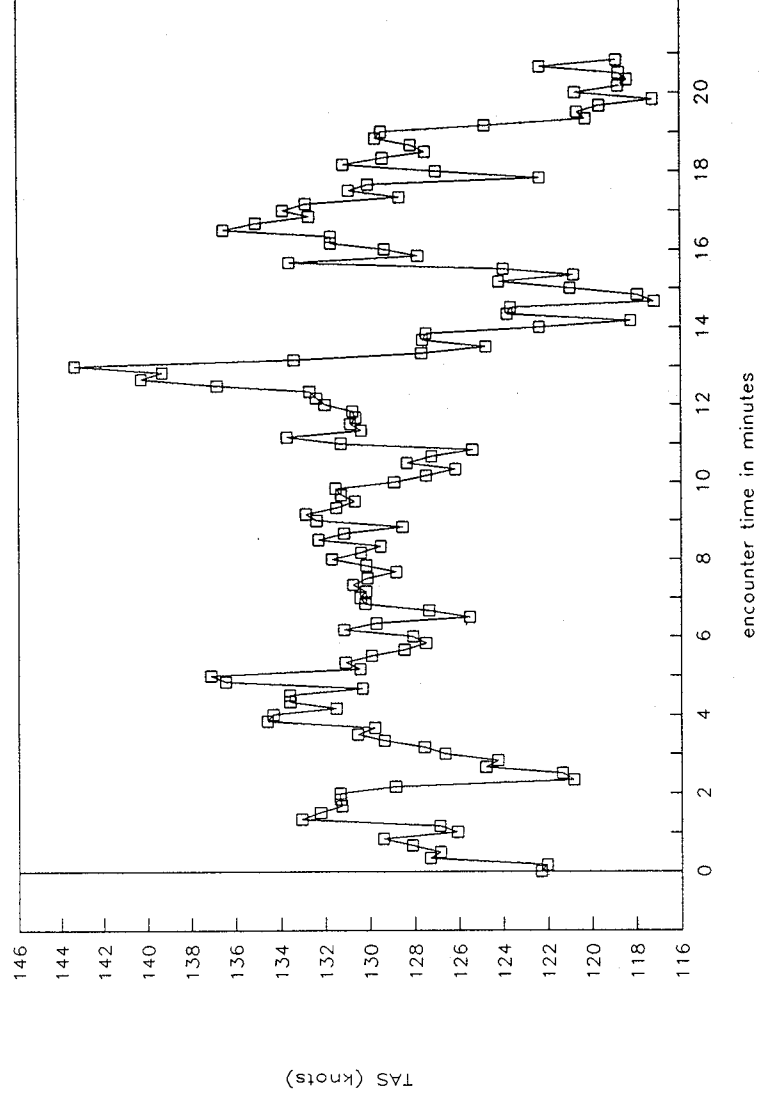
Figure 6a.—Aircraft true airspeed (in knots) for flight 90-5, run 1; average 128.6, standard deviation = 5.0.
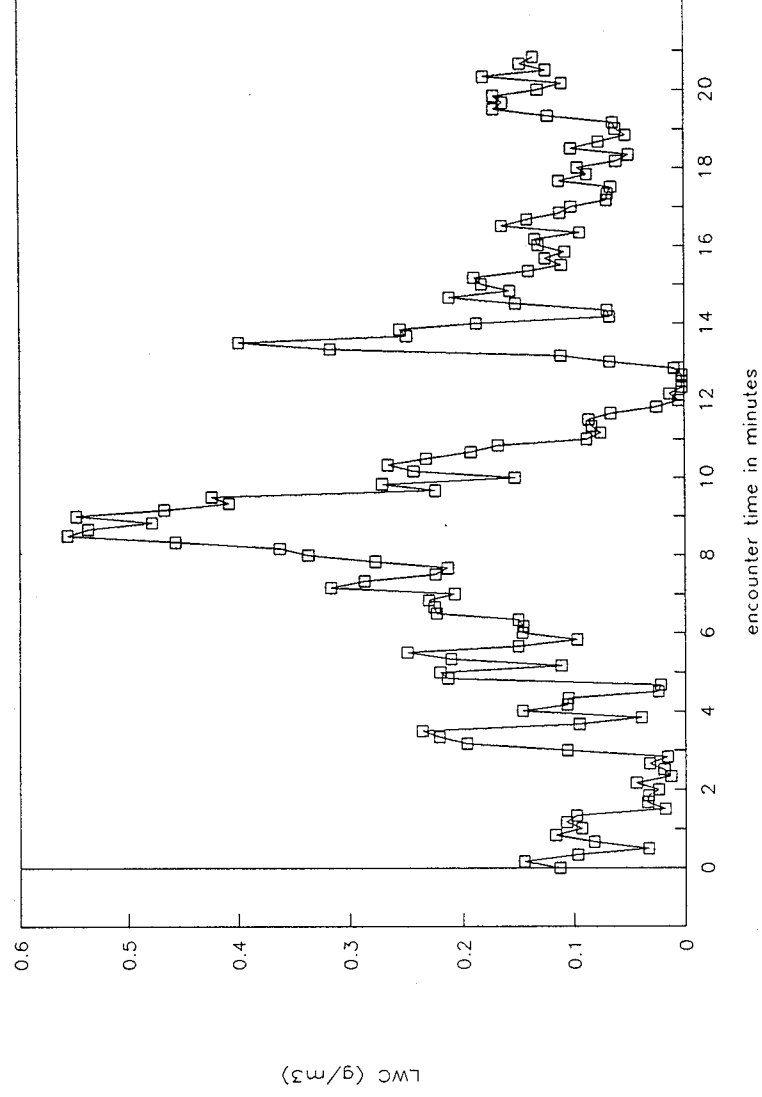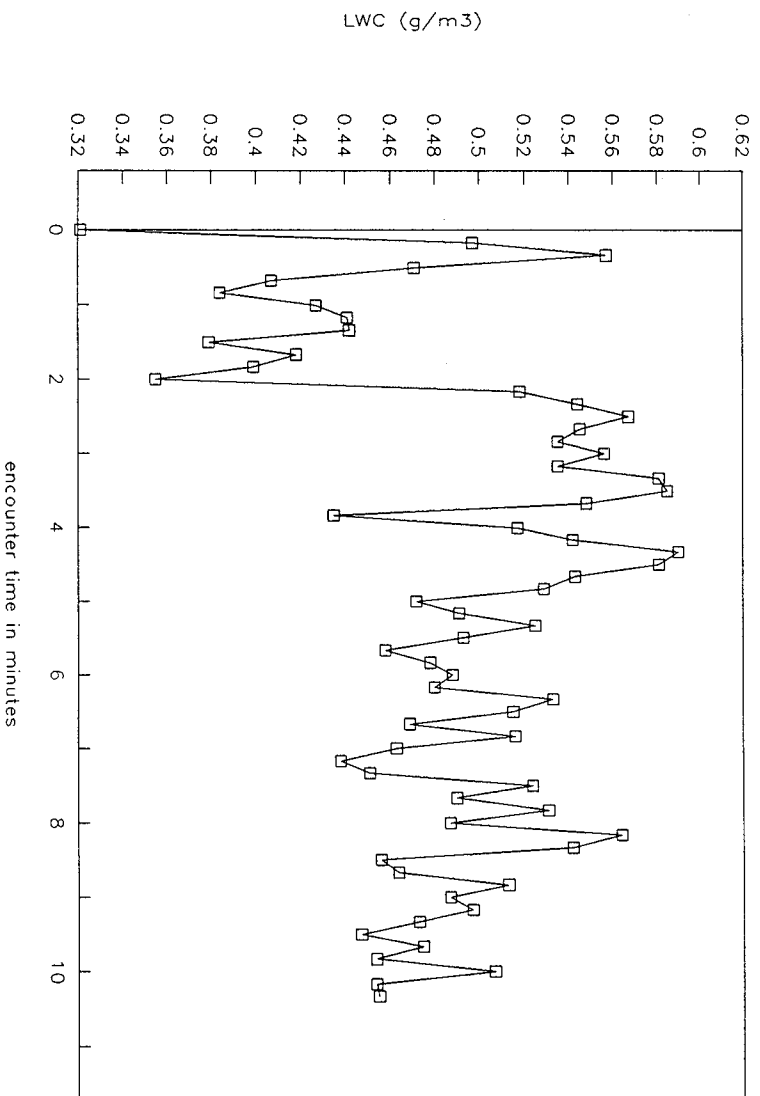

Figure 6b.—Johnson-Williams liquid water content for flight 90-5, run 1; average = .15, standard deviation = .12.
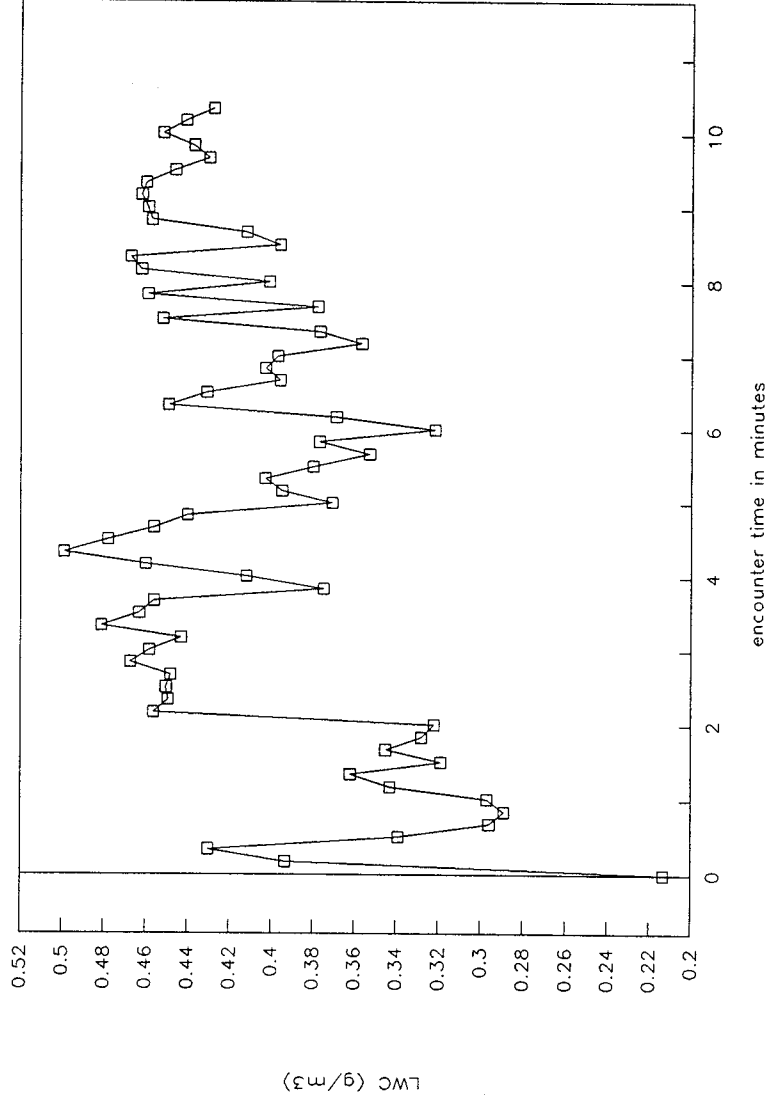
20
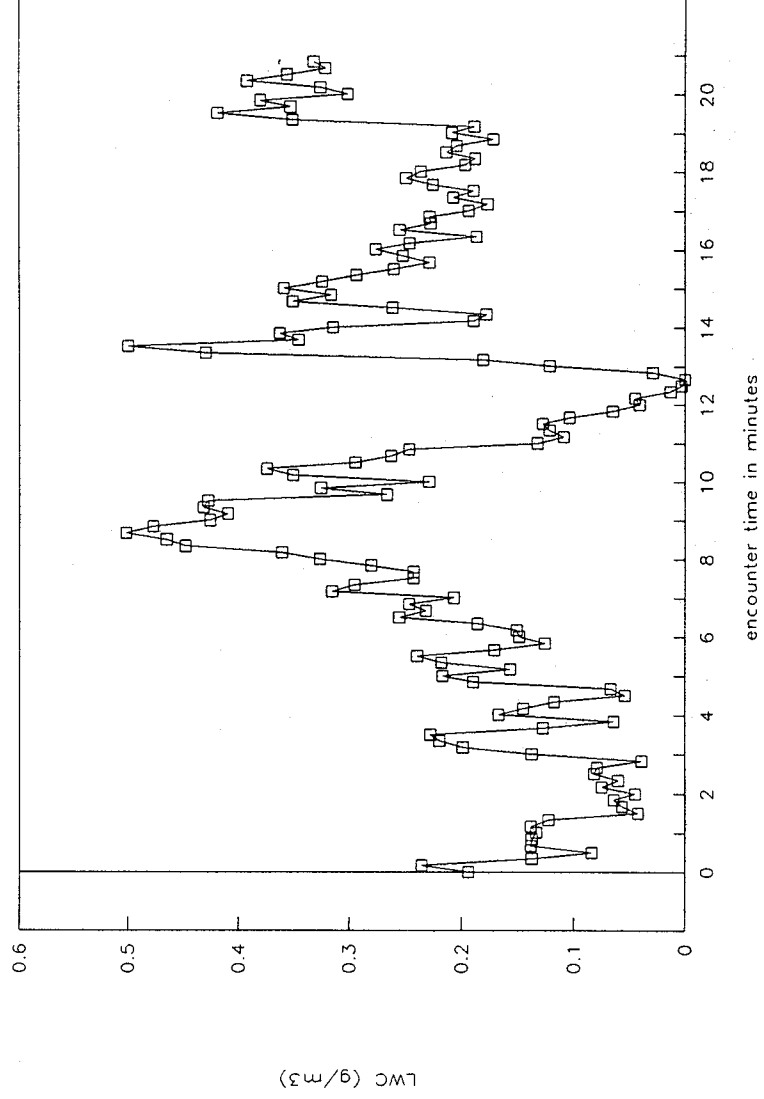
Figure 6c.—Laser probe liquid water content for flight 90-5, run 1; average = .22, standard deviation = .12.
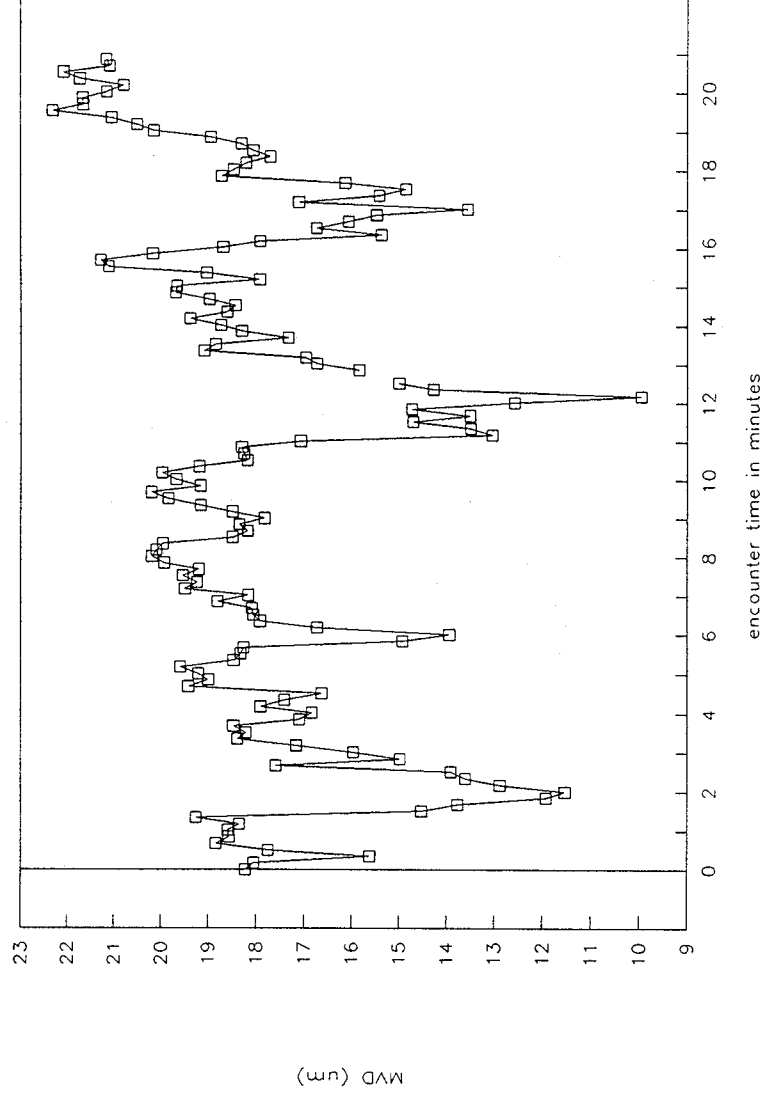
Figure 6d.—Droplet mean volume diameter for flight 90-5, run 1; average = 17.8, standard deviation = 2.4.

21

SAT (deg C)
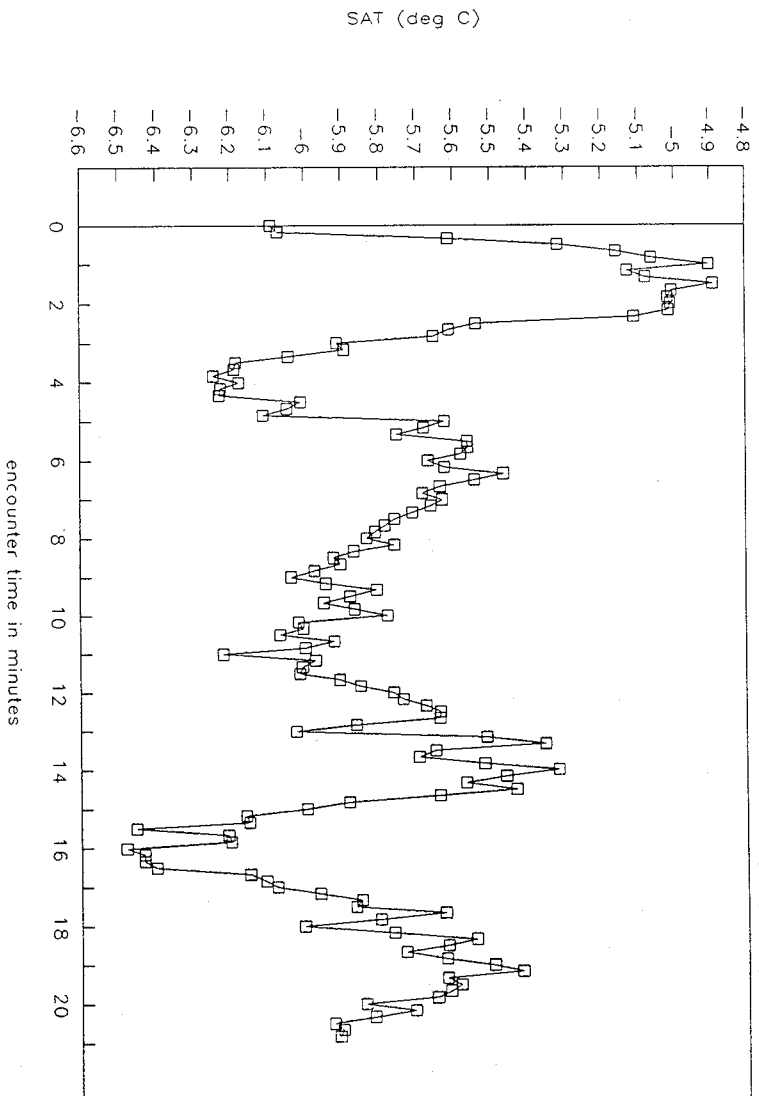
Figure 6e.—Static air temperature for flight 90-5, run 1; average = -5.77, standard deviation = .34.
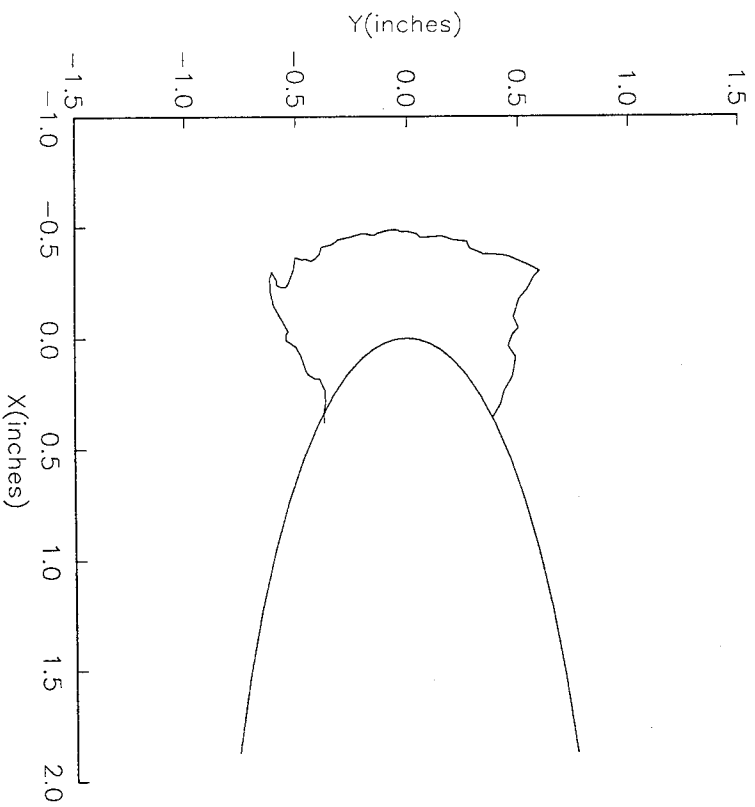
Figure 6f.—Center span tracing of ice from flight 90-5, run 1.
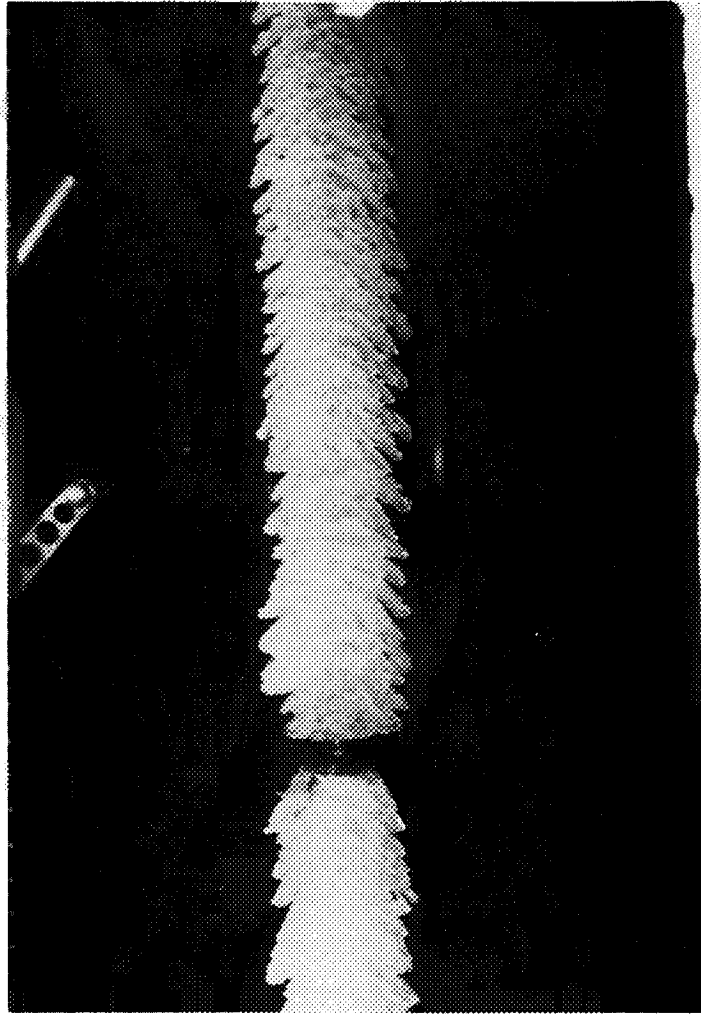
Figure 6g.—Photograph of ice from flight 90-5, run 1.
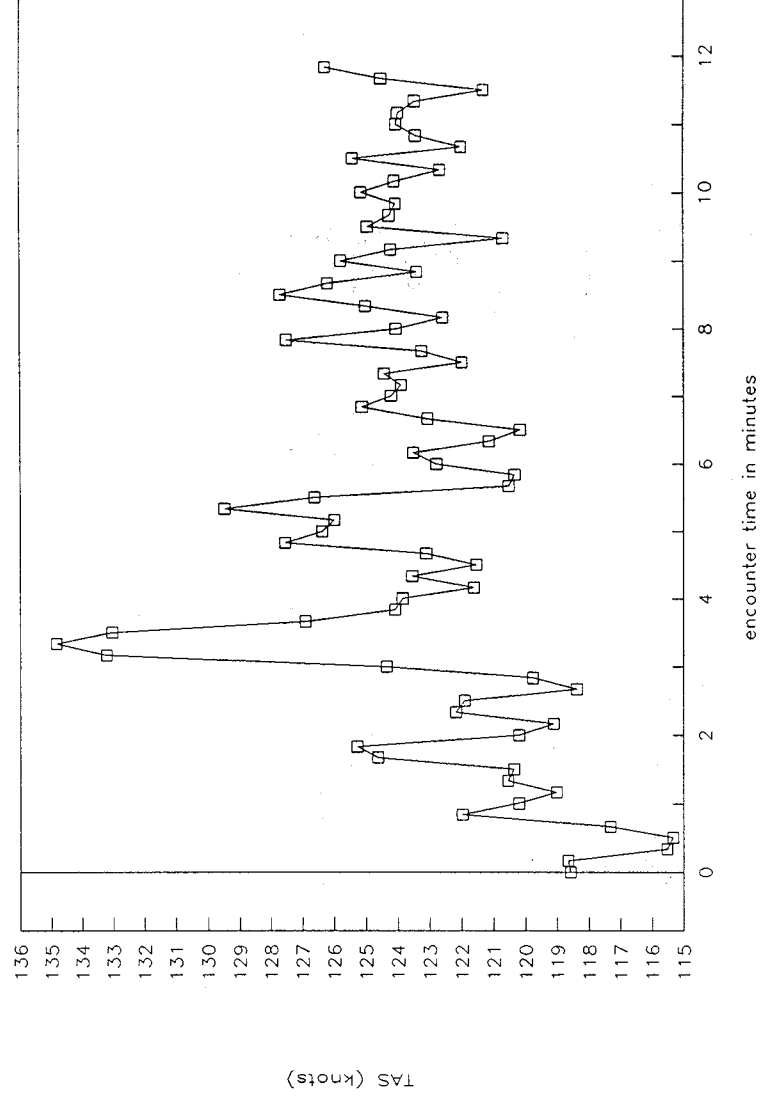
Figure 7a.—Aircraft true airspeed (in knots) for flight 90-5, run 2; average 123.4, standard deviation = 3.5.
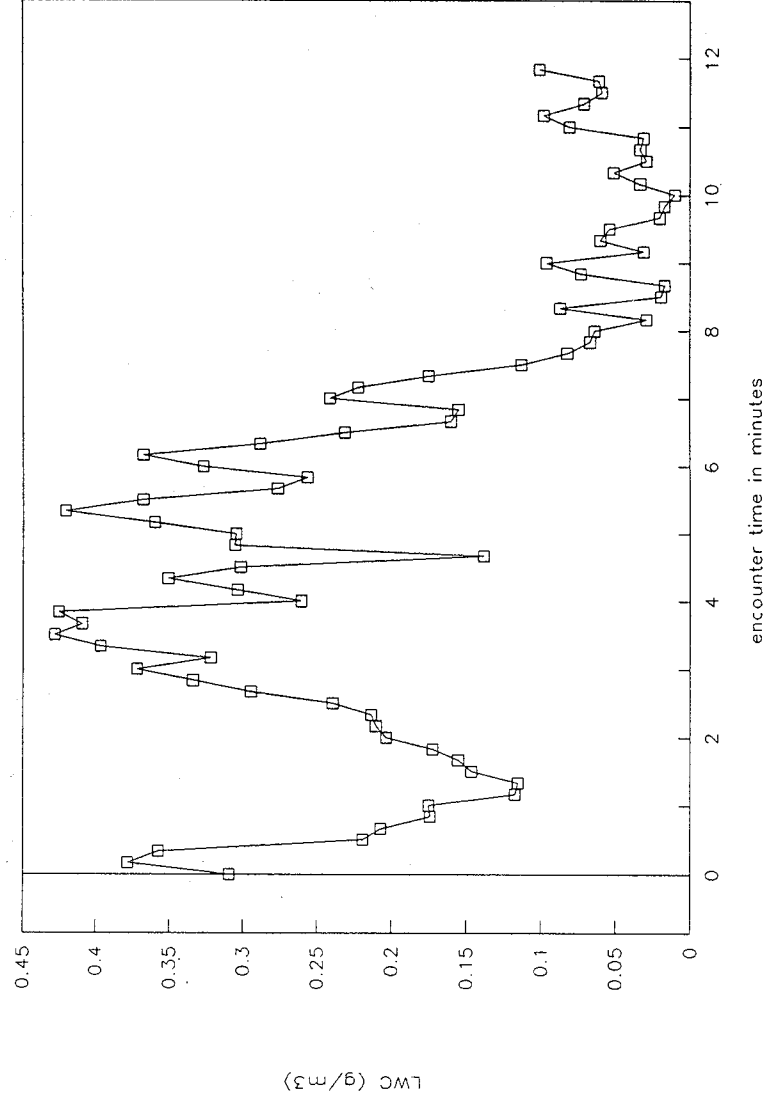
Figure 7b.—Johnson-Williams liquid water content for flight 90-5, run 2; average = .19, standard deviation = .13.
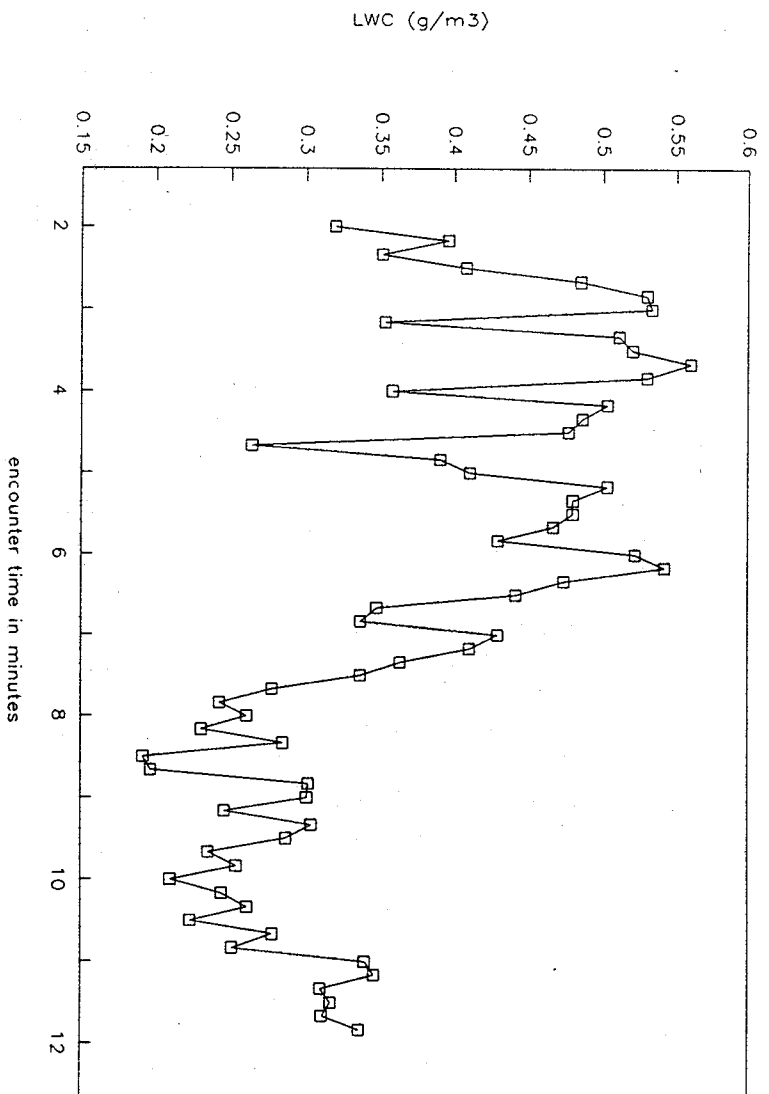
Figure 7c.—Laser probe liquid water content for flight 90-5, run 2 (minus first two minutes of data); average = .37, standard deviation = .1.
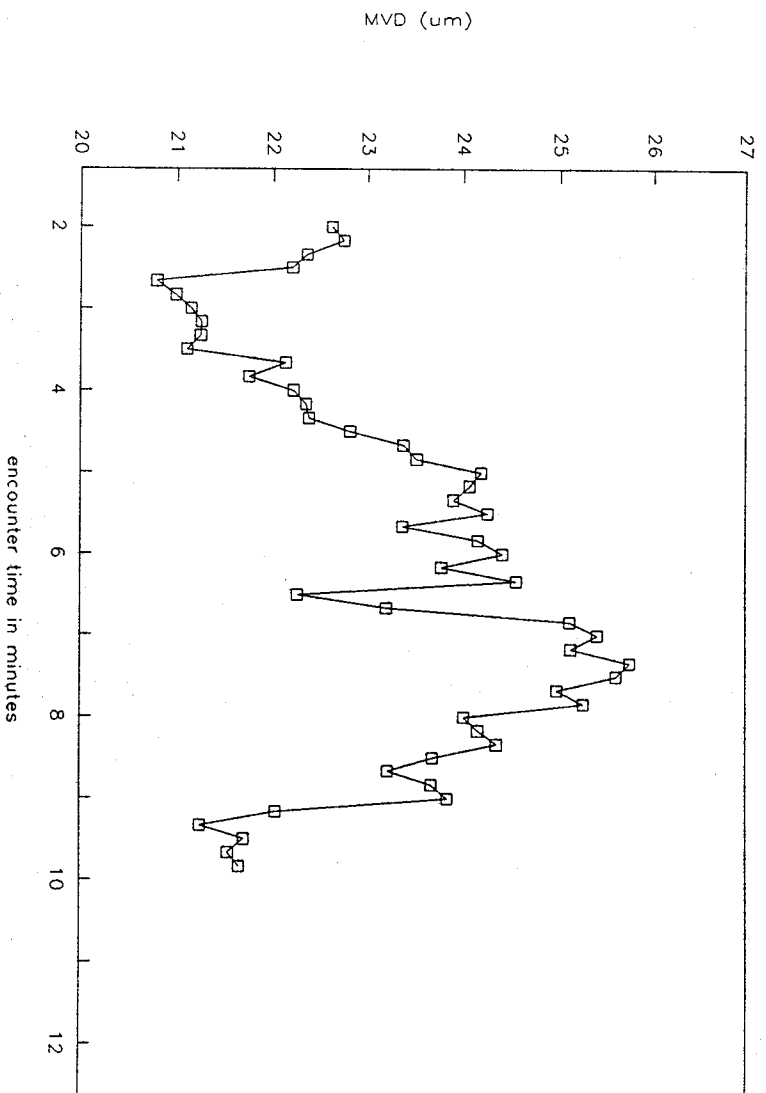
Figure 7d.—Droplet mean volume diameter for flight 90-5, run 2 (minus first two minutes of data); average = 23.5, standard deviation = 1.5.
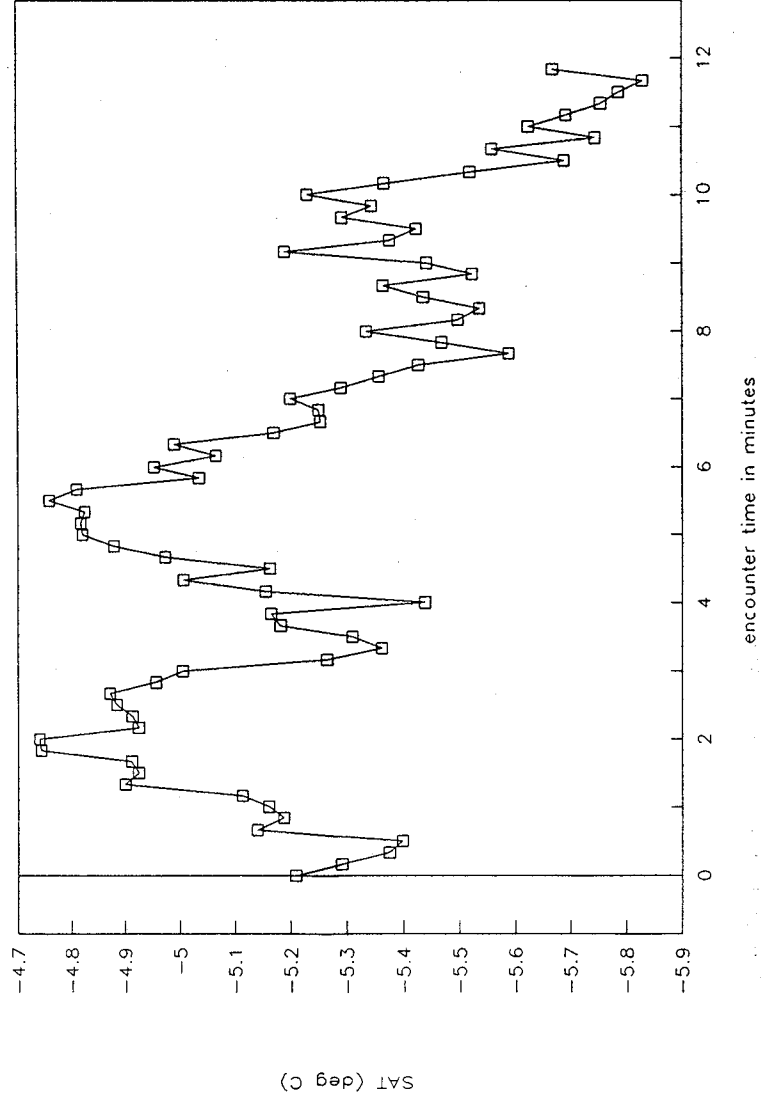
Figure 7e.—Static air temperature for flight 90-5, run 2; average = -5.23, standard deviation = .28.
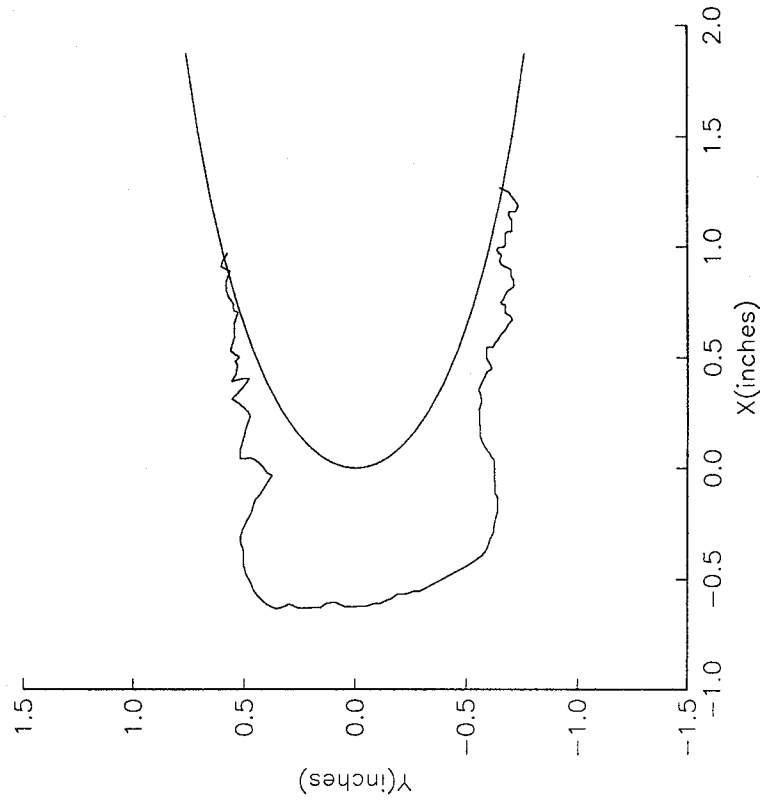
Figure 7f.—Center span tracing of ice from flight 90-5, run 2.

26

C-89-14068
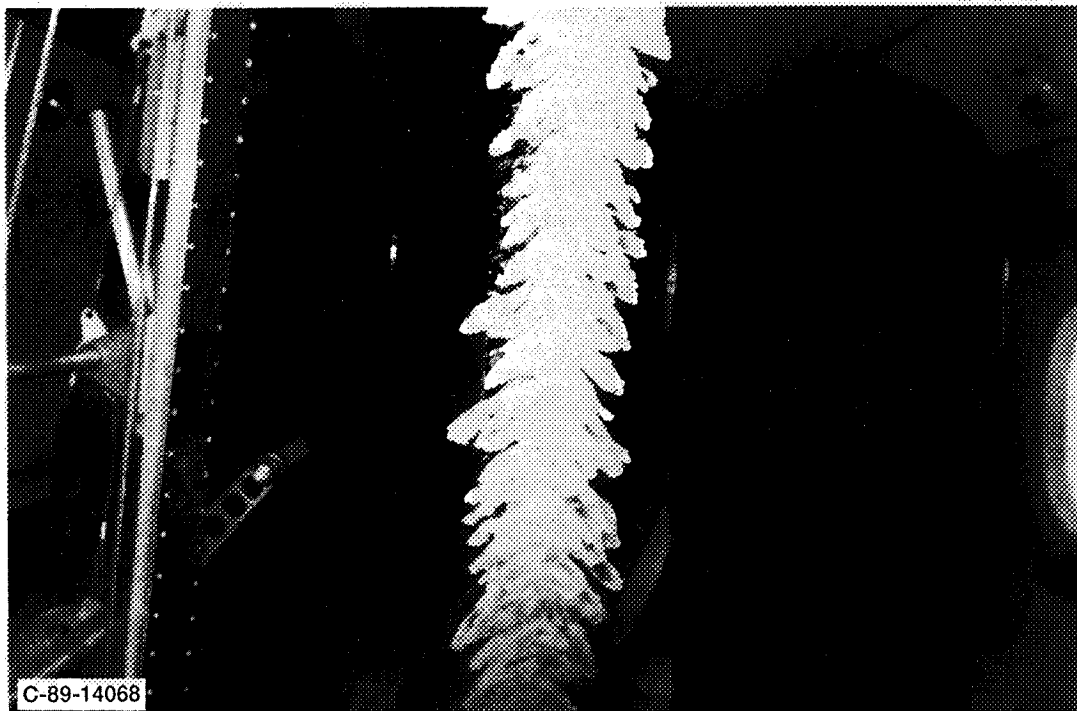
Figure 7g.—Photograph of ice from flight 90-5, run 2.

Figure 8a.—Aircraft true airspeed (in knots) for flight 90-7, run 1; average 126.0, standard deviation = 2.5.
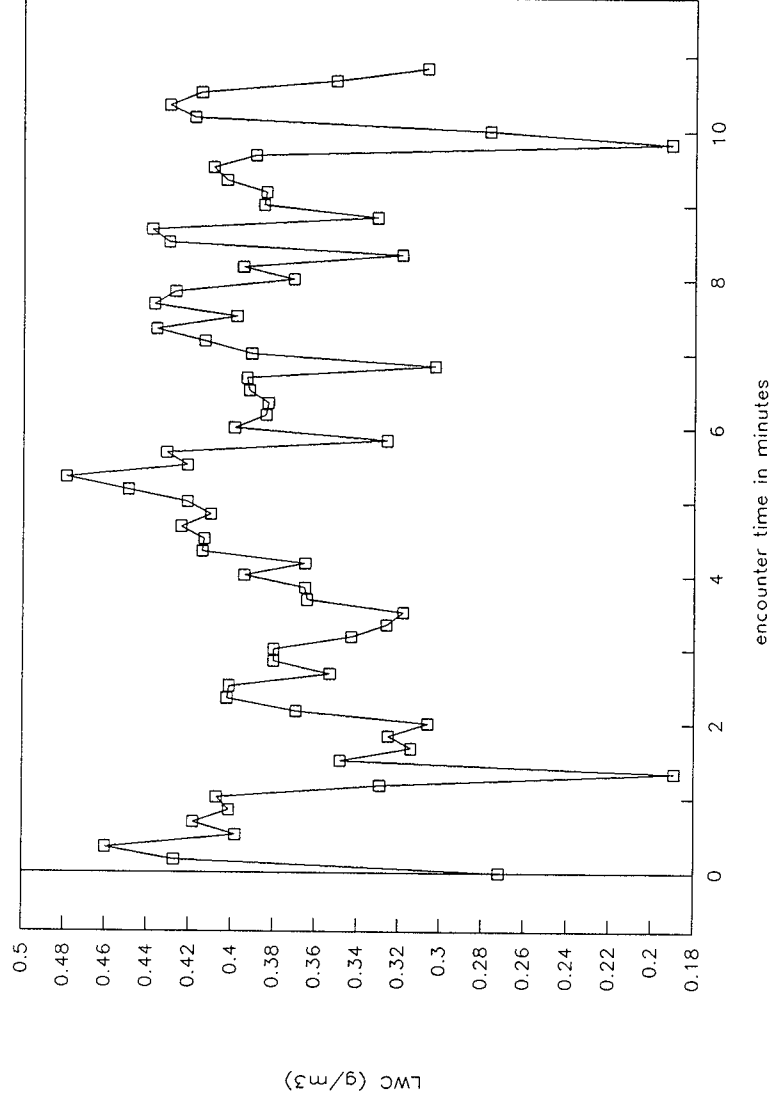

Figure 8b.—Johnson-Williams liquid water content for flight 90-7, run 1; average = .26, standard deviation = .04.

28

Figure 8c.—Laser probe liquid water content for flight 90-7, run 1; average = .30, standard deviation = .10.

Figure 8d.—Droplet mean volume diameter for flight 90-7, run 1; average = 15.14, standard deviation = 4.15.
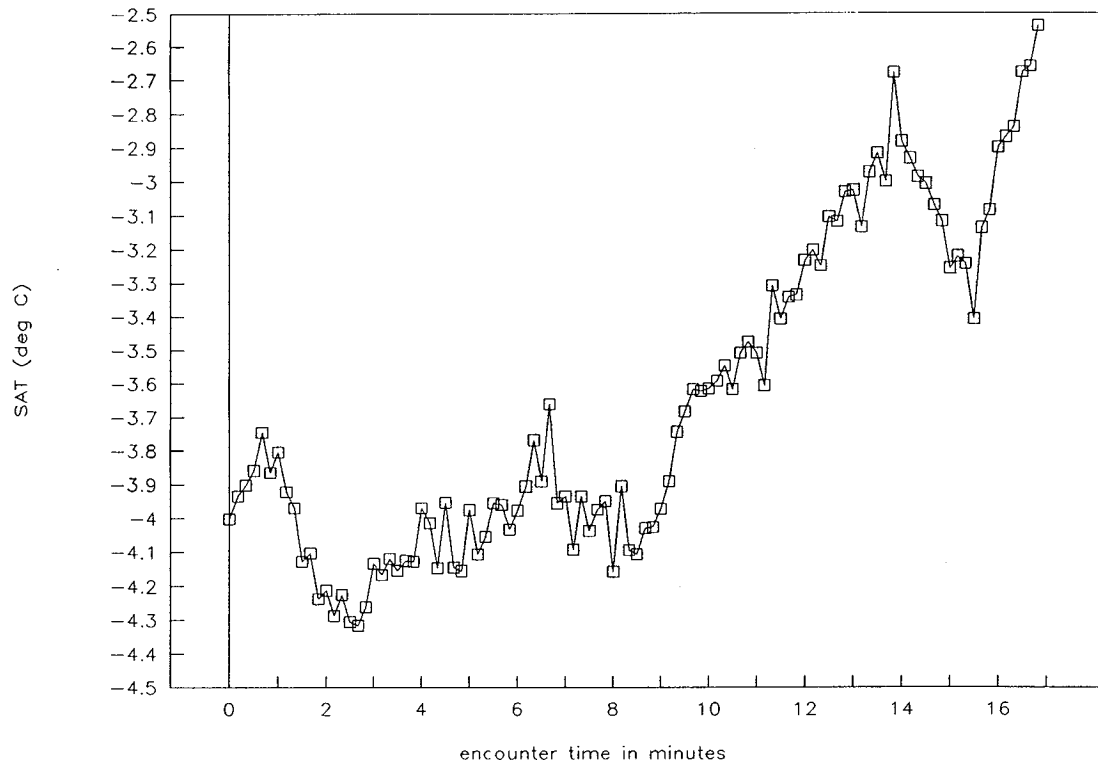
Figure 8e.—Static air temperature for flight 90-7, run 1; average = –3.65, standard deviation = .47.
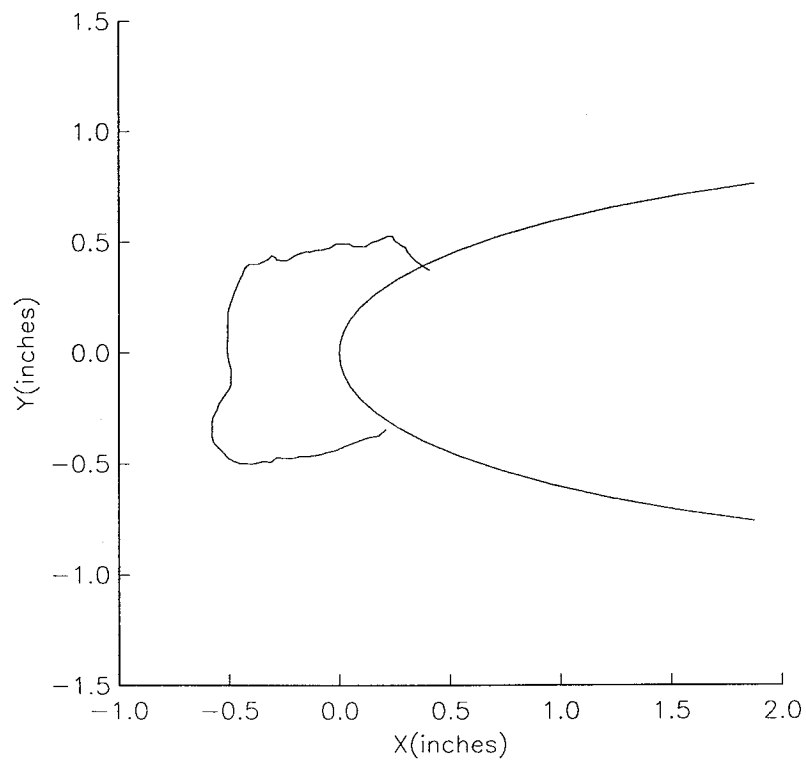
Figure 8f.—Center span tracing of ice from flight 90-7, run 1.

30
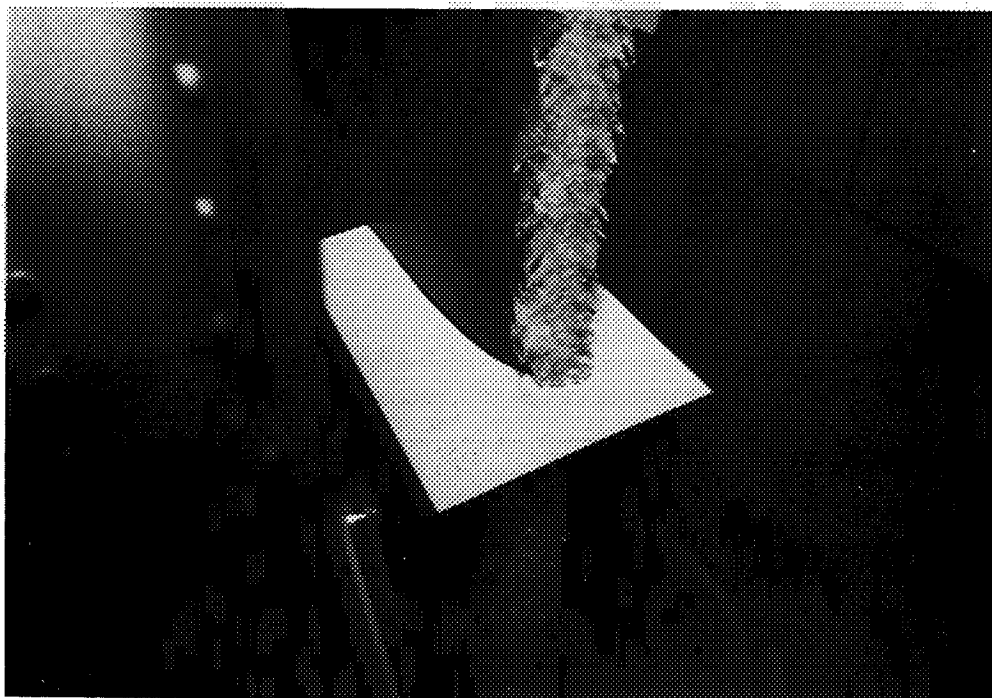
Figure 8g.—Photograph of ice from flight 90-7, run 1.

Figure 9a.—Aircraft true airspeed (in knots) for flight 90-7, run 2; average 127.6, standard deviation = 1.9.

Figure 9b.—Johnson-Williams liquid water content for flight 90-7, run 2; average = .22, standard deviation = .06.
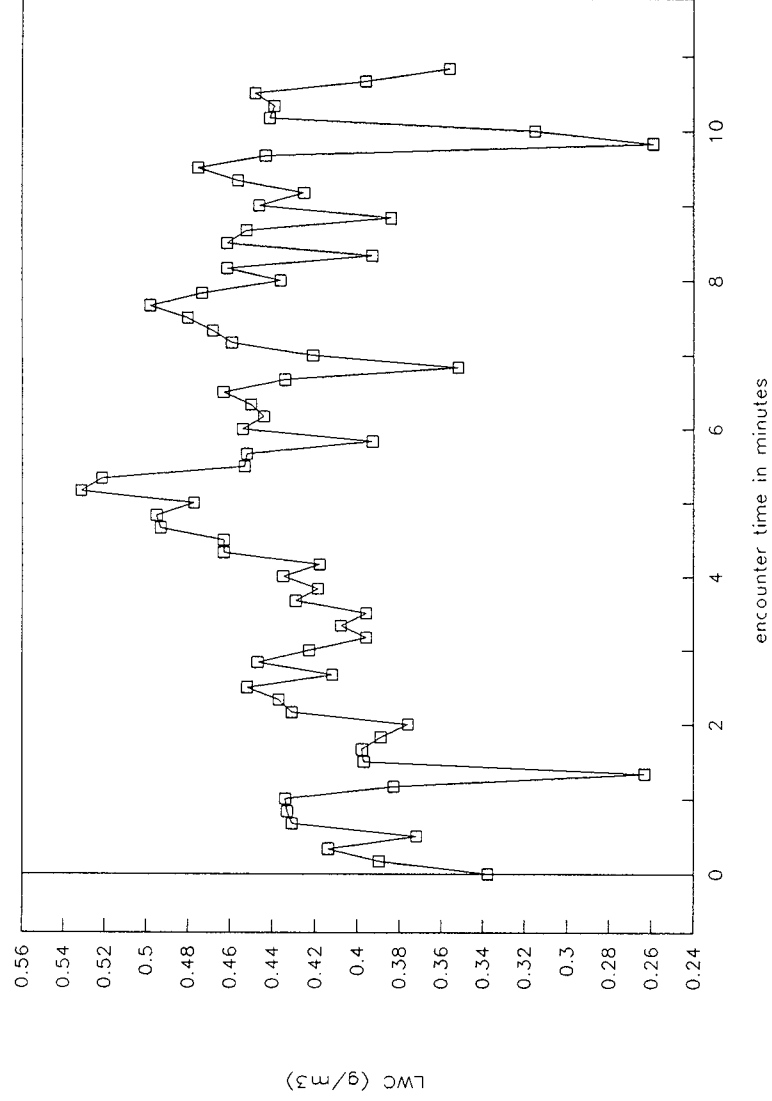
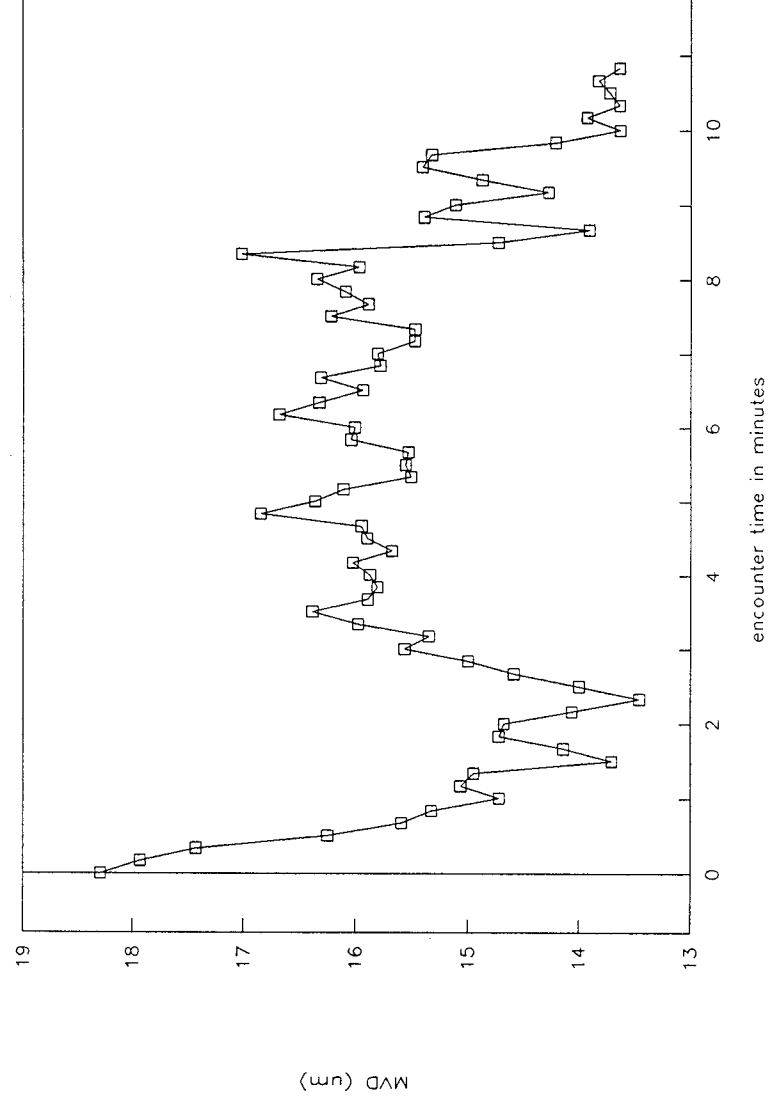Figure 9c.—Laser probe liquid water content for flight 90-7, run 2; average = .28, standard deviation = .07.
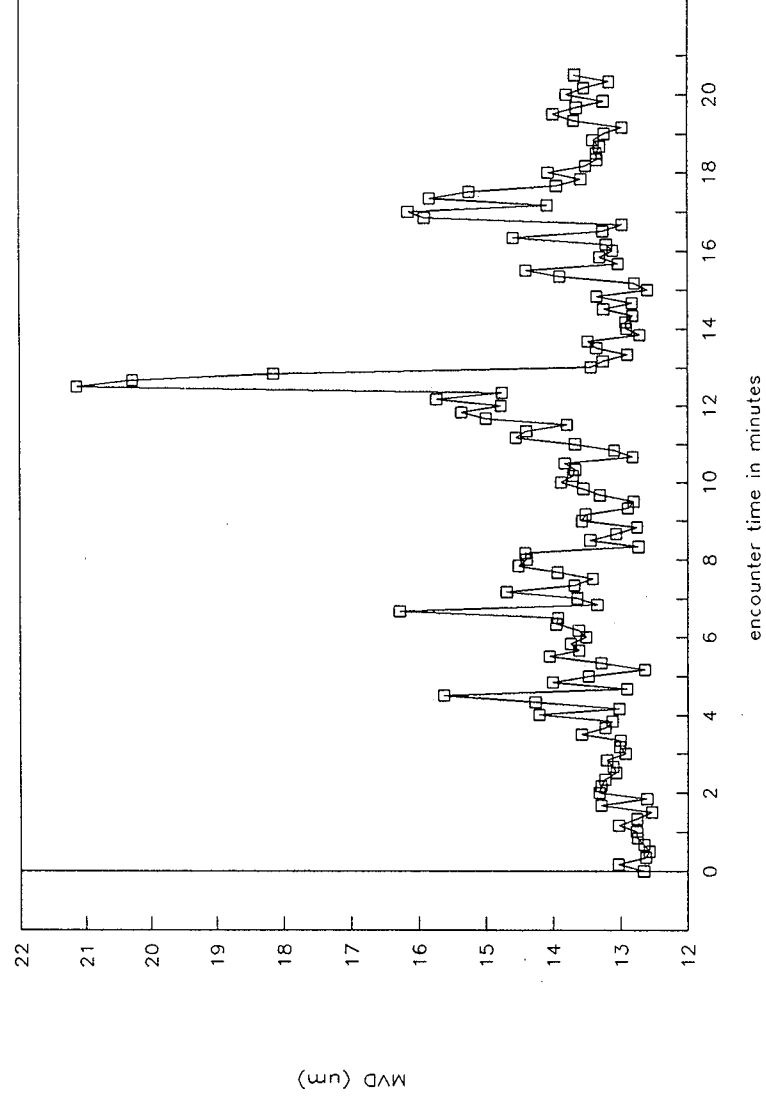
Figure 9d.—Droplet mean volume diameter for flight 90-7, run 2; average = 13.74, standard deviation = 1.26.

33
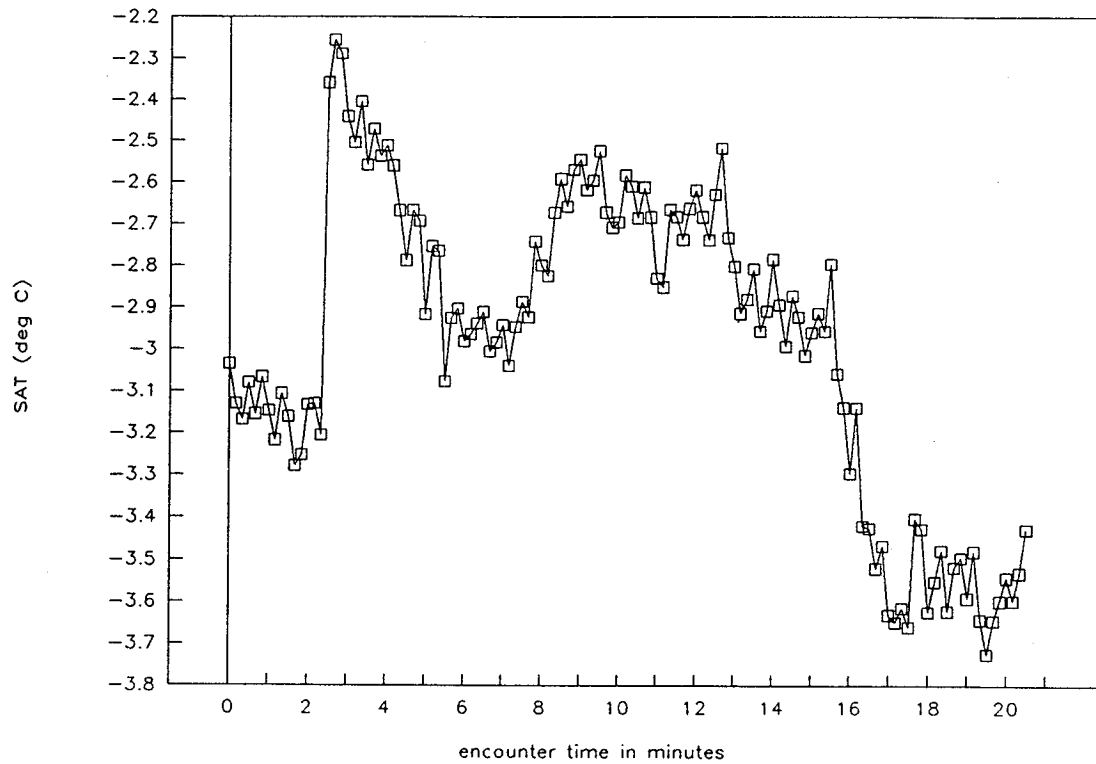
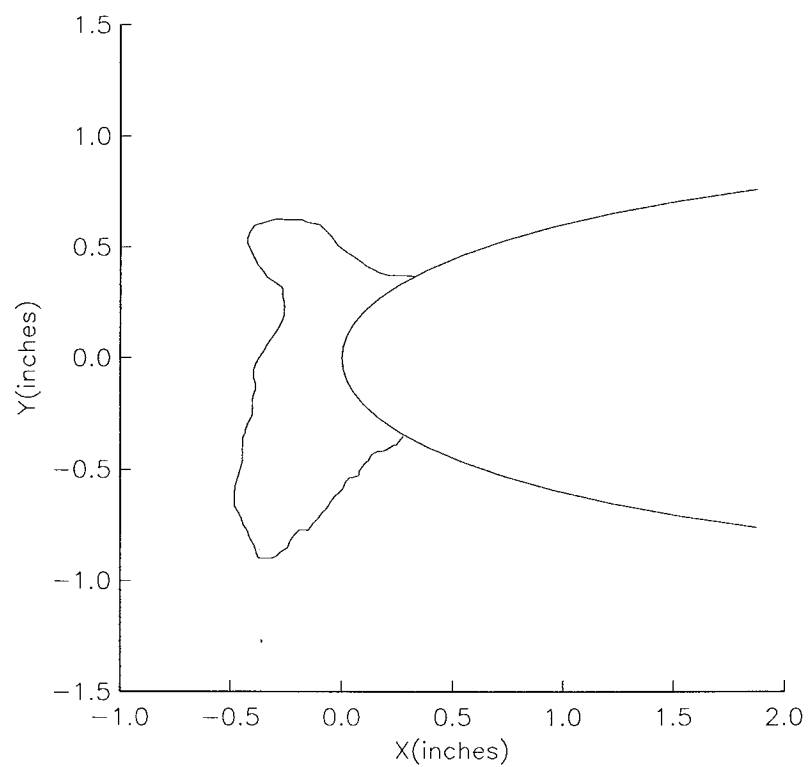Figure 9e.—Static air temperature for flight 90-7, run 2; average = –2.98, standard deviation = .36.
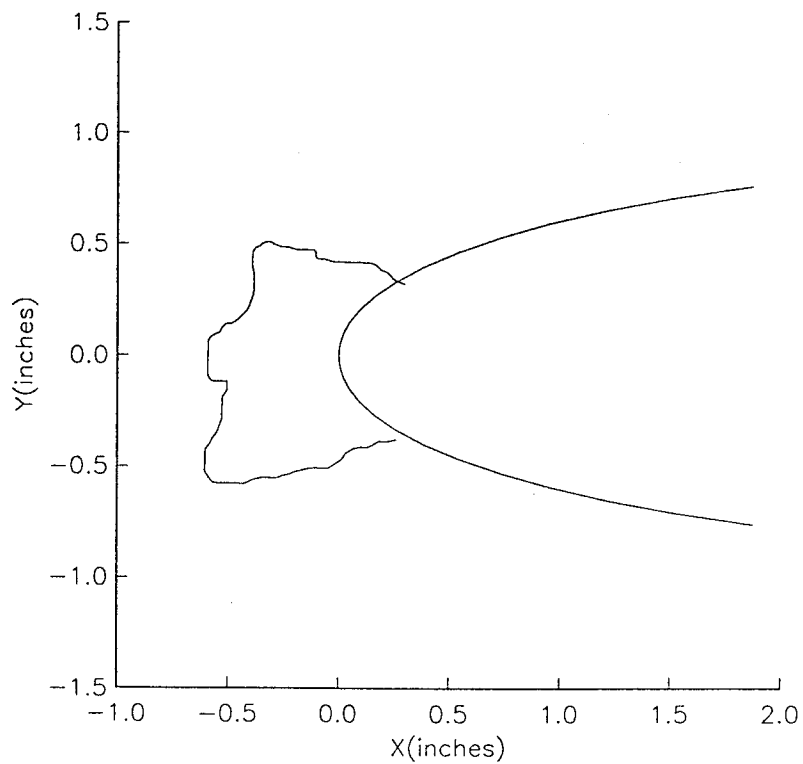
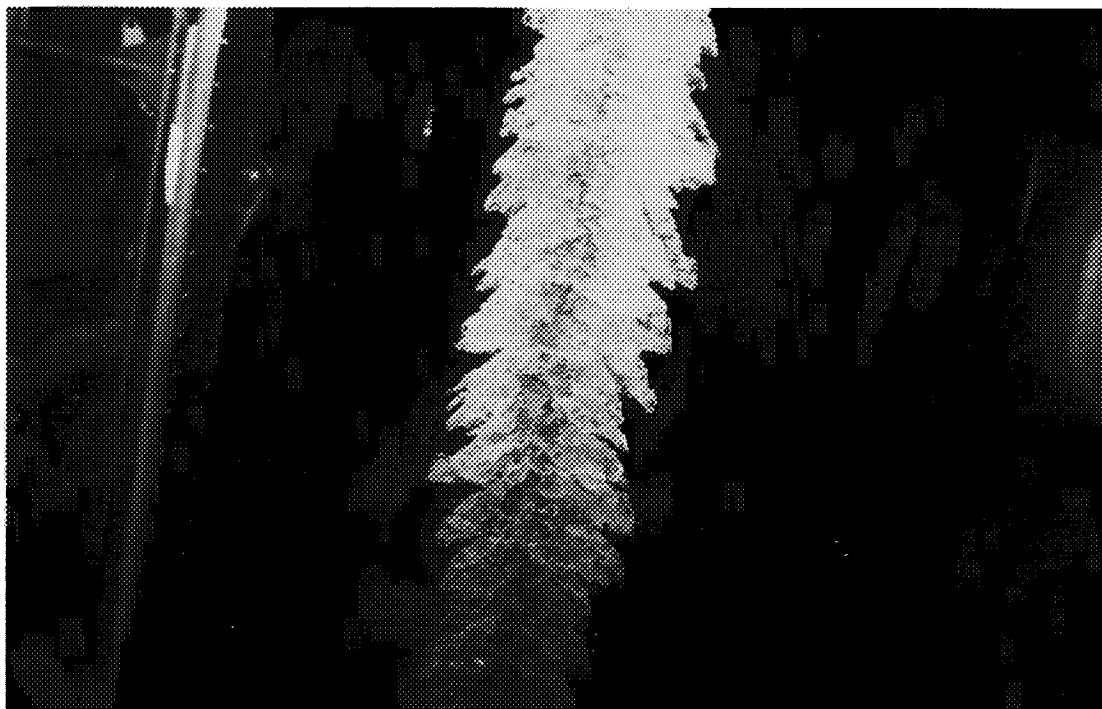Figure 9f.—Center span tracing of ice from flight 90-7, run 2.
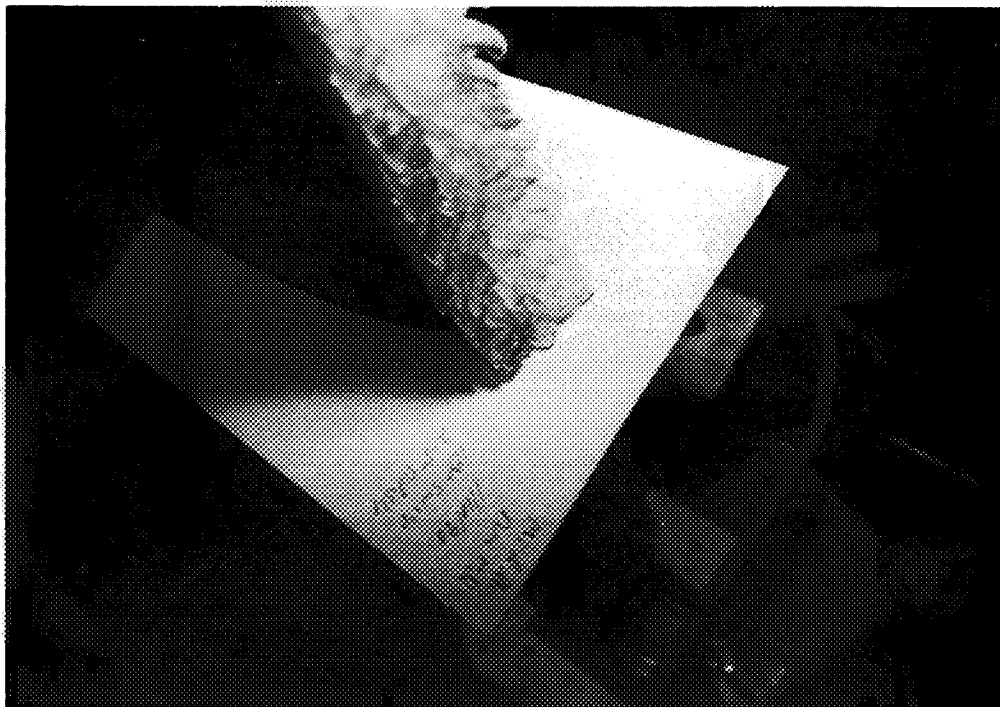
Figure 9g.—Photograph of ice from flight 90-7, run 2.

Figure 10a.—Aircraft true airspeed (in knots) for flight 90-7, run 3; average 124.0, standard deviation = 3.5.
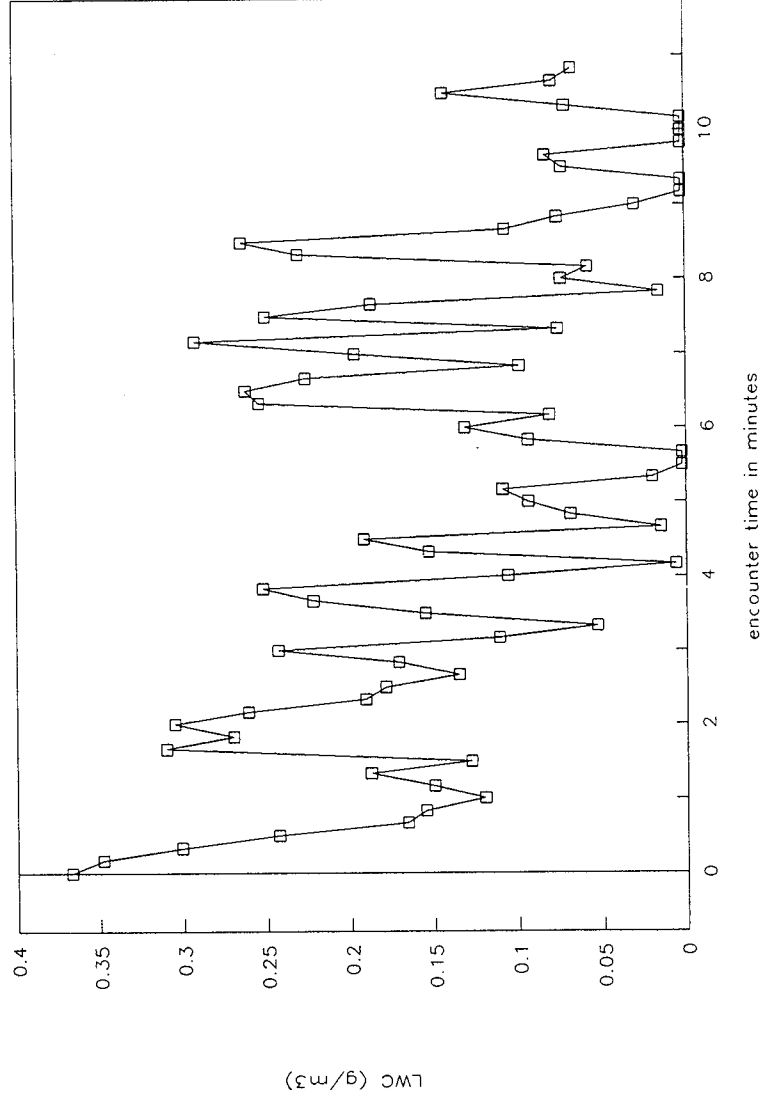

Figure 10b.—Johnson-Williams liquid water content for flight 90-7, run 3; average = .19, standard deviation = .09.

36

Figure 10c.—Laser probe liquid water content for flight 90-7, run 3 (with bad data removed); average = .28, standard deviation = .12.
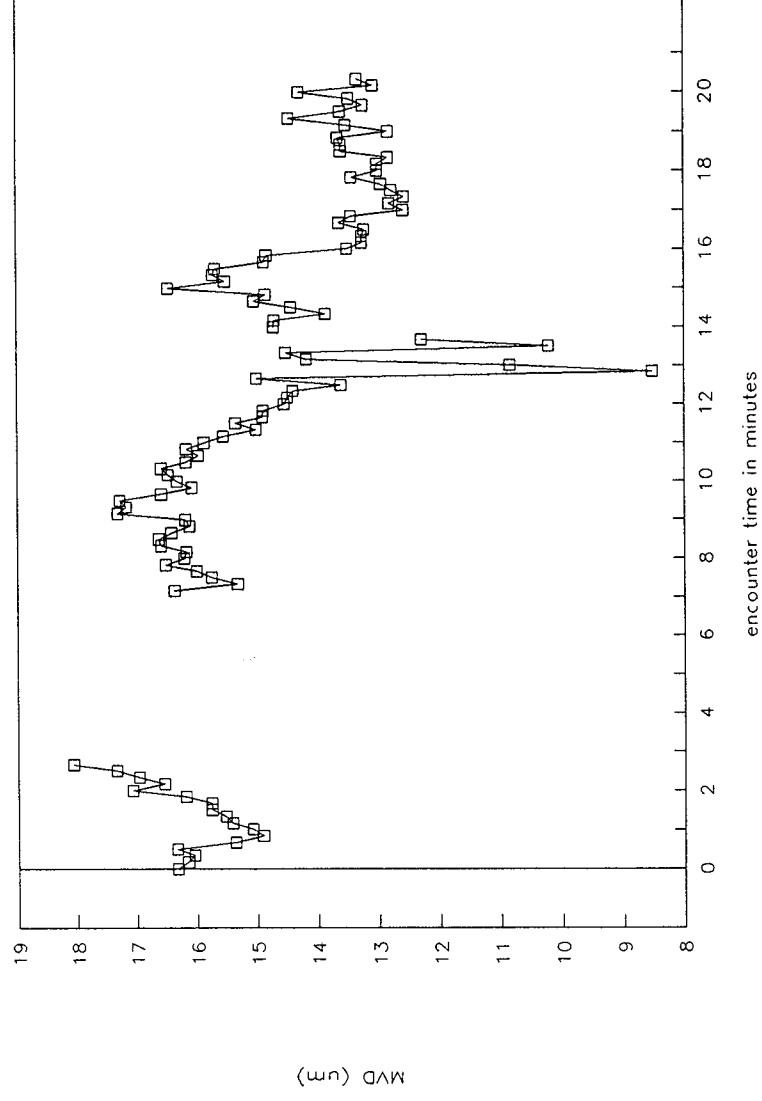
Figure 10d.—Droplet mean volume diameter for flight 90-7, run 3 (with bad data removed); average = 14.8, standard deviation = 1.65.

Figure 10e.—Static air temperature for flight 90-7, run 3; average = –4.72, standard deviation = .49.
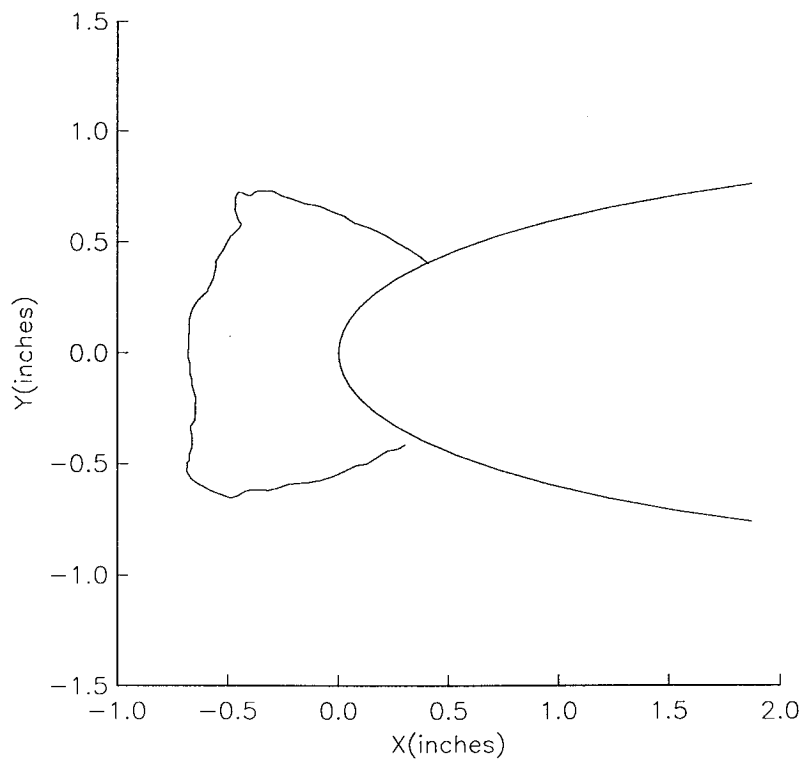
Figure 10f.—Center span tracing of ice from flight 90-7, run 3.

38

TAS (knots)
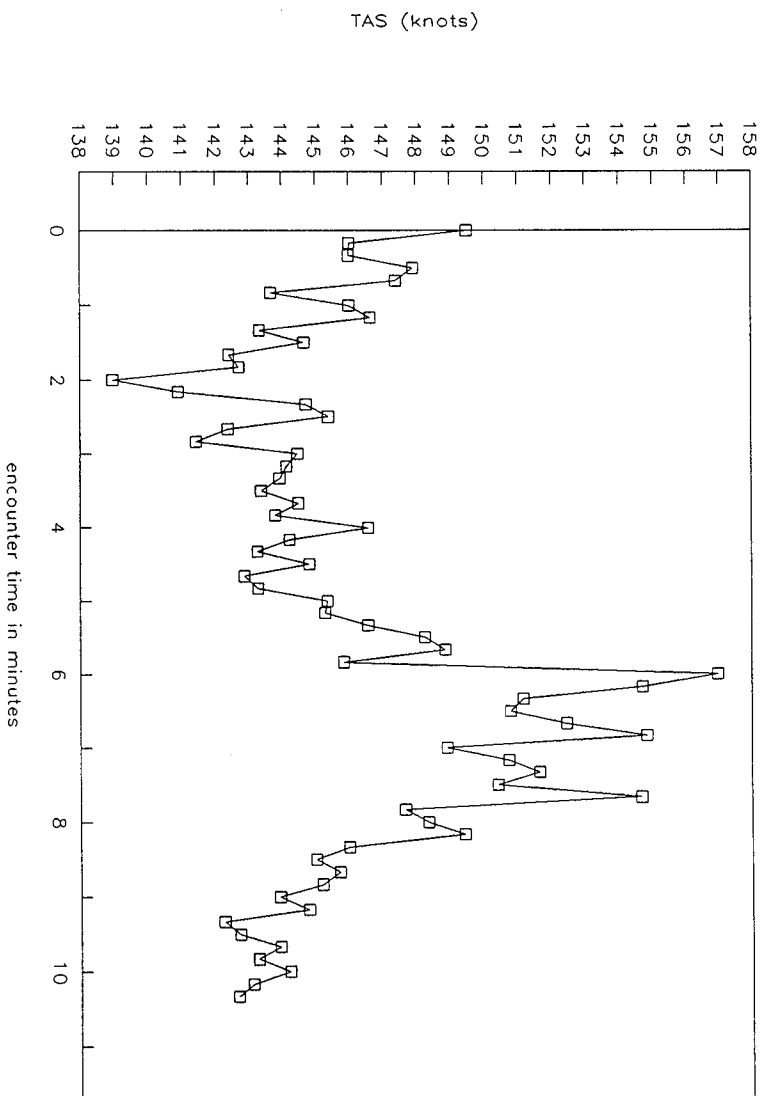
Figure 11a.—Aircraft true airspeed (in knots) for flight 90-8, run 1; average 146.0, standard deviation = 3.6.

encounter time in minutes

LWC (g/m3)

Figure 11b.—Johnson-Williams liquid water content for flight 90-8, run 1; average = .49, standard deviation = .06.
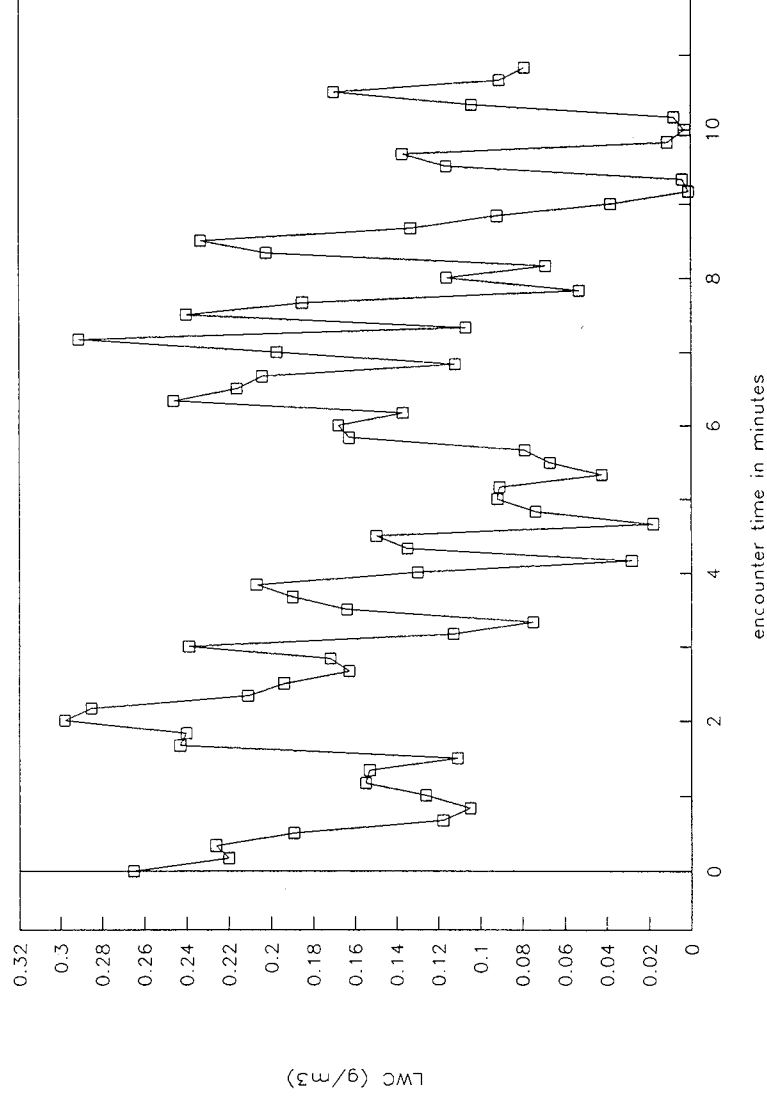
encounter time in minutes

Figure 11c.—Laser probe liquid water content for flight 90-8, run 1; average = .41, standard deviation = .06.
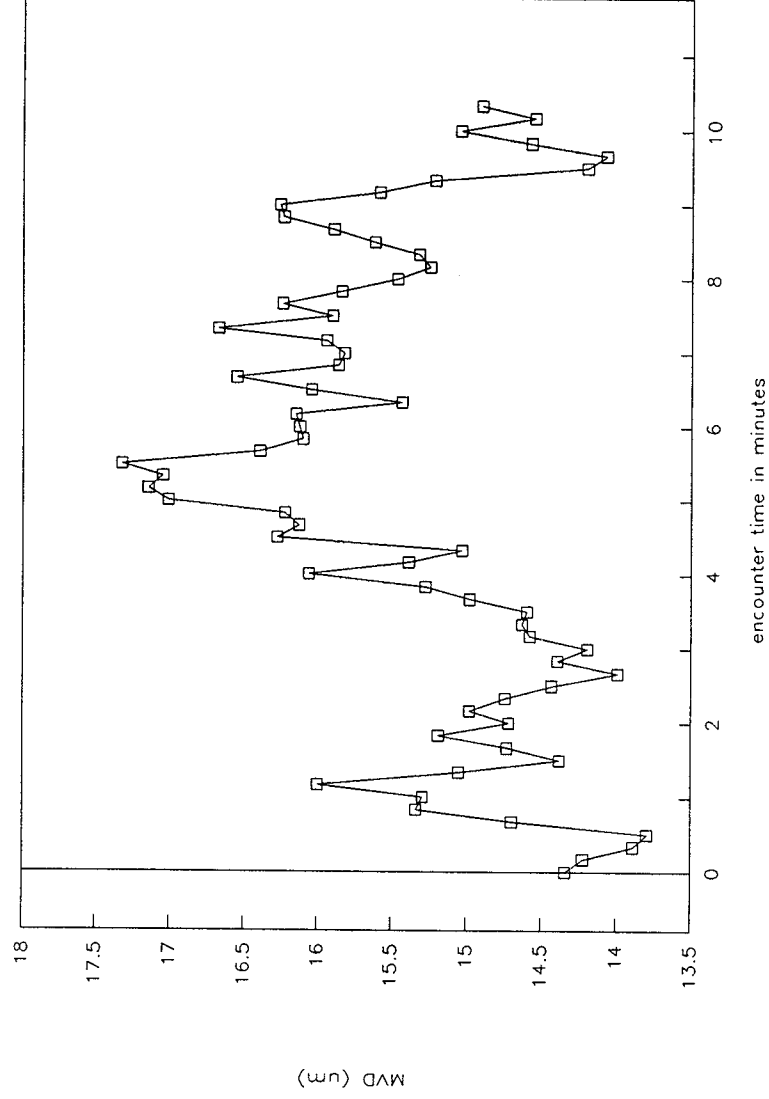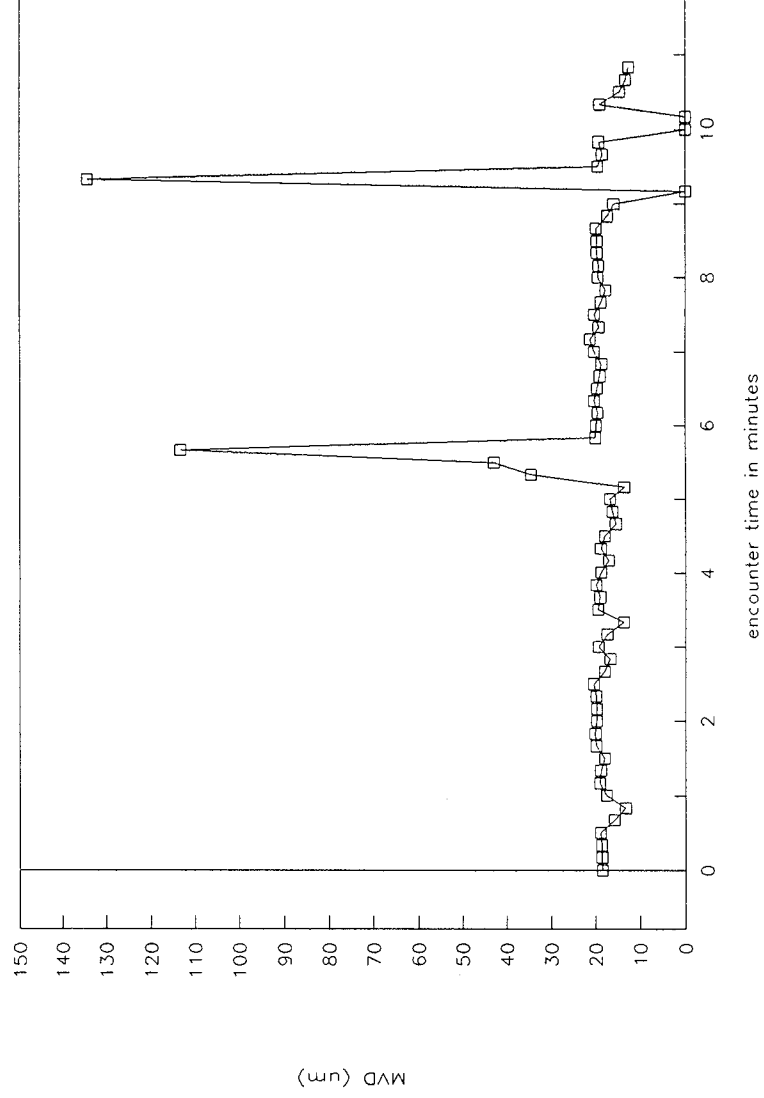

Figure 11d.—Droplet mean volume diameter for flight 90-8, run 1; average = 15.4, standard deviation = ?
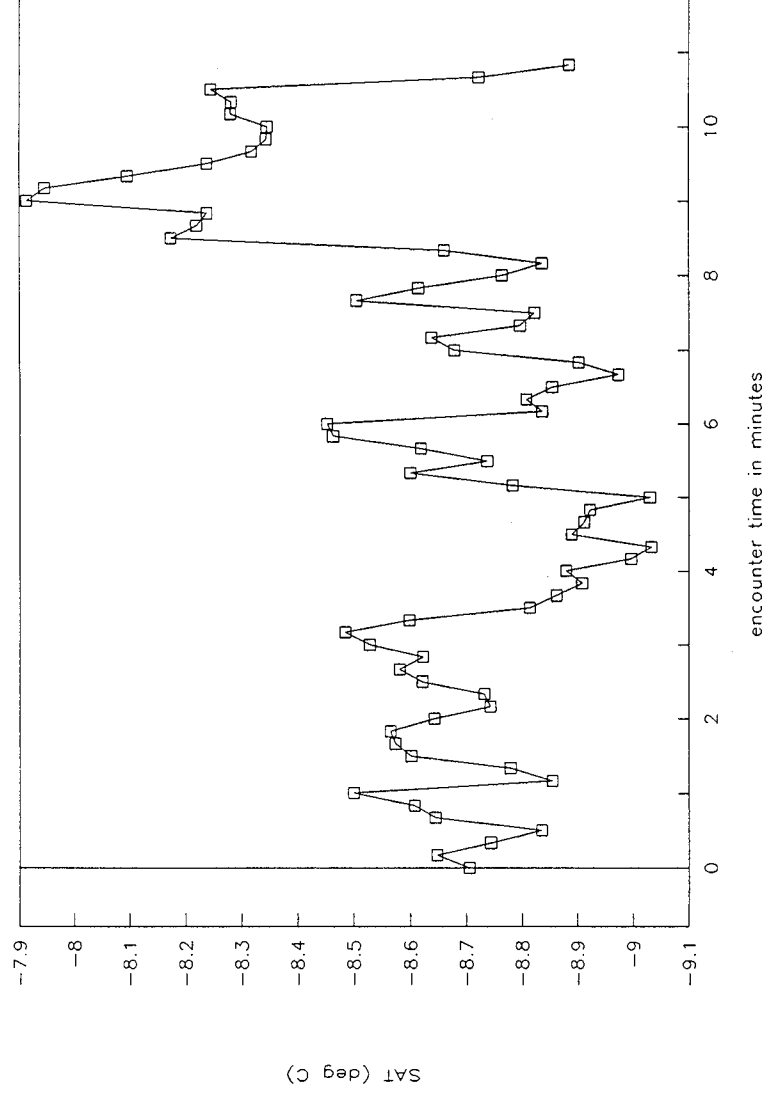
40
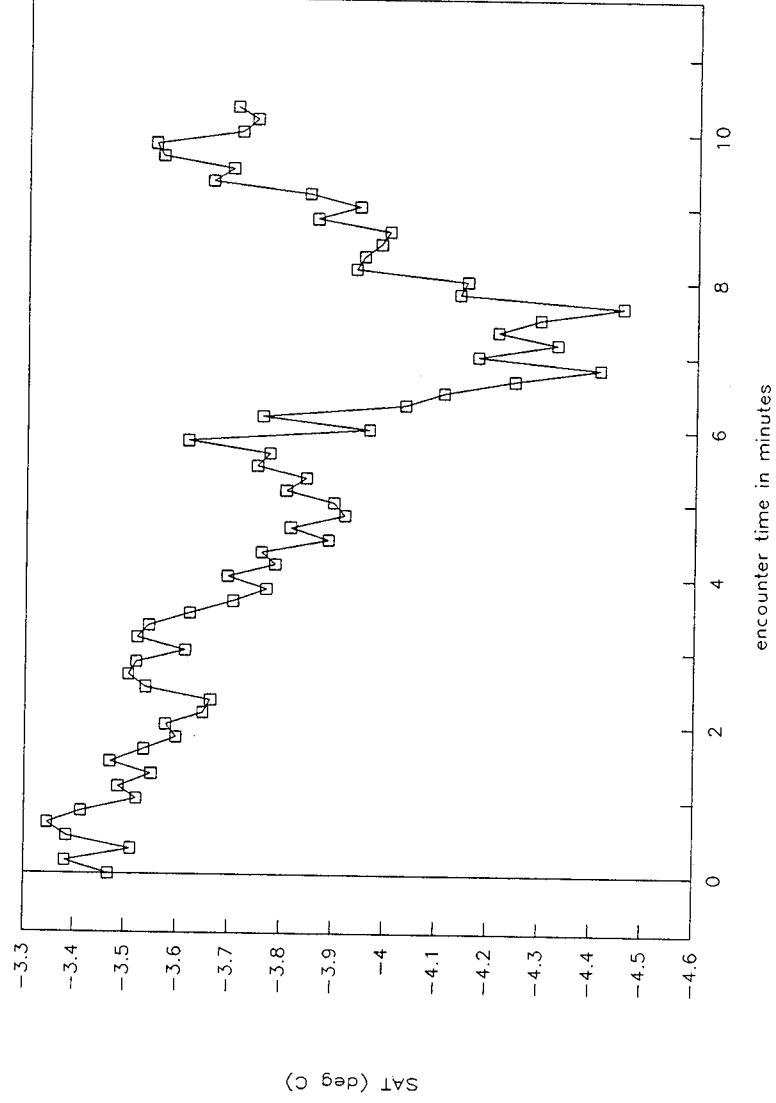
Figure 11e.—Static air temperature for flight 90-8, run 1; average = -3.77, standard deviation = .27.
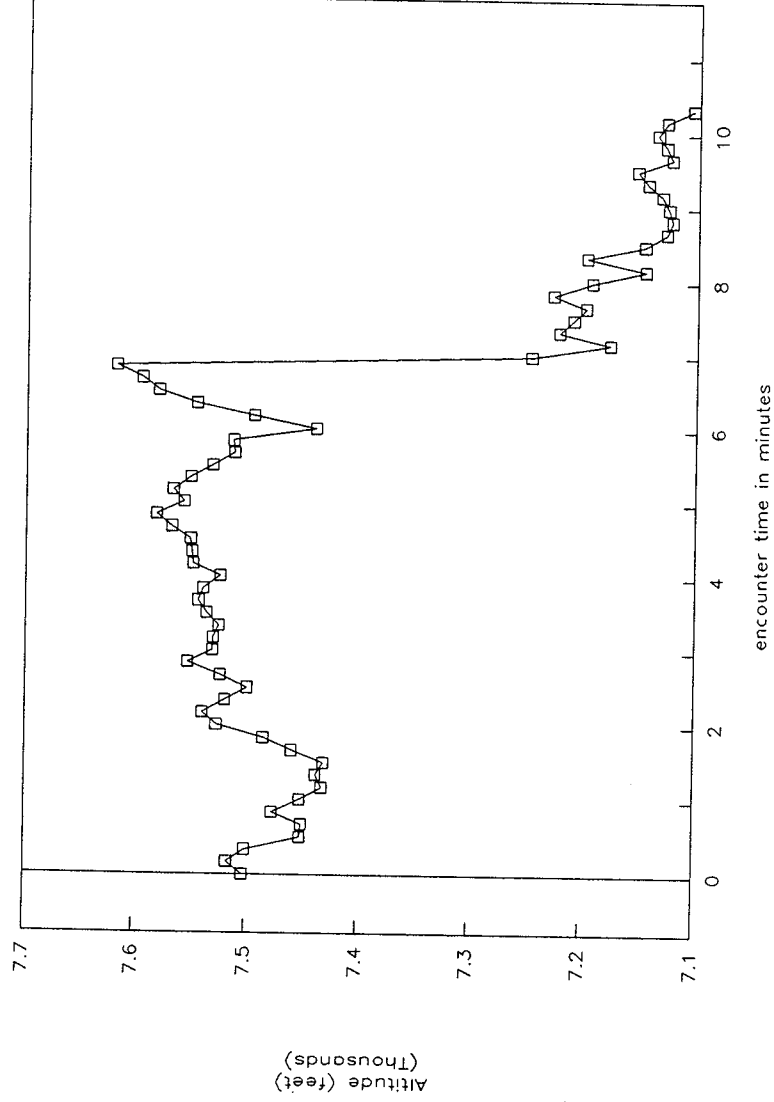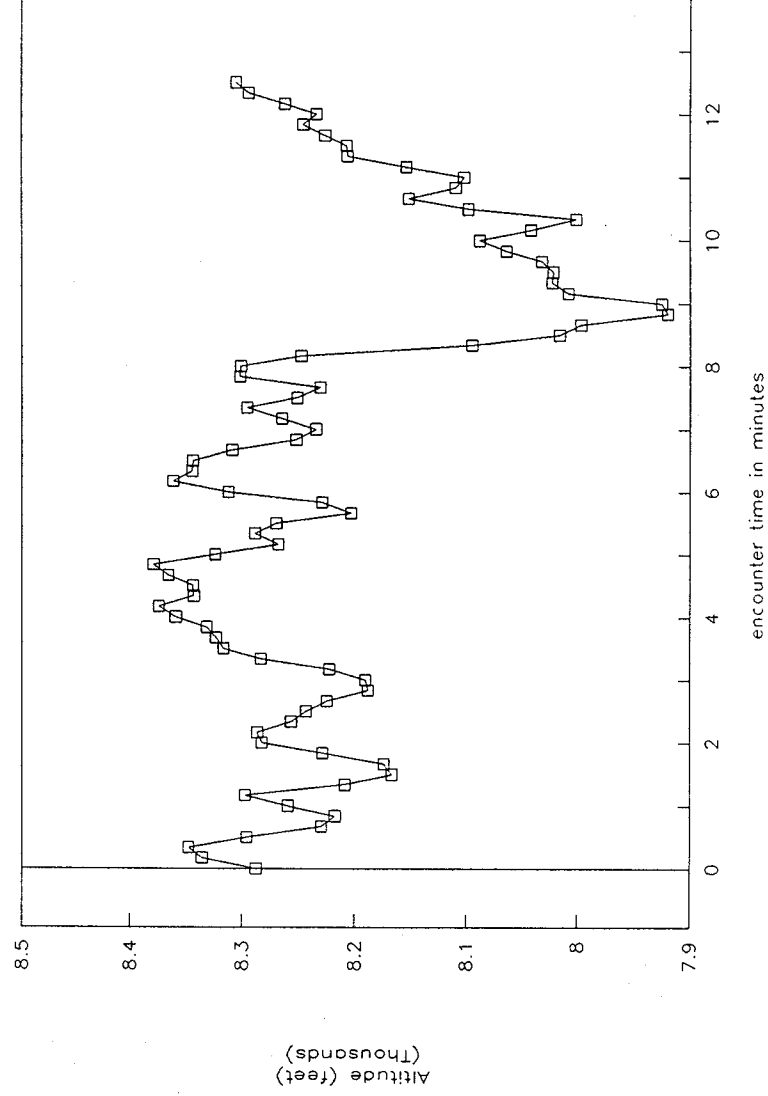

Figure 11f.—Aircraft altitude (in feet) for flight 90-8, run 1; average = 7399.0, standard deviation = 173.8.
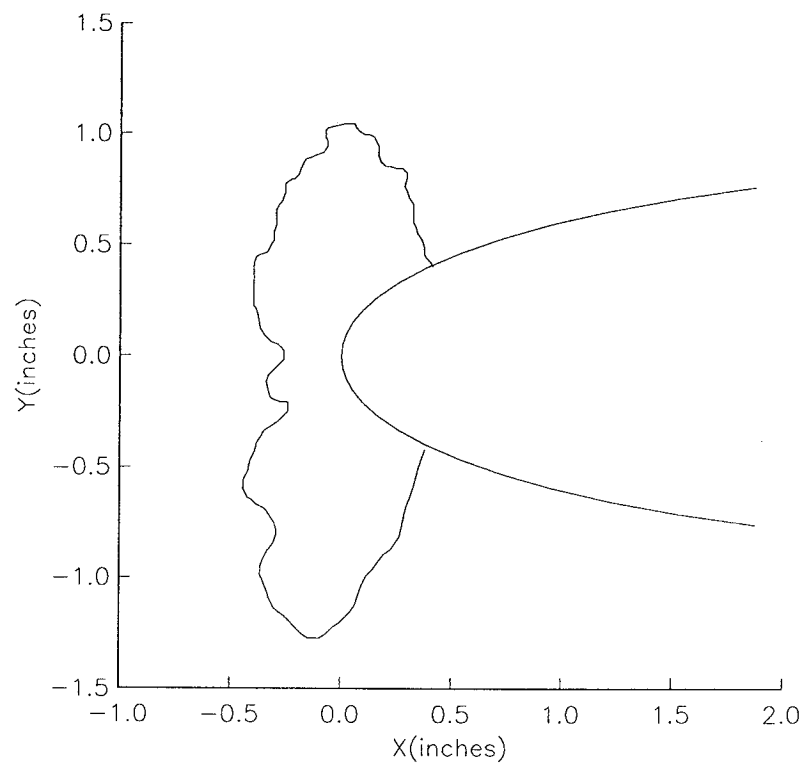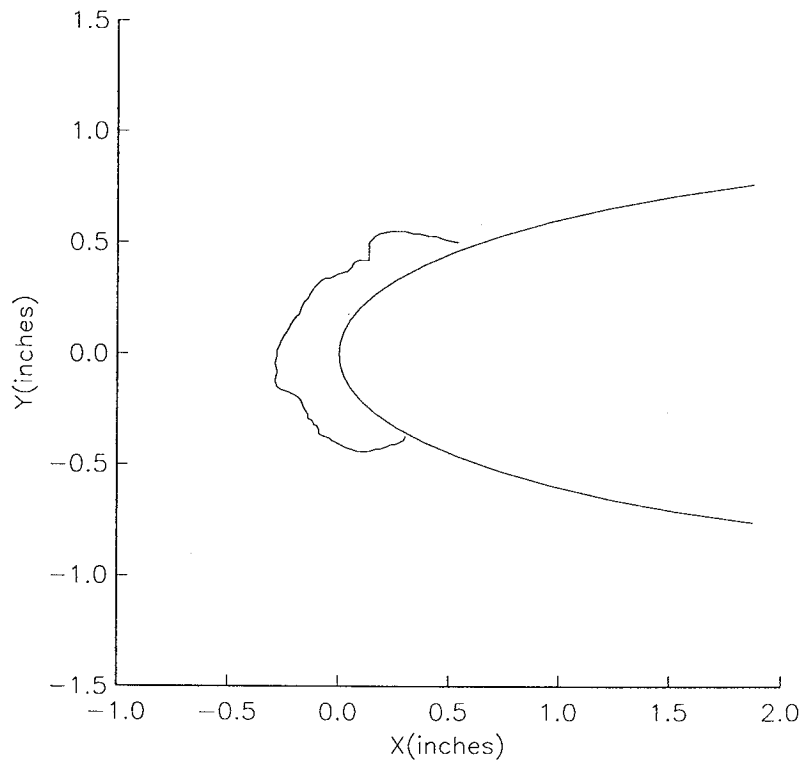
Figure 11g.—Center span tracing of ice from flight 90-8, run 1.

Figure 11h.—Photograph of ice from flight 90-8, run 1.

42
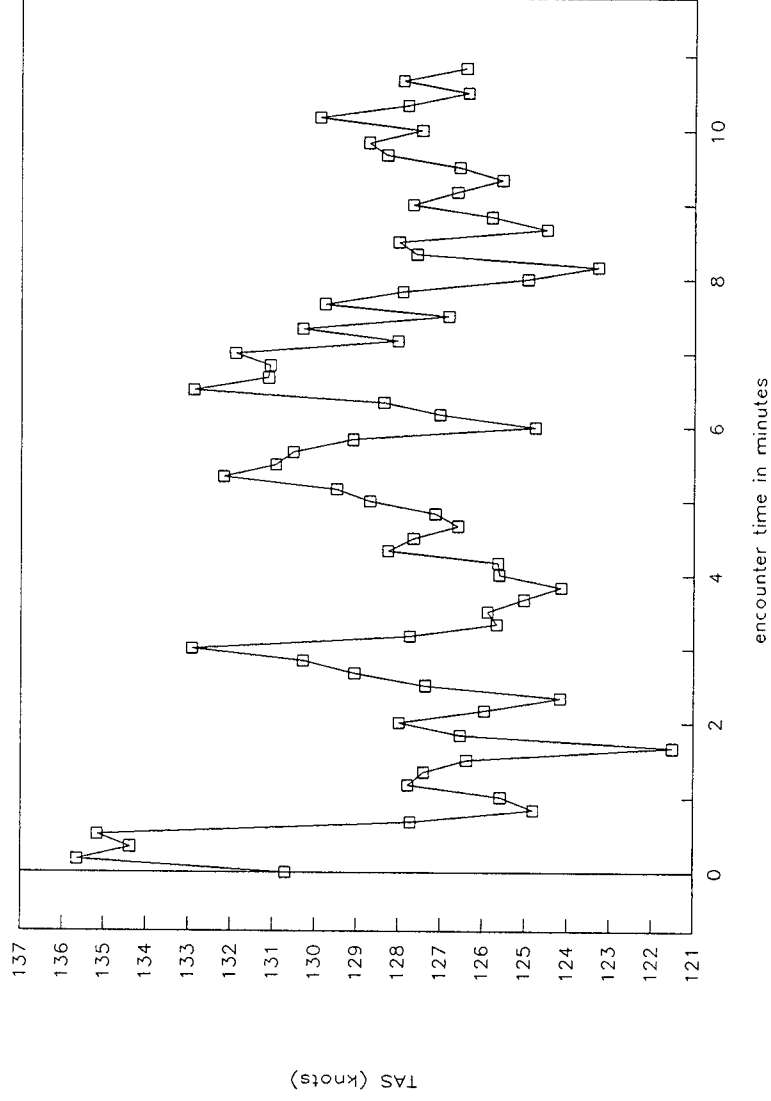
Figure 12a.—Aircraft true airspeed (in knots) for flight 90-8, run 2; average 128.0, standard deviation = 2.7.

Figure 12b.—Johnson-Williams liquid water content for flight 90-8, run 2; average = .38, standard deviation = .05.

43

Figure 12c.—Laser probe liquid water content for flight 90-8, run 2; average = .43, standard deviation = .05.

Figure 12d.—Droplet mean volume diameter for flight 90-8, run 2; average = 15.4, standard deviation = 1.1.

44
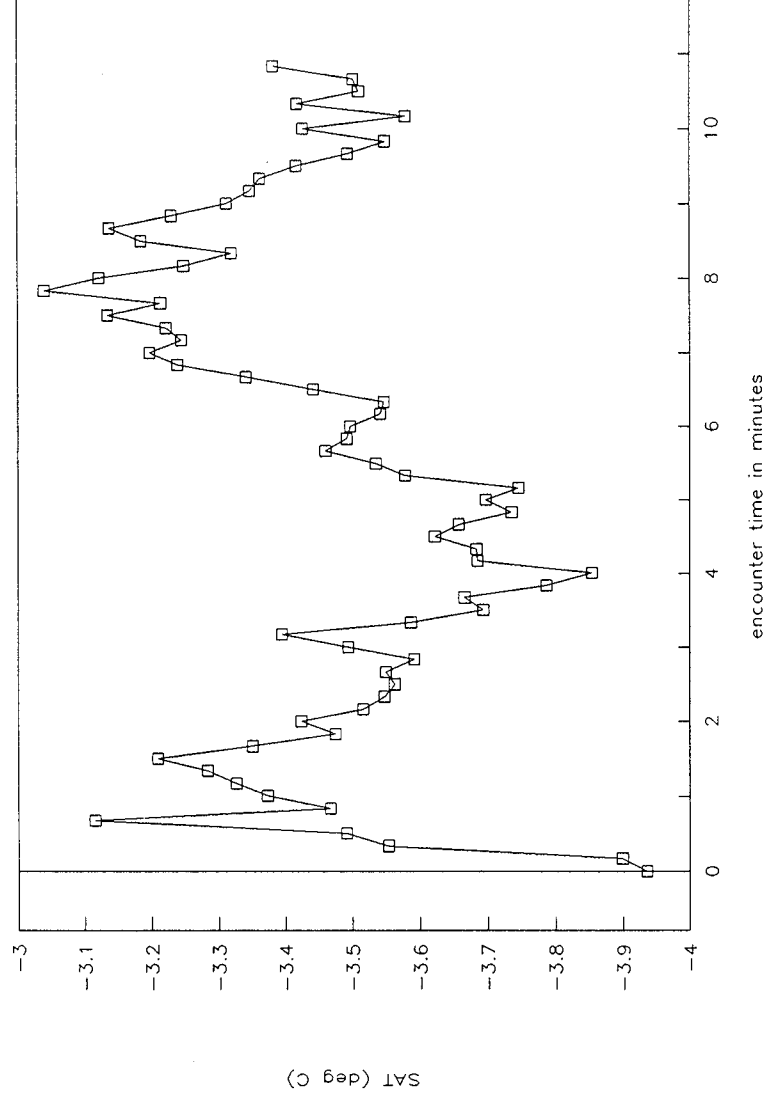
Figure 12e.—Static air temperature for flight 90-8, run 2; average = –3.4, standard deviation = .2.
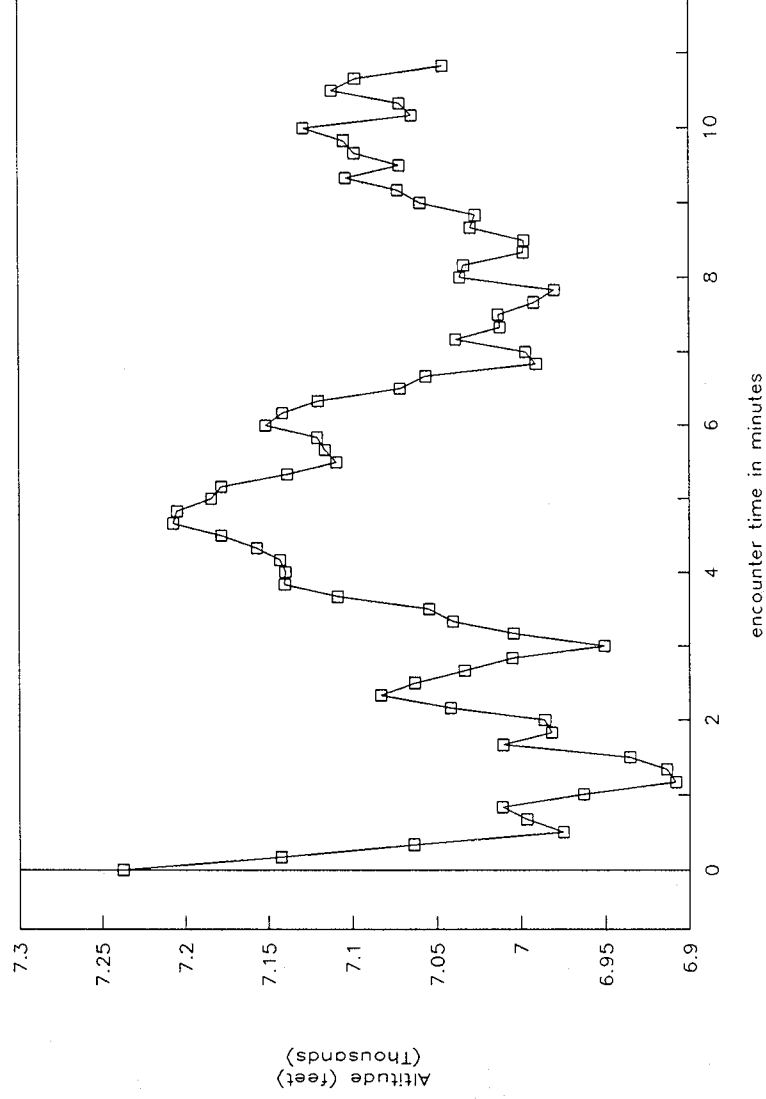
Figure 12f.—Aircraft altitude (in feet) for flight 90-8, run 2; average = 7064.0, standard deviation = 73.4.

45

Figure 12g.—Center span tracing of ice from flight 90-8, run 2.

Figure 12h.—Photograph of ice from flight 90-8, run 2.

46
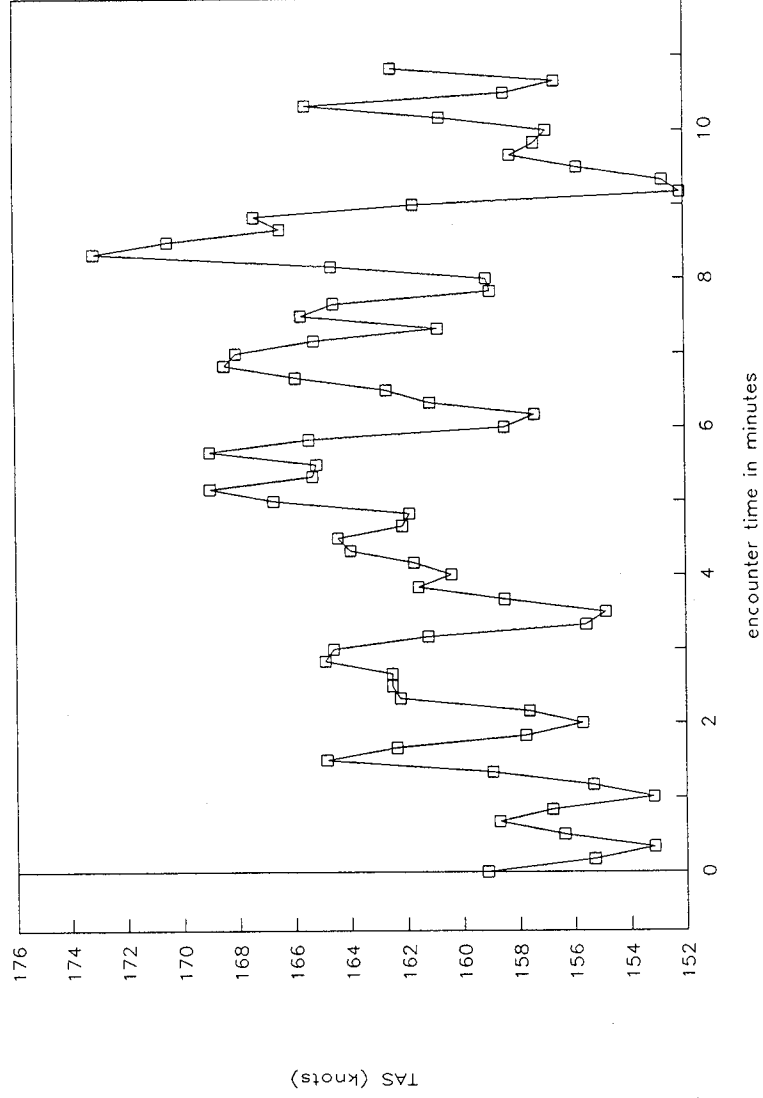
Figure 13a.—Aircraft true airspeed (in knots) for flight 90-11, run 1; average 160.9, standard deviation = 4.5.
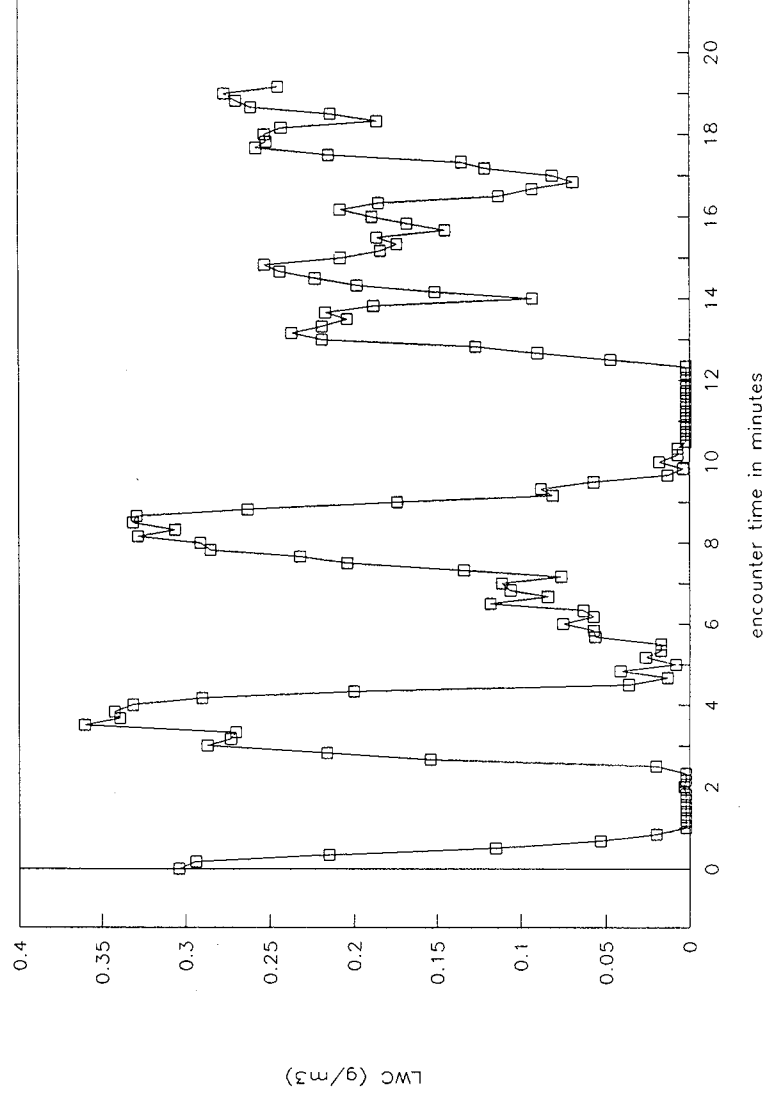

Figure 13b.—Johnson-Williams liquid water content for flight 90-11, run 1; average = .12, standard deviation = .1.
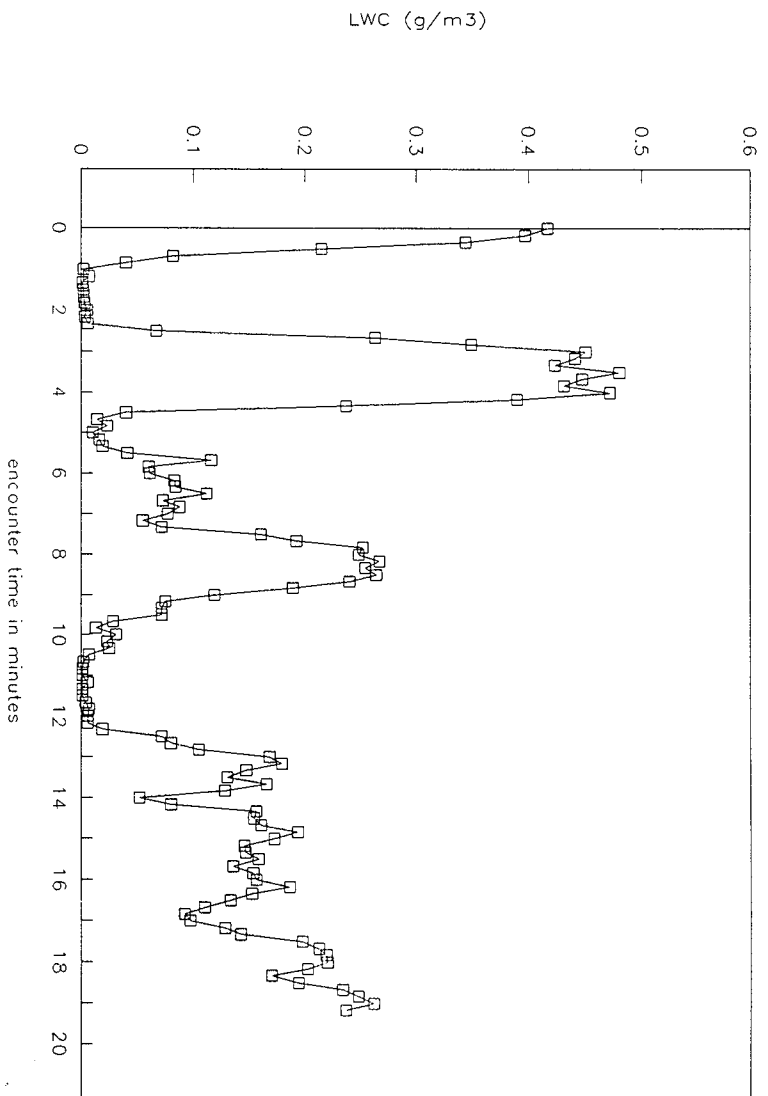
47

Figure 13c.—Laser probe liquid water content for flight 90-11, run 1; average = .12, standard deviation = .08.
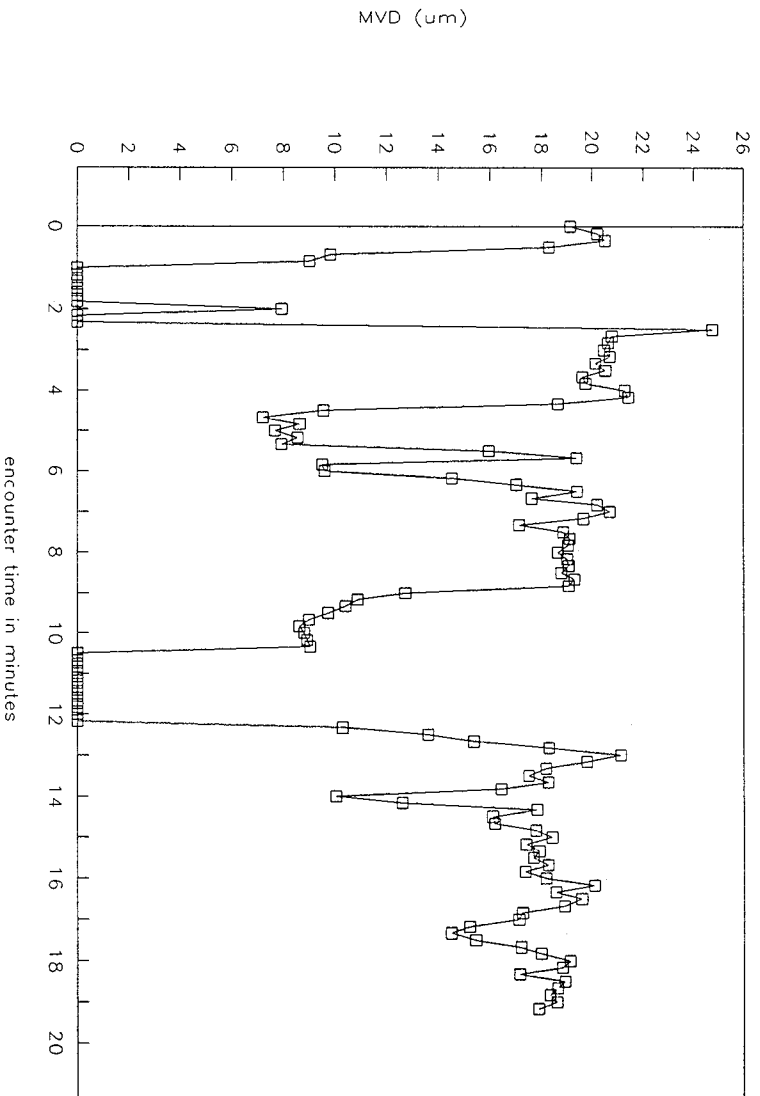

Figure 13d.—Droplet mean volume diameter for flight 90-11, run 1; average = 17.9, standard deviation = 2.4.
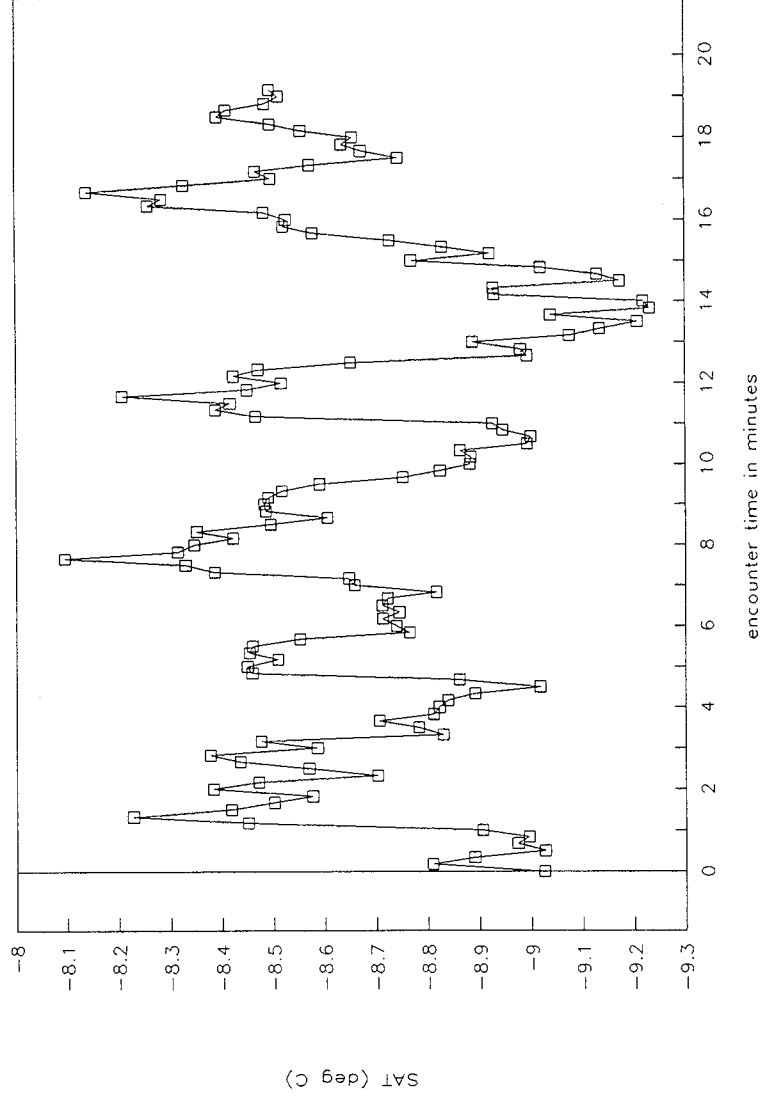
Figure 13e.—Static air temperature for flight 90-11, run 1; average = -8.7, standard deviation = .26.
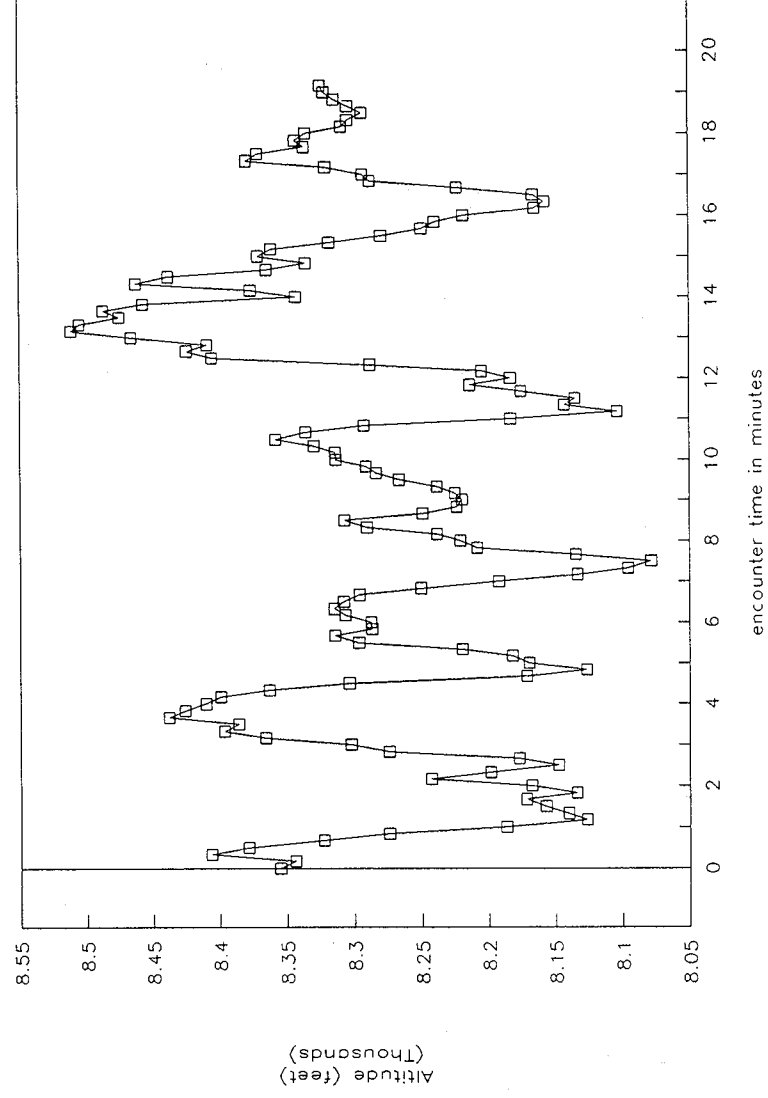

Figure 13f.—Aircraft altitude (in feet) for flight 90-11, run 1; average = 8221.0, standard deviation = 112.6.
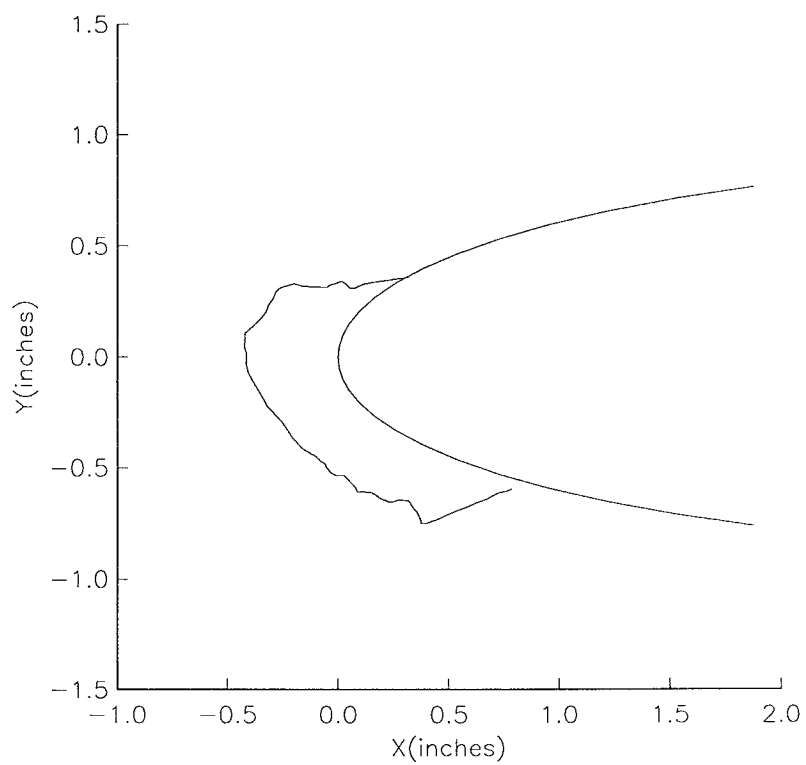
**Figure 13g.—Center span tracing of ice from flight 90-11, run 1.**
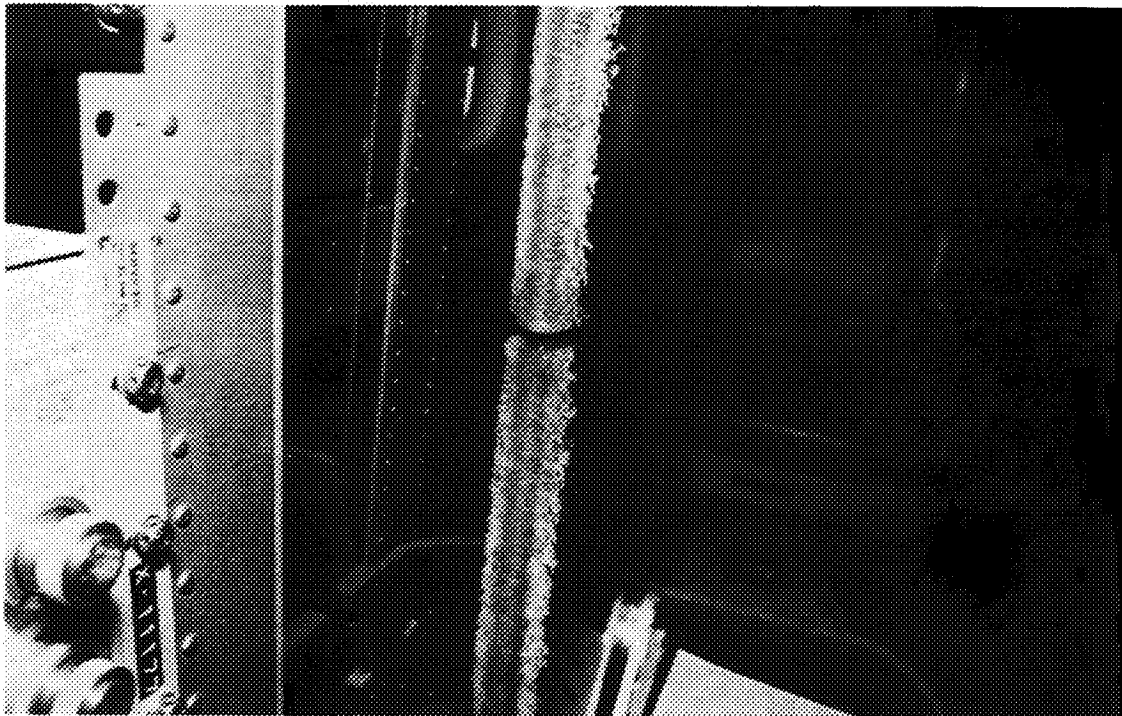
Figure 13h.—Photograph of ice from flight 90-11, run 1.
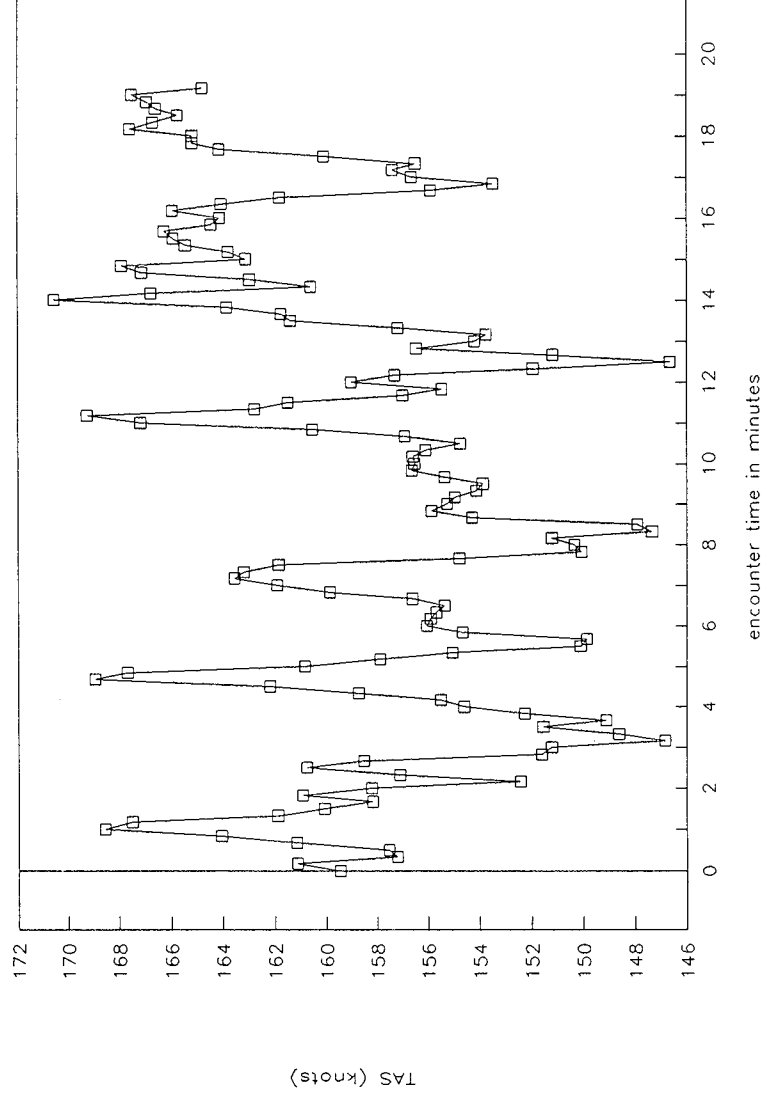
Figure 14a.—Aircraft true airspeed (in knots) for flight 90-11, run 2; average 158.9, standard deviation = 5.7.

Figure 14b.—Johnson-Williams liquid water content for flight 90-11, run 2; average = .14, standard deviation = .11.

51

Figure 14c.—Laser probe liquid water content for flight 90-11, run 2; average = .14, standard deviation = .12.

Figure 14d.—Droplet mean volume diameter for flight 90-11, run 2; average = 16.6, standard deviation = 4.1.

Figure 14e.—Static air temperature for flight 90-11, run 2; average = –8.7, standard deviation = .26.

SAT (deg C)

encounter time in minutes

Figure 14f.—Aircraft altitude (in feet) for flight 90-11, run 2; average = 8284.0, standard deviation = 98.6.

Altitude (feet)
(Thousands)

encounter time in minutes

53

Figure 14g.—Center span tracing of ice from flight 90-11, run 2.
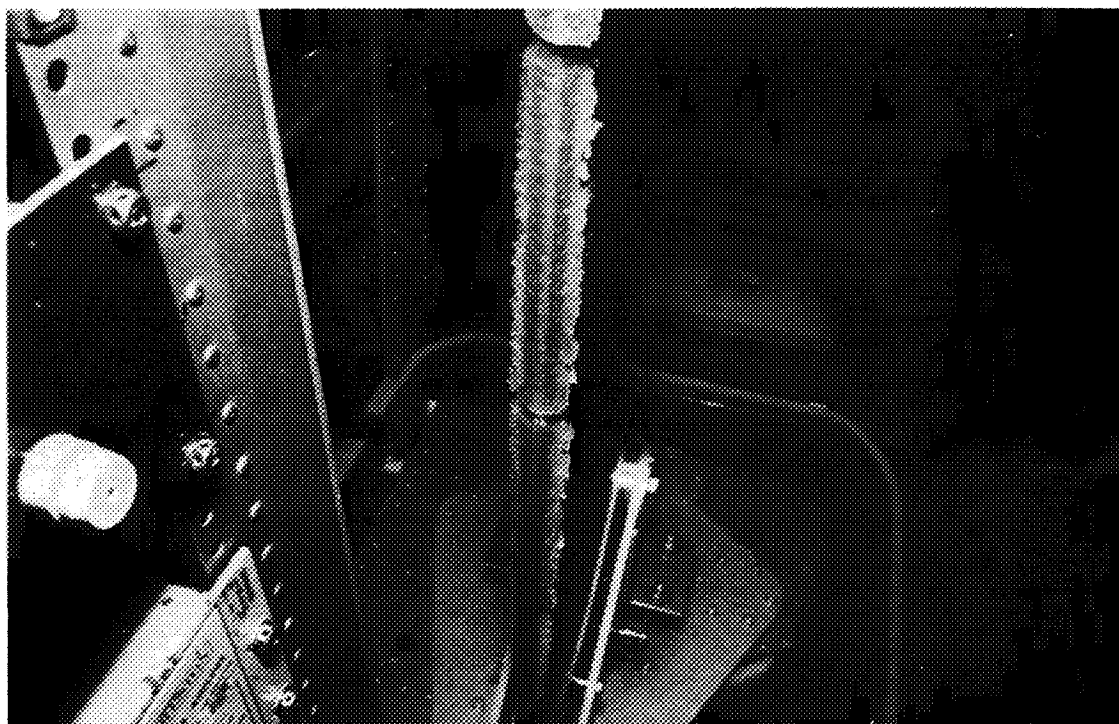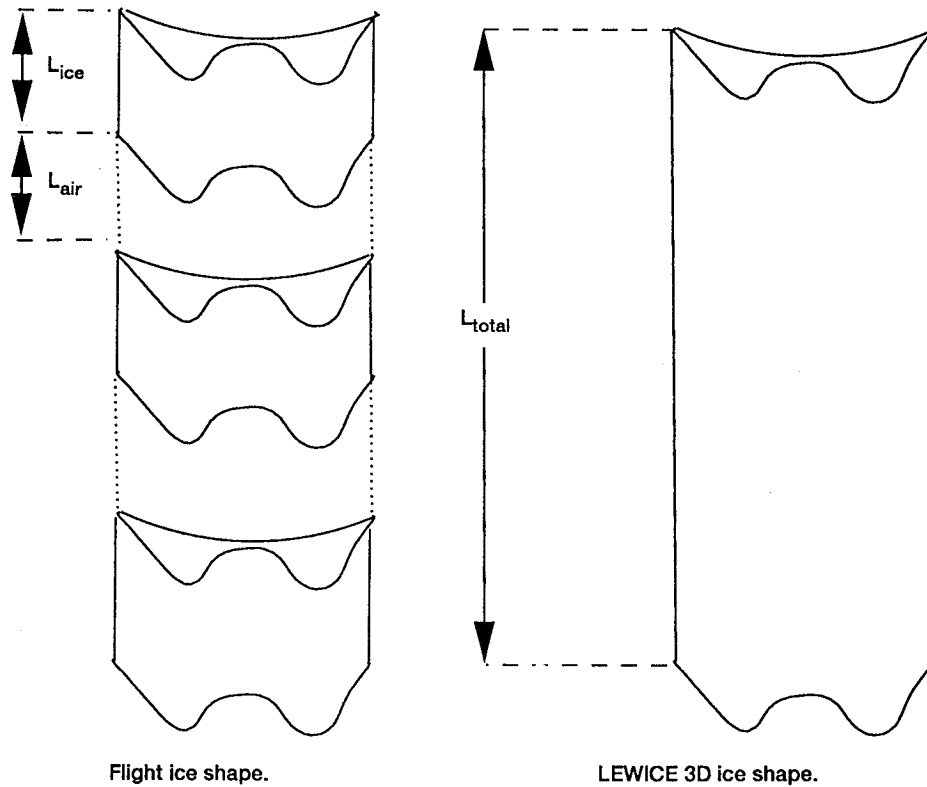

Figure 14h.—Photograph of ice from flight 90-11, run 2.
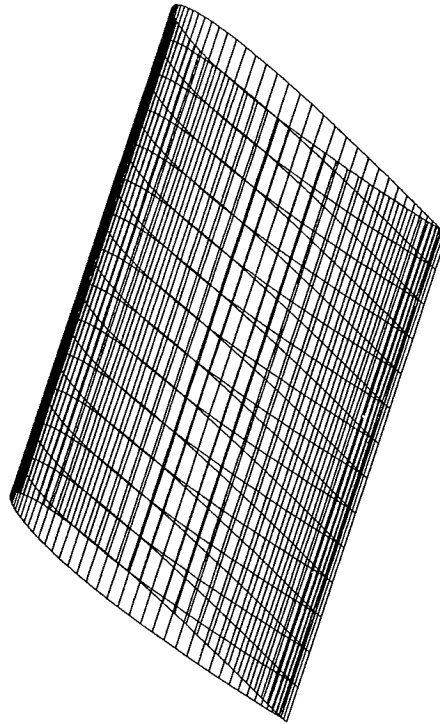
Figure 15.—LEWICE 3D airfoil model.

Flight ice shape.   LEWICE 3D ice shape.

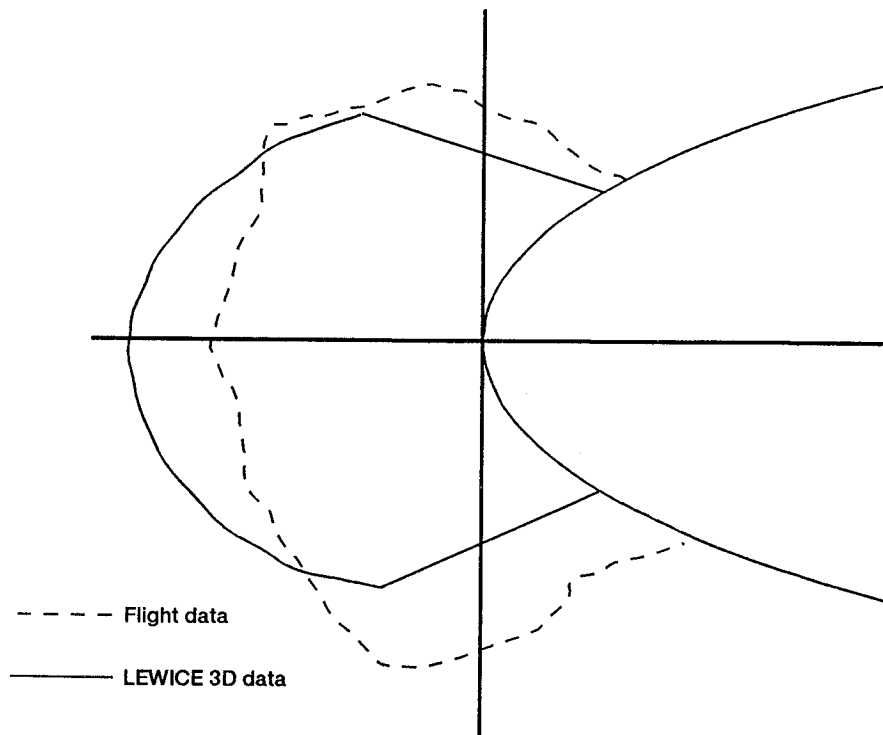Figure 16.—Derivation of AIRFAC density correction term.

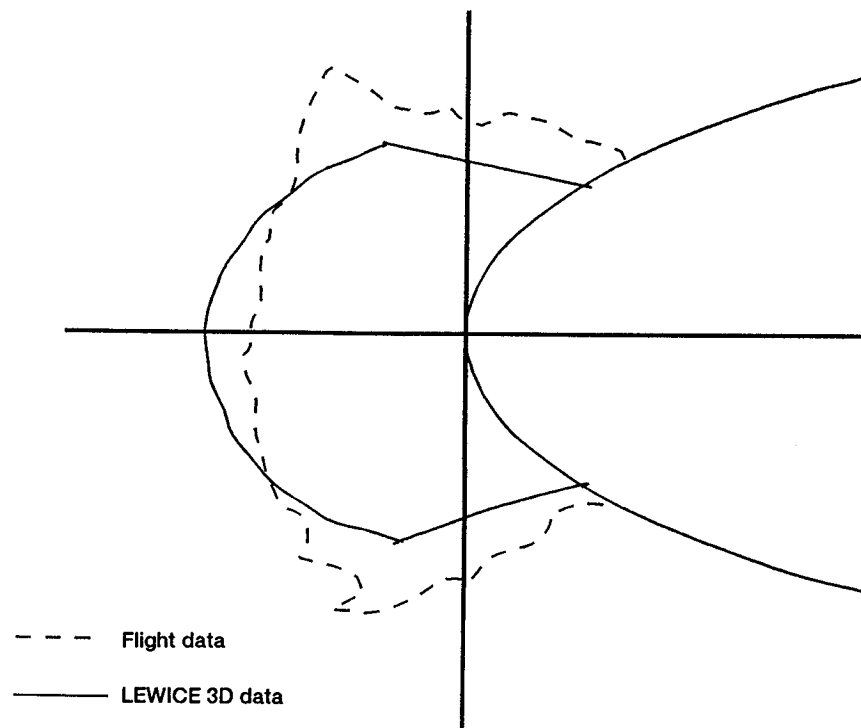Figure 17.—Comparison between flight and LEWICE 3D ice shapes for flight 90-4, run 1.

Figure 18.—Comparison between flight and LEWICE 3D ice shapes for flight 90-5, run 1.
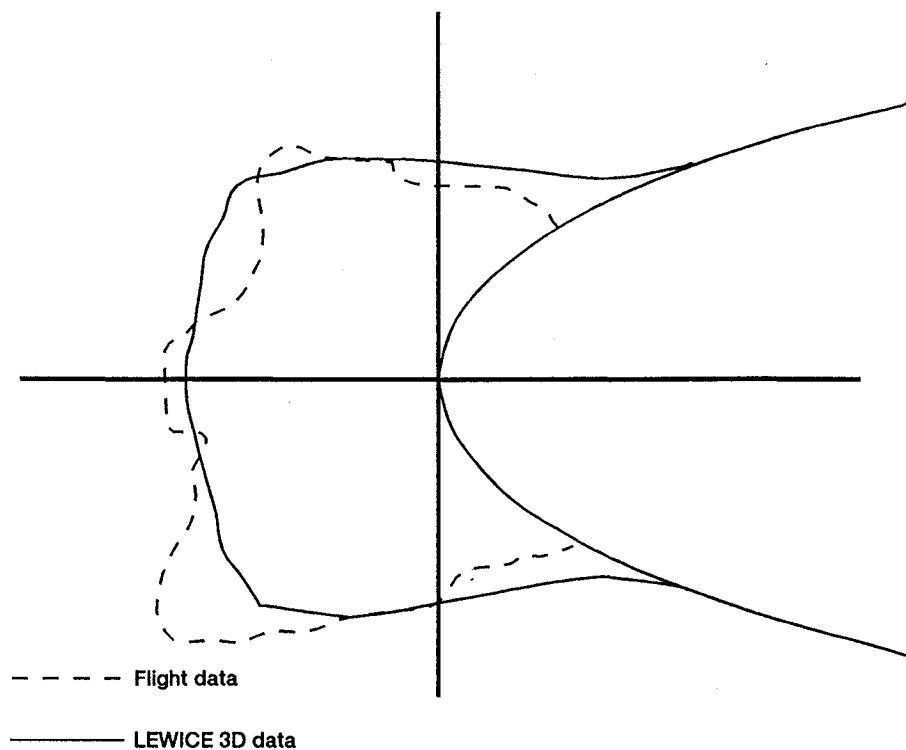
- - - - Flight data

———— LEWICE 3D data

Figure 19.—Comparison between flight and LEWICE 3D ice shapes for flight 90-7, run 2.

- - - - · Flight data
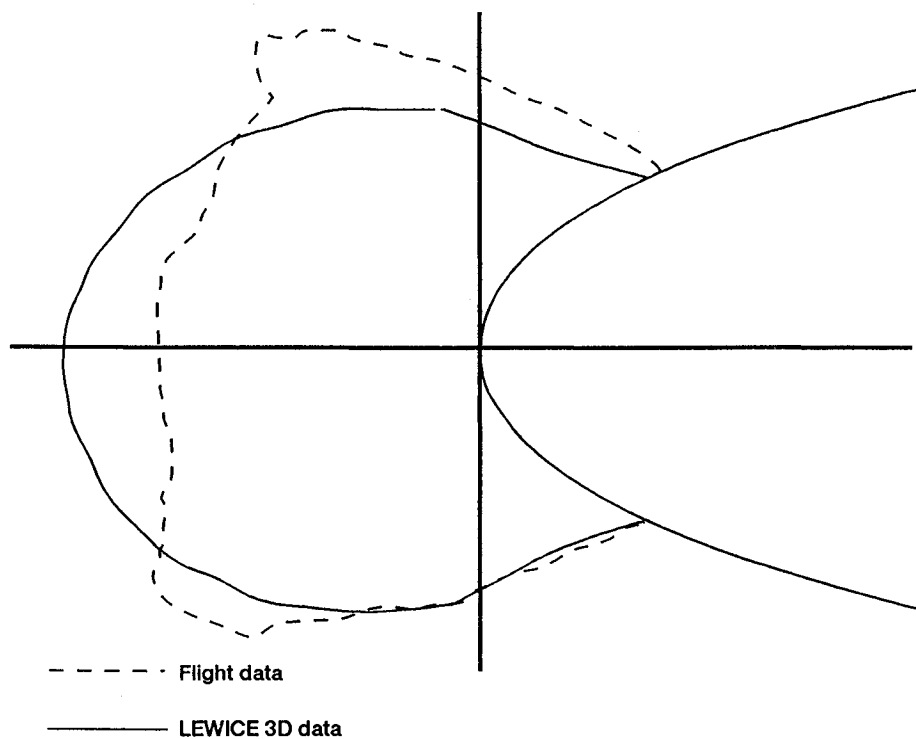
———— LEWICE 3D data

Figure 20.—Comparison between flight and LEWICE 3D ice shapes for flight 90-7, run 3.
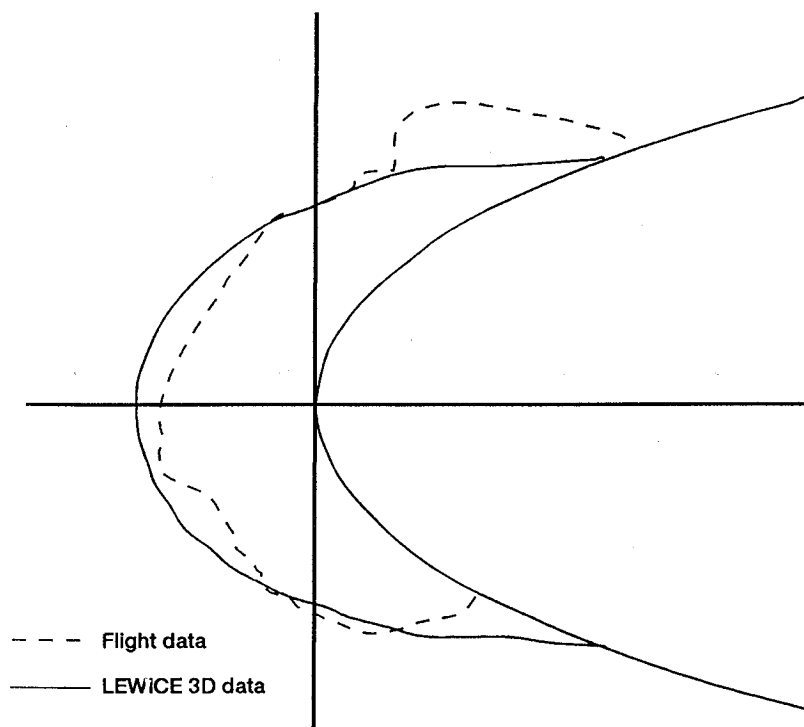
Figure 21.—Comparison between flight and LEWICE 3D ice shapes for flight 90-11, run 1.
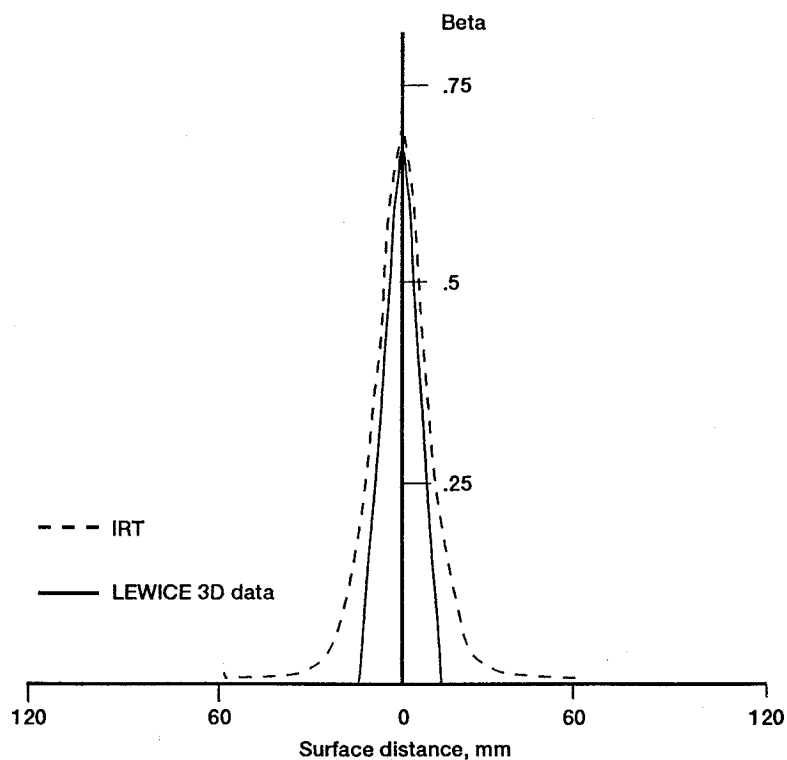

Figure 22.—Comparison between experimental and calculated local collection efficiencies for a NACA0012 airfoil swept to 30 degrees.

REPORT DOCUMENTATION PAGE

1. AGENCY USE ONLY (Leave blank)	2. REPORT DATE 1992	3. REPORT TYPE AND DATES COVERED Technical Memorandum

4. TITLE AND SUBTITLE

Prediction of Ice Accretion on a Swept NACA 0012 Airfoil and Comparisons to Flight Test Results

5. FUNDING NUMBERS

WU-505-68-10

6. AUTHOR(S)

Andrew L. Reehorst

7. PERFORMING ORGANIZATION NAME(S) AND ADDRESS(ES)

National Aeronautics and Space Administration
Lewis Research Center
Cleveland, Ohio 44135-3191

8. PERFORMING ORGANIZATION REPORT NUMBER

E-6746

9. SPONSORING/MONITORING AGENCY NAMES(S) AND ADDRESS(ES)

National Aeronautics and Space Administration
Washington, D.C. 20546-0001

10. SPONSORING/MONITORING AGENCY REPORT NUMBER

NASA TM-105368
AIAA-92-0043

11. SUPPLEMENTARY NOTES

12a. DISTRIBUTION/AVAILABILITY STATEMENT

Unclassified - Unlimited
Subject Category 02

12b. DISTRIBUTION CODE

13. ABSTRACT *(Maximum 200 words)*

In the winter of 1989-90, an icing research flight project was conducted to obtain swept wing ice accretion data. Utilizing the NASA Lewis Research Center's DHC-6 DeHavilland Twin Otter aircraft, research flights were made into known icing conditions in Northeastern Ohio. The icing cloud environment and aircraft flight data were measured and recorded by an onboard data acquisition system. Upon entry into the icing environment, a 24 inch span, 15 inch chord NACA 0012 airfoil was extended from the aircraft and set to the desired sweep angle. After the growth of a well defined ice shape, the airfoil was retracted into the aircraft cabin for ice shape documentation. The ice accretions were recorded by ice tracings and photographs. Ice accretions were mostly of the glaze type and exhibited scalloping. The ice was accreted at sweep angles of 0, 30, and 45 degrees. A 3-D ice accretion prediction code was used to predict ice profiles for five selected flight test runs, which include sweep angle of zero, 30, and 45 degrees. The code's roughness input parameter was adjusted for best agreement. A simple procedure was added to the code to account for 3-D ice scalloping effects. The predicted ice profiles are compared to their respective flight test counterparts. This is the first attempt to predict ice profiles on swept wings with significant scalloped ice formations.

14. SUBJECT TERMS

Aircraft icing; Three-dimensional ice accretion modeling; Flight test

15. NUMBER OF PAGES

16. PRICE CODE

17. SECURITY CLASSIFICATION OF REPORT Unclassified	18. SECURITY CLASSIFICATION OF THIS PAGE Unclassified	19. SECURITY CLASSIFICATION OF ABSTRACT Unclassified	20. LIMITATION OF ABSTRACT